Published in final edited form as:
Phys Med Biol. 2014 September 21; 59(18): R233–R302. doi:10.1088/0031-9155/59/18/R233.

An exponential growth of computational phantom research in radiation protection, imaging, and radiotherapy: A review of the fifty-year history

X. George Xu
Rensselaer Polytechnic Institute Troy, New York, USA

Abstract

Radiation dose calculation using models of the human anatomy has been a subject of great interest to radiation protection, medical imaging, and radiotherapy. However, early pioneers of this field did not foresee the exponential growth of research activity as observed today. This review article walks the reader through the history of the research and development in this field of study which started some 50 years ago. This review identifies a clear progression of computational phantom complexity which can be denoted by three distinct generations. The first generation of stylized phantoms, representing a grouping of less than dozen models, was initially developed in the 1960s at Oak Ridge National Laboratory to calculate internal doses from nuclear medicine procedures. Despite their anatomical simplicity, these computational phantoms were the best tools available at the time for internal/external dosimetry, image evaluation, and treatment dose evaluations. A second generation of a large number of voxelized phantoms arose rapidly in the late 1980s as a result of the increased availability of tomographic medical imaging and computers. Surprisingly, the last decade saw the emergence of the third generation of phantoms which are based on advanced geometries called boundary representation (BREP) in the form of Non-Uniform Rational B-Splines (NURBS) or polygonal meshes. This new class of phantoms now consists of over 287 models including those used for non-ionizing radiation applications. This review article aims to provide the reader with a general understanding of how the field of computational phantoms came about and the technical challenges it faced at different times. This goal is achieved by defining basic geometry modeling techniques and by analyzing selected phantoms in terms of geometrical features and dosimetric problems to be solved. The rich historical information is summarized in four tables that are aided by highlights in the text on how some of the most well-known phantoms were developed and used in practice. Some of the information covered in this review has not been previously reported, for example, the CAM and CAF phantoms developed in 1970s for space radiation applications. The author also clarifies confusion about “population-average” prospective dosimetry needed for radiological protection under the current ICRP radiation protection system and “individualized” retrospective dosimetry often performed for medical physics studies. To illustrate the impact of computational phantoms, a section of this article is devoted to examples from the author’s own research group. Finally the author explains an unexpected finding during the course of preparing for this article that the phantoms from the past 50 years followed a pattern of exponential growth. The review ends on a brief discussion of future research needs (A

supplementary file "3DPhantoms.pdf" to Figure 15 is available for download that will allow a reader to interactively visualize the phantoms in 3D).

1. Introduction

For more than 50 years, radiation dose assessment using computational models of the human anatomy has been a subject of great interest to the fields of radiation protection, medical imaging, and radiotherapy. Health physicists often need to understand how radiation interacts with the human body so that they can ensure the safety of workers and members of the public in accordance with complicated regulatory requirements. In diagnostic radiology and nuclear medicine, the imaging process—involving x-ray and gamma-ray photons powerful enough to traverse bodily tissues—must be optimized to achieve necessary image quality while minimizing potentially harmful radiobiological effects. Radiation therapy aims to deposit a lethal dose to the tumor—which may be subjected to organ motion—using focused external beams of x-ray and gamma-ray photons, electrons, protons, and heavy ions, or using internal sources that are less penetrating, while sparing healthy tissues from toxicity and secondary cancer. The anatomical modeling techniques evolved over time and new phantoms would emerge, as expected. However, the early pioneers of this field did not foresee the exponential growth of research activity that this review article has uncovered.

Radiation dosimetry is a basic science that has to do with the determination of the amount and distribution pattern of ionizing energy deposited in the object of interest. Accurate radiation dosimetry in the human body is quite challenging for several reasons: (1) exposure scenarios are diverse, often including complex and unique geometrical relationships between the source and human body; (2) an exposure can involve multiple radiation types, each of which transverse the human body and interact with tissues according to different radiation physics principles; (3) the human body consists of a very large number of anatomical structures that are heterogeneous in density and composition sometimes under in the influence of organ motion. For instance, cardiac and respiratory motion can result in complex 3-dimensional (3D) and 4-dimensional (4D) dose distribution patterns that must be accounted for during medical imaging or radiotherapy. This last point underscores the importance of anatomical models in radiation dosimetry because dose inside a living person cannot usually be directly measured. Instead, one must use computational or physical anatomical models to estimate the dose delivered to a worker or patient exposed to ionizing radiation. The accuracy of the dose estimate critically depends on how well the anatomical models account for the specific geometry and radiation attenuation properties of each individual—a quite daunting task in light of the fact that every person has a unique body shape and size.

It has been known for a long time that dose inside the body can be derived using either a physical phantom or a computational phantom that mimics human anatomical features. Historically, the term phantom was used in the radiological science literature to mean a physical device that mimics the human body. In the radiation protection community, phantom has also been used to refer to a mathematically defined anatomical model instead

of a physiologically based model such as a respiration or blood flow model. In this review article, “computational phantom” and “physical phantom” are used to avoid confusion.

Physical phantoms are made of solid materials which are radiologically equivalent to human tissues. Because the human body consists mostly of water, homogenized water or plastic phantoms are widely used for the calibration of radiation detectors and treatment systems. The simpler designs of these phantoms are useful for routine measurements where standardization between laboratories or hospitals is of critical importance (DeWerd and Kissick 2014). Another use of such homogeneous phantoms is to calibrate calculations by measuring the power output from a specific radiation-emitting machine. In contrast, anthropomorphic phantoms are more realistic and better represent the complex heterogeneity of the human body; they often consist of several tissue-equivalent materials that are molded into shapes of organs or bones to represent part or all of the body. For the ease of placing tiny radiation dosimeters, some of the physical phantoms for dose measurements come in slices with cavities in locations that match with organs of interest.

The approach of using such anthropomorphic physical phantoms for organ dose measurements can be expensive and time-consuming due to necessary experimental and radiation safety procedures. Furthermore, commercially available physical phantoms only come in a limited number of body sizes and do not fully reflect the diversity of the human population. Luckily, the advent of first-generation computers and Monte Carlo simulation methods originally designed for nuclear weapons research demonstrated the feasibility to calculate organ doses using computational phantoms. Such computational phantoms include extensive details of the exterior and interior features of the human body such as the shape, volume, and mass of radiosensitive organs. Coupled with information for tissue density and chemical composition, a computational phantom allows a researcher to simulate radiation interactions and energy deposition patterns in the body accurately. Although experimental work involving a whole-body physical phantom is still needed to verify the calculations especially when involving complex irradiation conditions, the computational approach is, in general, advantageous compared with the experimental approach in versatility, efficiency, precision, and safety. Furthermore, internally distributed radiation sources are best handled by the computational approach.

Since the 1960s, the development and application of computational phantoms have evolved into a specialized field of research that is integral to radiation protection, medical imaging, and radiotherapy. For non-ionizing radiation, similar computational phantoms have been developed over the years to study the biological effects caused by the heat produced by radiofrequency-emitting devices such as electric power lines and wireless cellular-phones. In the twenty years after the first computational phantom was developed in the 1960s, less than two dozen computational phantoms were developed and used by a small group of people in national laboratories who had access to computers. Computational phantoms became widely adopted in the 1980s with the advent of personal computers. By then, medical imaging had made it possible to visualize the anatomy in 3D. An international research community soon took shape and, over the years, several workshops were held to disseminate research ideas, facilitate collaboration, and develop roadmap for the future.

In 1996, Peter Dimbylow organized the first workshop on voxelized computational phantoms at the National Board of Radiological Protection (now Health Protection Agency) in the United Kingdom (Dimbylow 1996). In 2000, Keith Eckerman hosted a similar workshop at Oak Ridge National Laboratory in the United States (Eckerman 2000). The interest about computational phantoms was so widespread in the mid of 2000s that many colleagues decided to form the Consortium of Computational Human Phantoms (CCHP) during a dinner meeting at the Monte Carlo 2005 Topical Meeting, American Nuclear Society, Chattanooga, TN, April 17–21, 2005 (http://www.virtualphantoms.org). Under the umbrella of CCHP, George Xu and Keith Eckerman published the *Handbook of Anatomical Models for Radiation Dosimetry* in 2009 involved 64 authors from 13 countries (Xu and Eckerman 2009). In 2011, George Xu and Junli Li organized a workshop under the name of "The 3rd International Workshop on Computational Phantoms for Radiation Protection, Imaging and Radiotherapy," in Beijing, China (http://www.virtualphantoms.org/3rdWorkshopInBeijing.html). The Beijing Workshop was the first time that researchers from both ionizing and non-ionizing radiation communities attended. In Beijing, it was decided that the workshop would be held every other year. The 4th workshop (http://cp2013.org/) was then hosted by Niels Kuster of the Foundation for Research on Information Technologies in Society (IT'IS) in Zurich, Switzerland, May 20–22, 2013. At the Zurich workshop, it was decided to hold the next workshop in Seoul, Korea in 2015.

By 2009, approximately 121 computational phantoms had already been reported in the literature for studies involving ionizing and non-ionizing radiation (Xu and Eckerman 2009). Such a large number of computational phantoms was somewhat surprising at the time, given the fact that less than a dozen existed prior to the 1980s. Most of these phantoms were reported during the late 1980s and early 1990s due to the increased availability of advanced medical imaging technologies such as x-ray computed tomography (CT) and magnetic resonance imaging (MRI). It also became clear that organ surfaces could be defined in a variety of solid geometry modeling techniques including those we were familiar with, such as quadric equations and voxels, but also advanced geometries such as B-Splines, Non-Uniform Rational B-Splines (NURBS), and polygonal meshes. In the recent workshops, a number of questions were on people's minds:

- What are the fundamental challenges in phantom related research?
- Why did the computational phantoms evolve the way they did?
- Will the number of computational phantom stop increasing at some point of time?
- What are the differences between "population-average" prospective dosimetry needed for radiological protection under the current ICRP radiation protection system and "individualized" retrospective dosimetry often performed for medical physics studies?
- Is the concept of "Reference Man" in radiation protection obsolete?
- What are future research directions?

Answers to these questions, and many others, require an appreciation of the rationales and methods responsible for some of the most important computational phantoms. Through a

review about when and how various computational phantoms came about in the last 50 years, this article also attempts to learn insight into where this field of study may be heading in the future.

This article is organized into the following sections: (1) Introduction, (2) Solid-geometry modeling methods: CSG and BREP, (3) Monte Carlo Codes used with Computational Phantoms, (4) The Evolution of Computational Phantoms, (5) Physical Phantoms, (6) Examples of Computational Phantom Applications at RPI, (7) Discussion, and (8) Conclusion.

2. Solid-geometry modeling methods: CSG and BREP

It is essential to understand the geometrical shapes—the building blocks—of computational phantoms. The construction of a computational phantom must consider multiple factors such as anatomy, radiosensitivity of specific organs/tissues, computational efficiency, and geometrical compatibility with the Monte Carlo code that carries out the radiation transport calculation. As a first step, a phantom must be generated by explicitly defining the surfaces of an organ in which radiation interactions and energy depositions occur. The computer graphics community has dealt extensively with solid-geometry modeling for computer-aided-design (CAD). Two general modeling methods have been widely used: (1) constructive solid geometry (CSG) and (2) boundary representation (BREP) (Agostinelli *et al* 2003, Geant4 Team 2007, Leyton 2001, Stroud 2006). The topology—spatial location and relationship of the surfaces—is fundamentally different for these two methods.

CSG allows the modeler to create a solid object using Boolean operators (or the equivalent) to combine very simple shapes called primitives. Examples of these primitives include cuboids, cylinders, prisms, pyramids, spheres, cones and ellipsoids—surfaces that are easily described by quadric equations. CSG representations are easy to adopt and can yield good results when the objects are relatively simple in shape.

Modern CAD software systems, however, are based on the more powerful BREP methods. There are two types of information in BREP: topological and geometric. Topological information provides the relationships among vertices, edges, and faces. In addition to connectivity, topological information also includes orientation of edges and faces. In advanced BREP-based CAD, the exterior of an object can be defined as NURBS, which afford very smooth surfaces. The faces can alternatively be represented as polygons whose vertices are defined by a set of coordinate values x, y and z. A polygon mesh or unstructured grid is a collection of vertices and polygons that define the geometric shape of a polyhedral object in CAD. In principle, NURBS and polygonal meshes are interchangeable BREP data structures; however, unlike the CSG representation, BREP is much more flexible because a richer set of operation tools are available (e.g. extrusion, chamfering, blending, drafting, shelling, and tweaking). These features allow BREP-based models to include very complex anatomical features. Furthermore, the BREP technique is ideally suited for surface deformation—an operation necessary for the adjustment of organ size and for organ motion simulations and for changing the posture of phantoms to better simulate how humans interact with their environment.

For example, the left lung can be represented in the CSG method by "half an ellipsoid with a section removed" (Cristy and Eckerman 1987). The cut-out section, which is not specified by the original authors, can be defined by a Boolean operation subtracting one ellipsoid (B) from the other (A) to create the left lung, as described below:

$$A: \left(\frac{X-8.5}{5}\right)^2+\left(\frac{Y}{7.5}\right)^2+\left(\frac{Z-43.5}{24}\right)^2 \leq 1, Z \geq 43.5 \; B: \left(\frac{X-2.5}{5}\right)^2+\left(\frac{Y}{7.5}\right)^2+\left(\frac{Z-43.5}{24}\right)^2 \geq 1, if\, y<0$$

In Figure 1a and 1b, the 3D shapes of the left lung before and after the Boolean operation are illustrated. These surface equations are computationally efficient and are accepted by nearly all Monte Carlo codes. When using a Monte Carlo code, the geometry of the left lung is often further simplified by replacing the ellipsoid B with several planes. This type of phantoms is commonly referred to as "stylized" or "mathematical" phantoms. However, even with complicated and carefully designed Boolean operations, phantoms based on quadric surfaces are not anatomically accurate. The true shape of a human lung is more amorphous and cannot be described by a simple ellipsoid.

Using voxels as a CSG modeling technique, Figure 1c defines the left lung as an assembly of 3D cuboids. Medical image data can be converted to voxel geometry that provides a direct way of realistically describing the human anatomy. The geometry of a voxel is very easy for existing Monte Carlo codes to handle. On the other hand, each tomographic image slice needs to be treated by a "segmentation" process, which assigns each pixel to an organ or tissue of interest such as the lung, bone, or skin using a unique identification number. It can take a significant amount of time to prepare a voxel-based phantom because there is no automatic segmentation algorithm that works on all organs. Furthermore, a voxel phantom is based on images for one subject, therefore lacking the anatomical variability associated with organ size, shape, and location that are important in the current paradigm for radiation protection dosimetry. Furthermore, CT images do not generally distinguish between soft tissues well and are typically not whole-body images. Finally, the boundary of an organ is defined by uneven steps instead of a smooth surface, as shown in Figure 1c. As a result, the anatomical fidelity depends on the voxel size, especially for thin and small tissues such as the skin, eye lens, ribs, and bone marrow. An adjustment to the organ shape will likely involve all underlying voxels, which is computationally inefficient. These types of computational human body models are commonly referred to as "voxel" or "tomographic" phantoms.

The lung can also be defined by the advanced BREP modeling techniques involving NURBS or polygon mesh surfaces. The most common technique to create a BREP-based phantom involves the surface contour extraction of each organ from a tomographic image dataset using a commercial software package, followed by the integration of individual organs into a whole body assembly. In essence, the contours convert the voxels into NURBS or mesh surfaces that are smooth and anatomically realistic. These phantoms are commonly referred to as "NURBS," "mesh" or "BREP" phantoms. A misleading name for this type of phantom is "hybrid" which does not specify what two formats are actually used. Figure 1d

shows the triangular meshes of a left lung, which was derived from high-resolution tomographic images.

3. Monte Carlo Codes used with Computational Phantoms

Computational phantoms must be coupled with Monte Carlo codes that simulate radiation transport inside the human body for the purposes of determining the patterns of radiation interaction and energy deposition. Most health and medical physics applications employ photons and electrons with energies up to 20 MeV and protons up to 300 MeV. Health physics dosimetry, however, also considers neutron sources in nuclear reactors and particles with energies in the TeV range in high energy physics research or space radiation environment. Each type of radiation interacts with matter differently. For example, photons (x-rays or gamma-rays) deposit energy primarily via photoelectric effect, Compton scattering, and pair production processes (Attix 1986). The probability of a photon interaction occurring within an organ or tissue is determined by "cross sections" that are associated with the energy, the tissue electron density, and the tissue chemical composition. Mathematically, the differential cross section per electron for a photon undergoing the Compton scattering at angle ϕ per unit solid angle Ω is analytically determined by using the Klein-Nishina Equation (Attix 1986)

$$\frac{d\sigma}{d\Omega_{\varphi}} = \frac{r_o^2}{2}\left(\frac{h\nu'}{h\nu}\right)^2\left(\frac{h\nu}{h\nu'} + \frac{h\nu'}{h\nu} - \sin^2\varphi\right) \quad \text{(Eq. 2)}$$

where r_o is the classical electron radius, and *hv* and *hv'* are photon energies before and after the scattering, respectively. Extensive photon cross-section libraries have been developed for these purposes (Hubbell 1969, Storm and Israel 1970).

In general, Boltzmann radiation transport problems described by various differential, integral, and integro-differential equations can be solved by numerical computational methods including finite difference, finite element, discrete ordinates, and Monte Carlo. However, only the Monte Carlo methods are able to account for all aspects of particle interactions within 3D heterogeneous media such as the human body. Monte Carlo methods, which are based on statistical simulations, have a long history, but the real application to radiation transport simulations and the associated software development arose from nuclear weapons research at Los Alamos National Laboratory during World War II (Hammersley and Handscomb 1964).

In a Monte Carlo code, random numbers are used to determine the distance and fate of a particle by comparing interaction probabilities for every geometrical region of interest. This rather tedious process is repeated for an extremely large number of particles (nowadays often exceeding 1 billion), and each particle is tracked in the 3D anatomical model until all its energy is absorbed or the particle escapes from the transport geometry. The inherent statistical uncertainty can be controlled to be less than 1%, which is often more precise than an experimental result performed in a physical phantom using a dosimeter (for quantities such as the absorbed dose). Experiments with physical phantoms are often still needed, however, to validate the Monte Carlo calculations. This creates a peculiar situation where it

is not immediately clear whether the direct measurement in a simplistic physical phantom or the Monte Carlo calculation involving a more realistic compuational phantom provides the more accurate dose estimate. One reason for the rise in popularity of the Monte Carlo methods for dose estimation is the improvement in computer affordability and computing power over the last 30 years. The development of major Monte Carlo code packages is supported by national labs as well as by the user community at large. As a result, Monte Carlo codes are used today for many applications in nuclear engineering, health physics, and medical physics.

Most production Monte Carlo codes were originally developed for nuclear engineering and high energy physics research. Although these codes have been vigorously validated for radiation physics, the software packages are often difficult to use without extensive experience. Nearly all existing Monte Carlo codes can handle CSG shapes including the voxels. In the 1990s, some of these codes had trouble handling the very large numbers of voxels required for simulations involving whole-body computational phantoms (e.q., MCNP would limit the voxels to less than 25 millions).

There are many comprehensive reviews or introductory articles about the Monte Carlo methods for health physics and medical physics (Andreo 1991, Raeside 1976, Turner *et al* 1985, Zaidi 1999, Zaidi and Sgouros 2003, Rogers 2006). Some of the public-domain, general-purpose Monte Carlo codes used for radiation dose calculations include: EGS (NRC 2013), FLUKA (Battistoni *et al* 2006), GEANT4 (Allison *et al* 2006), MCNP (Brown 2003), MCNPX (Pelowitz 2005), MCNP6 (Goorley *et al* 2013), and PENELOPE (Salvat *et al* 2003). Specific codes for radiation therapy have also been developed (Rogers 2006).

4. The Evolution of Computational Phantoms

Previously published reviews on the historical development of computational phantoms have focused on a certain time period or a particular phantom type (Caon 2004, Zaidi and Xu 2007, Eckerman *et al* 2009, Zaidi and Tsui 2009). These reviews did not explicitly classify phantom modeling techniques, and since the time of their publication, many new phantoms have been developed using the BREP methods. An understanding of the modeling techniques and when the research community predominantly adopted each technique provides important insight into future directions. Based on chronological and technical information in the literature, this review article divides computational phantoms into three generations: (1) Stylized phantoms that are based on quadratic equations (1960s to 2000s); (2) Voxel phantoms that are based on tomographic images (1980s to present); (3) BREP phantoms that are based on advanced primitives and are deformable (2000s to present). Figure 2 contrasts these phantom generations in terms of their geometric sophistication.

4.1. Stylized Phantoms (1960s to 2000s)

The first-generation computational phantoms were developed for the purpose of better assessing organ doses from internally deposited radioactive materials for workers and patients (Eckerman *et al* 2009). Some of the earliest dose assessment techniques were developed in the first third of the 20th century primarily for use with interstitial radiation sources such as radium. According to Loevinger (1965a, 1965b, 1969), the dosimetry of

radioactive materials distributed in the body had been under consideration as early as the 1920s. Quimby has provided an excellent historical review of the early development of radiation dosimetry in nuclear medicine (Quimby 1970). The early techniques were adaptations of methods used for external dose assessment with assumptions and corrections applied to account for the different types of radiation used (NCRP 1985). However, rather than being able to measure the exposure or the absorbed dose, an internal dose assessment required a calculation.

Internal dose calculations were performed during early days using the formulation presented by Marinelli and his colleagues in the 1940s (Marinelli 1942, Marinelli *et al* 1948). These equations considered only the absorbed dose from beta-emitting radionuclides (classified as non-penetrating radiation) and from gamma-rays (penetrating radiation) emitted in the decay of these radiation sources.

In 1959, the International Commission on Radiological Protection (ICRP) used very simple models for the internal dosimetry calculations associated with the Report of ICRP Committee II (ICRP 1959). In these calculations, each organ of the body was represented as a sphere with an “effective radius.” The radionuclide of interest was assumed to be located at the center of the sphere and the “effective absorbed energy” was calculated for each organ. Corrections were made for the photon energy lost from the sphere. In this approach, the total body was represented as a 30-cm radius sphere. It is also interesting to note that the 30-cm radius sphere was used for an organ designated as “muscle” as well as for the small intestine and the entire gastrointestinal tract.

At the time, these approaches provided reasonably accurate estimates of the dose from a distributed radionuclide. However, most dosimetrists and researchers hoped for improved techniques and more accurate dosimetry estimates as technology developed. There was also a need for dose calculations for a number of new radionuclides introduced into nuclear medicine and more was known regarding the distribution and retention of these radionuclides in specific organs. Of course, the next step was to attempt to model individual organs of the body and ultimately the entire human body in a realistic manner. With the increase in the size and speed of computers, some progress occurred during the late 1950s and through the 1960s, eventually leading to the first-generation of stylized anthropomorphic phantoms.

Table 1 summarizes some of the most important and unique stylized phantoms developed since 1960s. This generation of stylized phantoms originated from work performed at Oak Ridge National Laboratory (ORNL) by Fisher and Snyder in the 1960s (Fisher and Snyder 1966, Fisher and Snyder 1967). Using CSG modeling techniques involving shapes such as elliptical cylinders and cones, they developed the so-called Fisher-Snyer adult phantom. The adult phantom was assumed to be standing erect with the arms at the sides of the body. Three specific regions were defined; the head and neck, the trunk including the arms, and the legs. The head and neck were represented by a 14 cm × 20 cm elliptical cylinder with a height of 24 cm. The trunk and arms were modeled as a larger elliptical cylinder, 20 cm × 40 cm with a height of 70 cm. The legs below the buttocks were modeled as a truncated elliptical cone with a height of 80 cm. Regions of little dosimetric importance were not

included, e.g., the hands, feet, ears, nose, etc. The composition of the phantom was assumed to be tissue distributed homogeneously throughout. No attempt was made to model the lungs or skeleton or to define the locations of specific organs in the phantom. Approximately 120 sub-regions were defined in the phantom, which were used to assign approximate values of the absorbed doses to organs located within specific regions. In some cases, absorbed dose estimates for large organs required the evaluation of the doses deposited in several of these regions. Even though the original phantom was designed for use with internally- deposited radionuclides, Snyder saw many other applications. For instance, Snyder used the phantom to study the distribution of dose in the body from external, point sources of gamma-rays (Snyder 1967). He studied four photon energies (0.07, 0.15, 0.5 and 1.0 MeV) and four different source locations at distances of one and two meters from the center of the phantom.

Fisher and Snyder also developed the “similitude” children phantoms which were scaled-down versions of the adult with added assumption that the entire body was a homogenous tissue (i.e. the lungs and skeleton were ignored) (see discussion by Eckerman *et al* 2009). These phantoms represented children of 0 (newborn), 1, 5, 10, and 15 years of age. These early phantom designs had outer dimensions representing the average height, surface area, and body mass of a children within each particular age group. These phantoms became known as the “similitude phantoms” because of their resemblance to children. This approach had its limitations because children, in general, are not just “little adults.” However, at the time, these phantoms helped answer a real need in the nuclear medicine community (Kereiakes *et al* 1965).

In 1969, Snyder and his colleagues reported the first heterogeneous phantom that became known as the “MIRD-5 Phantom,” a named derived from the Medical Internal Radiation Dosimetry (MIRD) Committee of the Society of Nuclear Medicine which adopted the phantom (Snyder *et al* 1969). This phantom was composed of a skeleton, a pair of lungs, and the remainder (soft tissue). The representation of internal organs in this mathematical phantom was crude, as the simple equations captured only the most general description of the position and geometry of each organ. The original model was intended to represent a healthy “average” adult male, the so-called Reference Man, as defined by the International Commission on Radiological Protection (ICRP). The characteristics of the Reference Man were the result of an extensive review of medical and other scientific literature on the European and North American populations (ICRP 1975). The Reference Man was defined as a 20- to 30-year-old Caucasian, 70 kg in weight and 170 cm in height (the height was later changed to 174 cm). In 1978, Snyder *et al* (1978) published an elaborative set of specific absorbed fractions using an improved version of their heterogeneous phantom which contained more than 20 organs and more detailed anatomical features.

The limitations associated with the approach of applying a set of scaling factors to the adult phantom to create age-dependent similitude phantoms were clear. Significant efforts were undertaken at ORNL during the mid-1970s to develop individual pediatric phantoms based upon a careful review of the existing literature for each particular age group. This effort produced the next generation of mathematical stylized phantoms that, although they appeared to be modeled after the adult, were designed independently. Three “individual phantoms” were designed by Hwang *et al* (1976). This set consisted of the newborn, the 1-

year old, and 5-year old models. A separate effort was undertaken by Jones *et al* (1976) for the 15-year old model, and Deus and Poston (Deus and Poston 1976) undertook the design of a 10-year old model after the other four designs were complete. The development of the 10-year old was significantly different from those for the other four ages. In fact, this design was intended to point the way to the next generation of more realistic phantoms (see discussion by Eckerman *et al* 2009). Even though the design was completed and used for a limited number of dose calculations, it was not popular because of the very complex geometry and, after Poston left ORNL, alternative approaches were developed.

Building upon previous work, Cristy reported the development of a new series of stylized phantoms in 1980 and then with Eckerman in 1987 in the report ORNL/TM-8381 (Cristy 1980, Cristy and Eckerman 1987). This series of "family" of phantoms consisted of an adult male, a newborn, and individuals of ages 1, 5, 10 and 15 (also representing an adult female with additional anatomical features). As shown in Figure 3, each phantom consists of three major sections: (1) an elliptical cylinder representing the trunk and arms; (2) two truncated circular cones representing the legs and feet; and (3) a circular cylinder on which sets an elliptical cylinder capped by half an ellipsoid representing the neck and head. Attached to the legs section is a small region with a planar front surface to contain the testes. The female phantom included two ellipsoids attached to the trunk to represent breasts (not shown in Figure 3). The arms are embedded in the trunk, and minor appendages such as fingers, feet, chin, and nose are omitted.

Drawings depicting the external features of all the family phantoms are shown in Figure 4. The pediatric phantoms were designed to form a developmentally consistent family with the existing Snyder adult phantom. The exterior of each phantom has approximately the form of the human body; but, as in their adult phantom, there has been no attempt to model for realistic details because these were presumed to have only small effect on the scattering of photons. Similarly, the description of the interior organs, while approximately correct as to size, shape, position, composition and density, are simplified to provide formulas which could be easily modeled on the computers available at the time. Figure 5 shows a schematic view of the principal organs.

4.1.1. Pregnant Woman Phantoms—In 1995, Stabin and his colleagues at ORNL adapted the adult female phantom in this family to represent a pregnant woman at the end of each trimester of pregnancy (Stabin *et al* 1995). This set of three stylized pregnant female phantoms were used for various internal nuclear medicine applications. Figure 6 shows a drawing of the cross sectional view of the uterine region at 9-months in the pregnant female phantom series by Stabin *et al* (1995).

4.1.2. GSF Gender-specific ADAM and EVA Phantoms—In parallel with the efforts at ORNL by Cristy and Eckerman to revise the MIRD-5 Phantom, a group at GSF—National Research Center for Environment and Health in Germany (now known as HZM—the German Research Center for Environmental Health) used the anatomical descriptions of the hermaphrodite MIRD-5 phantom to develop a pair of gender-specific adult phantoms later known as the ADAM and EVA for external dosimetry studies (Kramer *et al* 1982). The EVA phantom was derived by scaling down all relevant volumes of the MIRD-5 phantom

with the total whole body mass ratio of 0.83 that was based on the analysis of ICRP reference organ masses. Then, the female organ masses were modified to create space for neighboring organs. Finally, sex-specific organ such as testes, ovaries, uterus and breasts were introduced into the appropriate phantom to yield ADAM and EVA, respectively. The chin was introduced by removing a section of the neck to created a more realistic external irradiation geometry for the thyroid. The female breasts were represented by two ellipsoid sections attached to the trunk of EVA. There are a number of minor anatomical differences, such as breast sizes, from those reported by Cristy and Eckerman (Kramer *et al* 1982, Cristy and Eckerman 1987).

4.1.3. CAM and CAF Phantoms for Space Radiation Dosimetry—The Computational Anatomical Man (CAM) and CAF (Computerized Anatomical Female) phantoms, developed by Billings and Yucker in 1973 for the National Aeronautics and Space Administration (NASA), demonstrated a very different and aggressive approach in stylized modeling because the phantoms reportedly consisted of 1100 unique geometric surfaces and 2450 solid regions (Billings and Yucker 1973). According to the authors, internal body geometries such as organs, voids, bones, and bone marrow were explicitly modeled using CSG modeling techniques. A computer program called CAMERA was also developed for performing analyses with the CAM and CAF phantoms. The authors state that "extremely detailed geometrical model of the human anatomy, the most detailed yet prepared, has been developed for use in investigations dealing with exposure of astronauts to the natural space radiation environment". According to the authors, the model was equally applicable to investigations dealing with exposure of humans to radiation associated with nuclear weapon and nuclear power system environments as well as medical applications such as radiotherapy and radiography (Billings and Yucker 1973). Indeed the surface geometry was so detailed that one may wonder how this was possible using computers in the 1970s. Unfortunately, the CAM and CAF phantoms were never adopted for applications outside the aerospace industry and very little information about the work was accessible by the radiation dosimetry community until Tom Jordan who worked for years for NASA as a contractor recently released some of the images (CMPWG 2013). It is interesting to note one unique exterior anatomical feature of these phantoms: the arms are seperated from the trunk, unlike the MIRD-5 phantom and its successors developed around the same time. Two images of the CAM phantom are shown in Figure 7.

4.1.4. MIRD Committee Work—Since the publication of the stylized dosimetry model of Snyder *et al* in MIRD Pamphlet 5 Revised (Snyder *et al* 1978), SNM's MIRD Committee has refined several internal organs to support the development of radiopharmaceutical tracers and therapeutic nuclear medicine. Modifications to the MIRD stylized model have been published as MIRD Pamphlets, which include equations of the new geometries, tabulated absorbed fractions of energy for monoenergetic photons and electrons, and tabulated radionuclide S-values. In 1999, the MIRD Committee adopted 6 new age-specific models of the head and brain for a newborn, 1-year old, 5-year old, 10-year old, 15-year old (also representing the average adult female), and adult male (Bouchet *et al* 1999). Similar to previous stylized models, simplistic geometrical shapes were used to represent the different regions of the head and brain, with volumes derived from published reference masses and

shapes from analysis of MRI images. Later, the MIRD Committee also adopted an age-dependent series of stylized kidney models that are used widely in therapy nuclear medicine for renal toxicity predictions (Bouchet *et al* 2003).

4.1.5. MCAT Phantom for SPECT and PET Imaging—The stylized modeling technique was also adopted by one group for medical applications. The Mathematical Cardiac Torso (MCAT) phantom, which includes the major thoracic structures and organs, was developed by a research group led by Benjamin Tsui (currently with Johns Hopkins University) at the University of North Carolina for use in nuclear medicine imaging research, specifically single-photon emission computed tomography (SPECT) and positron emission tomography (PET) (Pretorius *et al* 1997, Tsui *et al* 1993, Tsui *et al* 1994). The same group, especially Paul Segars (who was a Ph.D. student of Tsui at the time), later developed more advanced phantoms that are discussed later in this article.

4.1.6. Other Stylized Phantom Works—Table 1 also lists several additional efforts related to stylized phantoms. In the early 1990s, it was clear that the research community no longer favored stylized phantom modeling methods. However, several groups continued to develop stylized phantoms for particular methods. Two groups developed computational phantoms of an embryo and fetus for space radiation dosimetry (Chen 2004) and an adult representing the Korean population (Park *et al* 2006). A group at the Nagoya Institute of Technology developed two new stylized phantoms of a 9-month old Japanese infant (Hirata *et al* 2008). Around the same time, researchers at Tsinghua University in Beijing created a new mathematical phantom named the Chinese Mathematical Phantom (CMP) using anatomical data for the Reference Asian Man and the Chinese Reference Man (Qiu *et al* 2008). A new MIRD phantom based on reference data for the standard Korean male was developed at the Catholic University in Pusan, Bugok (Kim *et al* 2010). This latter phantom was used to model a patient implanted with ^{192}Ir for brachytherapy treatment of prostate cancer. Bento *et al* (2011) at the Nuclear and Technological Institute (ITN) in Portugal also developed a new mathematical phantom to simulate the reference male BOMAB phantom. This phantom was used to simulate the detection of internal sources of radiation with a whole body counter (WBC). A series of four mathematical phantoms were developed at the Bhaba Atomic Research Centre in India to simulate the calibration of whole body monitoring systems for internal radionuclide contamination using BOMAB phantoms (Bhati *et al* 2011). More recently, Gardumi *et al* converted MIRD-type mathematical phantoms to NURBS before voxelizing them to investigate the so-called “voxel effect” which arises because of the stairstepped approximation of smooth surfaces with cubic voxels (Gardumi *et al* 2013).

For nearly 50 years since the first stylized phantom was reported, these anatomically simplified phantoms have been used as the *de facto* “standard” representations of the ICRP “Reference Man” methodology which is based on “population-average” 50th-percentile anatomical parameters specified in ICRP-23 (ICRP 1975) and ICRP-89 (ICRP 2002a). Applications of stylized phantoms have eventually included many aspects of radiation protection, radionuclide therapy, and medical imaging (ICRU 1992). In addition, national and international bodies have adopted organ dose estimates derived from these stylized

phantoms in guidelines and regulations related to industrial and medical uses of ionizing radiation.

Although stylized phantoms made it possible to carry out Monte Carlo computations during times when computers were much less powerful, the original developers recognized the obvious shortcomings. Human anatomy is too complex to be realistically modeled with a limited set of surface equations. Many anatomical details in these models were compromised that sometimes led to inaccurate results. For example, when such phantoms were applied to nuclear medicine procedures where precise dosimetry is necessary, the calculated average organ and marrow doses did not produced strong correlations with observed marrow toxicity (Lim *et al* 1997). Most nuclear medicine physicians consequently tend to administer lower-than-optimal amounts of radioactivity to avoid toxicity. For CT dose reporting, most existing commercial software systems were based on the stylized patient models that are known to cause very large errors for low-energy x-rays (Gu *et al* 2008a). Similar stylized models have also been used to derive dose-response relationships for Japanese atomic bomb survivors and for medical patients in epidemiological studies. In the external-beam radiotherapy community, a stylized homogenous phantom was used by the Radiation Epidemiology Branch of the National Cancer Institute (NCI) in studies related to assessing secondary organ doses of theraputically irradiated patients (Stovall *et al* 1989). By the late 1980s, a few groups of researchers began to seek new ways to develop anatomically realistic phantoms. The underlying motivation was the belief was that new anatomically realistic phantoms would not only take advantage of improvements in computer modeling technology, but would ultimately lead to improved estimates for assessing the risks of patients or workers exposed to radiation.

4.2. Voxel Phantoms (1980s to Present)

The development of anatomically realistic models was desirable but impossible until early 1980s when powerful computer and tomographic imaging technologies became available. With the advent of medical imaging techniques such as CT and MRI, researchers could, for the first time, visualize the internal structures of the body in 3D and store the images in versatile digital formats. These advantages brought about the exciting and prolific era of the so-called voxel or tomographic phantoms. Table 2 summarizes a total of 84 phantoms that were constructed, typically from one of three types of tomographic images: CT and MR images of live subjects, and cross-sectional photographs of cadavers. In two previously published review articles, a total of 21 voxel phantoms was reported by Caon (2004) and 38 by Zaidi and Xu (2007). The notable increase in the number of phantom due to a more exhaustive literature search, recent developments, and the inclusion of phantoms developed for use solely in non-ionizing radiation applications.

In terms of solid-geometry modeling techniques, a cubic voxel—one of the basic CSG primatives—is simply a 3D representation of a pixel; however, compared with the medical applications such as radiation treatment planning, the task of developing reference human phantoms presented some unique and intractable challenges: (1) to construct a whole-body phantom, image slices should ideally cover the entire body—a process not normally carried out in rountine medical examinations because of the need to minimize x-ray exposures or

the lengthy time required for MRI procedures; (2) a large amount of internal organs/tissues must be identified and segmented for organ dose calculations, whereas, in radiotherapy, only the tumor volume and adjacent regions are routinely outlined; (3) the image data size of a whole-body model, especially when high-resolution images are used, can be potentially too great for a computer to handle; and (4) a standardized patient phantom is often used to study diverse radiation types such as photons, electrons, neutrons, and protons, thus requiring considerable Monte Carlo simulation capabilities.

In terms of the developmental process, tomographic phantoms are fundamentally different from the stylized ones. A tomographic image data set is composed of many slices, each displaying a 2-dimensional (2D) pixel map of the anatomy. The 3D volume of a voxel is measured by multiplying the pixel size by the thickness of an image slice. Unlike stylized phantoms, which are based on quadric surface equations, a voxel phantom contains a huge number of tiny cubes grouped to represent various anatomical structures. However, both quadric surface equations and cubic voxels belong to the same class of CGS geometries.

The creation of a tomographic phantom involves four general steps: (1) acquire a set of tomographic images (e.g. CT, MR, or anatomical photography) that cover the entire volume of the body; (2) identify (or segment) organs or tissues of interest (e.g. lungs, liver, skin, etc.) from the original image slice by assigning every pixel with an identification number; (3) specify the density (e.g., soft tissue, hard bone, air, etc.) and chemical composition of organs or tissues; and (4) Register the segmented image slices into a 3D volume that can be used for 3D visualization (for checking anatomical structures) and for Monte Carlo calculations. Figure 8 illsutrates these steps using the VIP-Man phantom (Xu *et al* 2000).

The earliest effort to create an image-based phantom for radiation dosimetry is believed to have been reported by S. Julian Gibbs, a radiology professor at Vanderbilt University (Pujol and Gibbs 1982, Gibbs *et al* 1984, Gibbs *et al* 1987). In these pioneering studies, Gibbs and her co-workers explored the use of 2D x-ray images as the basis to form an anatomically realistic model of the patient. They used this information in Monte Carlo calculations to assess doses received by patients who underwent dental radiologic procedures.

Zankl and her colleagues at the GSF, Germany decided in the late 1980s to use 3D CT imaging on healthy volunteers and patients to develop what eventually became a family of 12 voxel phantoms: BABY, CHILD, DONNA, FRANK, HELGA, IRENE, GOLEM, GODWIN, VISIBLE HUMAN, LAURA, KLARA, and KATJA (Williams *et al* 1986, Zankl *et al* 1988, Smith et al 2000, Petoussi-Henss *et al* 2002, Zankl *et al* 2002, Fill *et al* 2004, Becker *et al* 2007, Zankl *et al* 2005). The adult male phantoms were developed first, followed by the adult female, pediatric, and pregnant-woman phantoms.

In its annual report for 2002, ICRP (2002b) states: "*An important issue for Committee 2 is the substitution of an anatomically realistic voxel phantom, obtained digitally in magnetic resonance tomography and/or computed tomography, for the MIRD phantom which is a mathematical representation of a human body*." The ICRP Committee 2 has a task group on Dose Calculations (DOCAL) that was directly responsible for the development of a set of standard voxel phantoms. DOCAL is made of active researchers as members and consultants

on internal and external dosimetry. The GOLEM and LAURA phantoms later underwent significant revision by the group led by Zankl at GSF, to yield the REX and REGINA phantoms which were released to the public as the ICRP adult Reference Male and Reference Female shown in Figure 9 (ICRP 2009, Schlattl *et al* 2007). Interestingly, ICRP did not endorse the first-generation stylized phantoms. Figure 9 shows the ICRP adult Reference Male and Female phantoms (ICRP 2009).

Several processes were considered to develop the ICRP reference phantoms: (1) CT image datasets of individuals close to the Reference Man and Woman (height and weight) were needed, (2) the datasets were segmented, (3) the body heights were adjusted to reference values by scaling the voxels, (4) the skeletal masses were adjusted to the reference values, and (5) individual organs were adjusted to reference values by adding and subtracting voxels. These processes were extremely time-consuming as the voxel data format is difficult to deform, unlike more advanced BREP geometries. While the ICRP reference phantoms filled a blank in the standardization of phantom-based radiation protection dosimetry, these phantoms had a relatively large slice thickness (up to 8 mm) compared to many phantoms reported later. At these voxel sizes, small organs cannot be realistically defined and the skin and walled organs reportedly contain small holes. To address this problem, A Korean group Yeom *et al* (2013) recently developed a polygon-surface version of the ICRP Reference Male by converting voxels to polygon-surfaces.

In 1994, Zubal *et al* (1994) from Yale University published a head-torso model called VoxelMan, which was developed from CT images. The original phantom was used for optimizing nuclear medicine imaging. Improvements to the original phantom were made with an MRI scan data of a human brain. This phantom is commonly known as the “Zubal Phantom” and registered users can freely download the original data from the internet. Two early users later revised the original data to report what are known as the MANTISSUE3-6 and VOXTISS8 phantoms by attaching arms and legs in two different positions to the original torso phantom (Dawson *et al* 1997, Sjögreen *et al* 2001). Adopting this publically available data, Kramer *et al* from Brazil developed an adult male phantom named MAX (Male Adult voXel) in 2003 (Kramer *et al* 2003) and later an adult female phantom named FAX in 2004 (Kramer *et al* 2004), both adjusted in accordance with ICRP-89 reference body height and organ masses. Kramer *et al* revised the skeletons (cortical bone, spongiosa, medullary yellow bone marrow, and cartilage) of MAX and FAX in 2006 to improve their compatibility with the latest ICRP-103 recommendations. These revised phantoms are known as MAX06 and FAX06. The work by Kramer *et al* is one of the earliest efforts to create a ICRP-89 compatible voxel phantoms for radiation protection dosimetry.

In 1996, Dimbylow from the National Radiological Protection Board (NRPB) (now known as the Health Protection Agency) in the United Kingdom reported the development of an adult male phantom known as NORMAN from MR images (Dimbylow 1996). NORMAN, which has a body height similar to the ICRP Reference Man, was first used by Dimbylow in a finite-element simulation code to determine the specific energy absorption rate from exposures to non-ionizing electromagnetic fields (Dimbylow 1997). In 1997, his colleague Jones adopted NORMAN to estimate organ doses from external and internal photon sources (Jones 1997). In 2005, Dimbylow developed an adult female phantom, NAOMI, also from

MRI scans (Dimbylow 2005a). The phantom was rescaled to a height of 1.63 m and a mass of 60 kg, the dimensions of the ICRP Reference Woman. However, to date, the NAOMI phantom has been used only in non-ionizing radiation calculations. In 2005, a revised version of the NORMAN phantom, called NORMAN-5, was created by Ferrari & Gualdrini from ENEA-ION Istituto di Radioprotezione in Italy to derive external photon dose data (Ferrari and Gualdrini 2005). One year later, Dimbylow merged the NAOMI with the stylized fetal phantoms developed by Chen from Canada to create a series of hybrid phantoms for pregnant women (Dimbylow 2006). The process of adjusting two types of geometrical information was reported to be cumbersome.

In 1999, Caon *et al* from Flinders University in Australia reported a torso phantom named ADELAIDE created from CT images of a 14-year old girl (Caon *et al* 1999, Caon *et al* 2000). This phantom was interesting because, for some time, it was the only set of voxel data for a non-adult, and at the time, their studies likely provided the most reliable CT dose estimates for this patient group. Caon later reviewed his and other researchers' experiences on voxel phantoms (Caon 2004).

The VIP-Man (Visible Photographic Man) voxel phantom was reported in 2000 by Xu and two of his students at Rensselaer Polytechnic Institute (RPI) in the U.S. (Xu *et al* 2000). VIP-Man was the first phantom based on cross-sectional color photographic images of a cadaver — a 39-year-old male through the National Library of Medicine's famous Visible Human Project (VHP). The color transversal photos digitally captured at the 0.33 mm×0.33 mm pixel resolution and each photograph was taken after the removal (by shaving) of each successive 1 mm layer of the frozen cadaver by a cryomacrotome (Xu *et al* 2000). Although the original images were segmented to yield more than 1400 organs and tissues for the purposes of teaching anatomy (Spitzer and Whitlock 1998), only approximately 80 organs and tissues were adopted at RPI for radiation dosimetry purposes. Ultra-fine and color image analysis allowed the RPI group to explicitly segment a number of small and radiosensitive tissues including the stomach mucosa, skin, and red bone marrow. Given the extremely small voxel size, the VIP-Man phantom consists of more than 3.7 billion voxels—the most of any phantom reported at the time. The finalized VIP-Man phantom was unique because it represented an individual with a heavy body mass of 103 kg. Keith Eckerman from ORNL, who headed the ICRP DOCAL Committee at that time, encouraged this effort at RPI because VIP-Man could serve as an interesting variation from the ICRP reference value. However, because the phantom was developed from a cadaver, the lungs of the VIP-Man are deflated and smaller than might normally be expected for a living, breathing individual. Figure 10 is an image that highlights the anatomical differences between the stylized and the voxelized VIP-Man. The VIP-Man was used for a large number of studies in health and medical physics which are discussed on more detail later in this article. It is worth noting that VISIBLE HUMAN developed at GSF was based on CT images at 2–4 mm resolution of the same individual before the body was frozen. The RPI group later also reported a pregnant patient phantom using CT images of a 30-week pregnant female and compared internal dose data with those derived from a stylized phantom (Shi and Xu 2004; Shi *et al* 2008).

Realizing the need for additional phantoms representing children of various ages, Bolch and colleagues from the University of Florida (UF) developed a series of pediatric voxel phantoms that appeared between 2002 and 2006, representing children with ages ranging from newborn to 15 years old (Lee *et al* 2005, Lee *et al* 2006, Nipper *et al* 2002). This approach was later extended to two groups (Groups A and B) of phantoms. Group A is composed of male and female voxel phantoms of a newborn, a 1-year old, a 5-year old, a 10-year old, and a 15-year old for whom the phantom stature, total weight, and individual organ masses are within 1% of ICRP-89 reference values. Group B phantoms are constructed by scaling the Group A phantoms up and down to yield phantom at each 1-year age interval, from newborn to 15-years old. The intent of the UF pediatric series was to provide a reference library of phantoms that could be matched to individual patients for age-specific organ dose assessment.

Two Japanese groups were noted in Table 2 for their independent efforts to develop voxel phantoms since 2001. Saito *et al* (2001) from the Japanese Atomic Energy Research Institute (JAERI) developed an adult male model named Otoko (the first Asian phantom) and an adult female phantom named Onago. More recently, Sato *et al* developed the JM, JM2, and JF phantoms which have a refined vertical slice thickness (Sato *et al* 2007a, Sato *et al* 2007b, Saito *et al* 2008). These phantoms were used mainly for radiation dosimetry applications in Japan were influenced by earlier projects at the GSF. The other group, Nagaoka *et al*, from the National Institute of Information and Communications Technology (NIICT) in Japan reported an adult male model, named TARO, and an adult female model, named HANAKO, developed from MR images for radio-frequency electromagnetic-field studies (Nagaoka *et* al 2004). Later *Nagaoka et al* (2008) would use a free-form deformation (FFD) to change the exterior features of the adult male phantom to develop Deformed Children phantoms of 3-, 5- and 7-year olds. The authors reported that it was difficult to develop these phantoms with the FFD algorithm and the internal organs are not adjusted to age-dependent values. The Otoko phantom was recently used in a study to calculate dose conversion coefficients for the Japanese population (Takahashi *et al* 2011).

Several Korean phantoms have been developed by researchers at Hanyang University in Korea from various image sources: Korean Man (KORMAN), Korean Typical MAN-1 (KTMAN-1), Korean Typical Man-2 (KTMAN-2), High-Definition Reference Korean (HDRK), and Korean WOMAN (KORWOMAN). The HDRK phantom was based on sectioned color photographs of an adult male cadaver that has high image resolution (Choi *et al* 2006, Kim *et al* 2008). The KTMAN-2 phantom has been used by Lee *et al* (2011) to measure the effects of selective collimation in cephalography. Kim *et al* (2010) from the Korea Atomic Energy Institute have developed a series of voxel phantoms of different body shapes in order to better calculate counting efficiencies for whole-body counters instead of using physical BOMAB phantom that has a fixed size.

Zhang *et al* (2009) summarized three Chinese voxel phantoms developed by three separate groups in China: Chinese Man (CNMAN) produced from color photographs of a cadaver by the China Institute for Radiation Protection (Zhang *et al* 2007a), Visible Chinese Human (VCH) produced from a different set of cadaver color photographs by the Huazhong University of Science and Technology (HUST) (Zhang *et al* 2007b, Zhang *et al* 2008a,

Zhang *et al* 2008b), and Chinese Voxel Phantom (CVP) produced from MRI images by Tsinghua University (Li *et al* 2009, Zeng *et al* 2006). The lead developer of the CNMAN phantom, Binquan Zhang, served as a visiting scholar at RPI during 2007–2008. The Chinese government undertook the Chinese version of the Visible Human Project through the so-called Xiang Shan Conference in early 2000s that resulted in multiple cadaver image datasets, some with a slice thickness as fine as 0.1 mm. Figure 11 depicts the VCH phantom which is based on extremely high-resolution cadaver images (Zhang *et al* 2008b). The HUST group also reported a rat model (Xie et al 2010). Recently, Sun *et al* (2013) adopted NURBS to construct the VCH-F Astronaut (VCH-FA) phantom for dose calculations in the space radiation environment, incorporating statistical body characteristics of Chinese female astronauts as well as ICRP reference organ mass data. Tung *et al* (2011) from the Chang Gung University of Taiwan developed a voxel phantom of the Reference Taiwanese Adult using CT images from thirty Taiwanese adults.

A voxel phantom named NUDEL (NUmerical moDEL) was developed by Ferrari in Italy (2010) for use in radiation protection studies. A computational phantom was constructed from CT data of the plastic physical AMOS (Anthropomorphic MOdel for dosimetric Studies) phantom. Dose calculations for several types of nuclide exposure were run in MCNPX code and were compared to experimentally measured values with the physical AMOS phantom. The calculations were also compared to values obtained from the NORMAN-05, GOLEM, DONNA, VOXELMAN, VIP-MAN, REX, and REGINA voxel phantoms.

A radiological accident that occurred in South America in 2009 prompted the construction of a personalized voxel phantom to numerically calculate the dose the victim received. Courageot *et al* (2011) of the Institute for Radiological Protection and Nuclear Safety (IRSN) converted CT scans into a voxel phantom using the Simulation of External Source Accident with Medical Images (SESAME) tool. Courageot *et al* (2010) reported the Simulation of External Source Accident with Medical Images (SESAME) tool that allows the use of NURBS to model a victim's morphology and posture.

Researchers at the French National Institute of Health and Medical Research (INSERM), a public institute focused on biomedical research, designed a series of virtual whole-body patient models (WBPM) for usage in radiotherapy (Alziar *et al* 2009). They used CT data and the software tools IMAgo and ISOgray to model the phantoms. The phantoms accommodate different radiotherapy treatment positions, genders, and age groups. Alzier *et al* (2009) developed a software tool to take patient data and adjust the phantom's anatomy in order to better match that of a specific individual.

Members of the MATSIM Project (MATROSHKA Simulation) at the Austrian Institute of Technology coordinated research to numerically simulate the effects of irradiation under reference radiation fields in outer space (Beck *et al* 2011). They created a two part voxel phantom using the FLUKA Monte Carlo code and CT images from a physical RANDO phantom. The voxel phantom was split into the MATSIM torso and head. The results of the simulations were within one standard deviation of experimental values. Taddei *et al* (2009) at the M.D. Anderson Cancer Center developed a voxel phantom in MCNPX code to assess

the radiation does to pediatric patients receiving craniospinal irradiation with proton beams. An Iranian and Japanese team (Mofrad *et al* 2010a) developed a race-specified voxelized organ, specifically a Japanese male liver that contains statistical parameters, for nuclear medicine and internal dosimetry purposes. Patni *et al* (2011) of the Bhabha Atomic Research Centre in India published dose conversion coefficients obtained from the ICRP adult voxel phantoms. In 2008, Akkurt *et al* (2008) from ORNL reported their work involving a hybrid of voxel and stylized geometries.

4.3 BREP phantoms (2000s to present)

The past decade has seen a surprising surge in BREP phantom development. The number of such phantoms is increasingly each month. A non-inclusive list of 10 groups, reporting a total of 183 BREP-based phantoms, are summarized in Table 3.

4.3.1. Work at UCSU, JHU, and Duke—Segars and Tsui (2009) summarized their work in a book chapter. Paul Segars's Ph.D. thesis at the University of North Carolina was the first publication that systematically described the anatomical modeling using the NURBS-based techniques (Segars 2001). The well-known NCAT phantom was developed from the Visible Human CT image data set and the 3D anatomy was later extended into the 4^{th} dimension to model cardiac and respiratory motions. The beating heart model of the 4D NCAT was based on 4D tagged MRI data from a real patient. The 4D NCAT phantom offers a vast improvement over the stylized MCAT phantom—a stylized version experimented on earlier by the same group—with more realistic models of the anatomy and the cardiac system, and the respiratory motion (Segars and Tsui 2009). The 4D NCAT has gained a widespread use particularly in nuclear medicine imaging research for evaluating and improving myocardial SPECT imaging. The conceptual design of the NCAT phantom also served as basis for the development of a 4D digital mouse phantom named MOBY (Segars *et al* 2004, Segars and Tsui 2007, Segars *et al* 2009). Figure 12 shows the original MIRD phantom together with MCAT, NCAT, XCAT, MOBY and ROBY phantoms provided by Paul Segars.

Figure 13 shows the 4D Extended Cardiac-torso (XCAT) phantom family recently developed as the next version of the 4D NCAT provided by Paul Segars. The XCAT phantom family includes whole-body male and female anatomies based on the high-resolution Visible Male and Female anatomical datasets. In addition to the basic anatomy, the cardiac and respiratory motions were also updated in the XCAT phantom. The series includes 47 phantoms based on of the XCAT phantom representing the cardiac and repiratory motions of multiple patients. The XCAT phantom was mapped to patient CT data to produce the series, Segars ran simulations of PET, SPECT, and CT to demonstrate the applicability of the phantoms. Mishra *et al* used a modified XCAT phantom to evaluate 3D fluoroscopic image generation from a single planar treatment image (Mishra *et al* 2013). Then Segars *et al* (2013) extended the XCAT beyond these reference anatomies to a library of 35 male and 23 female 4D computational phantoms by developing a series of anatomically variable 4D XCAT adult phantoms for imaging research. The NCAT and XCAT phantoms have been used by other research groups to simulate radiation dose from radiography (Tabary *et al* 2009, Niu *et al* 2010) and radiotherapy (McGurk *et al* 2010). A

research group constructed a version of the XCAT heart to enhance the range of cardiac disorders that can be studied using the phantom (Veress *et al* 2011). Tward *et al* (2011) developed a series of pediatric phantoms from a base adult XCAT phantom. An algorithm to modify the XCAT phantom was developed and used to generate 24 male pediatric patients with 8 organs each.

4.3.2. Work at RPI—In 2005, the research group led by Xu at RPI used the VIP-Man phantom to simulate respiratory motions by adopting the gated respiratory motion data of the NCAT phantom (Xu and Shi 2005). The 4D VIP-Man Chest phantom was used to study external-beam treatment planning for a lung cancer patient (Zhang *et al* 2008c).

From 2005 to 2007, using the BREP modeling technique, Xu *et al* from RPI reported a set of phantoms at the end of three gestational periods of 3, 6 and 9 months—called RPI-P3, RPI-P6 and RPI-P9 (Xu *et al* 2007). Unlike the stylized models and the voxel models, these BREP-based models were found to be more flexible. These features allow BREP models to realistically change the size and shape for geometrically complex organs. Figure 14 shows the polygonal mesh model of the 9-month old fetus. Organs in the un-pregnant female are also individually adjusted to the ICRP-89 values and then deformed to allow for the fetus to be inserted using reference information and the help from an experienced anatomist.

Continuing their BREP technique involving triangular meshes, the RPI group reported in 2008 the development of a pair of phantoms called RPI Adult Male and Adult Female (Zhang *et al* 2009b). Shown in Figure 15, this pair of adult phantoms was carefully adjusted to match the ICRP-89 reference values for more than 70 organs and 45 bones (including cortical bone, spongiosa, and cavities) as well as muscles. Several software algorithms were systematically developed to automate the deformation and organ overlap detection that were based entirely on about 126 sets of triangle meshes (Download a supplementary file "3DPhantoms.pdf" to this figure to interactively visualize the phantoms in 3D). In a subsequent work, as shown in Figure 16, the RPI Adult Male and Adult Female phantoms were extended into weight-specific phantoms representing the 5th, 25th, 50th, 75th, and 95th weight percentiles (Na *et al* 2010).

The RPI Adult Female phantom was used to create phantoms of female workers with different breast sizes for the purpose of studying the effect of this parameter on the lung counting of internally deposited radionuclides (Hegenbart *et al* 2008). This was one of the first efforts to perform the so-called "virtual calibration" for bioassay measurement of internally deposited radionuclides in workers. Existing physical phantoms for this purpose come in a limited number of body sizes. In comparison, computational methods detector efficiency calculation provide a more convenient means of for determining the internal radioactivity content in people across a spectrum of different body shapes and sizes.

Using the same BREP deformable modeling methods, Ding *et al* (2012) modified the RPI Adult Male and Female phantoms to produce 10 phantoms representing overweight and obese individuals with a Body Mass Indices from 26 to 48. These phantoms consist of more than 100 deformable organs defined in the mesh-geometry format. Two main classes of adipose tissue in the human body were considered: (1) subcutaneous adipose tissue (SAT)

located beneath the skin and (2) visceral adipose tissue (VAT) which surrounds the abdominal organs as illustrated in Figure 17.

Figure 18 shows 3D views of the RPI BMI-adjustable male and female phantoms. As the first ever set of phantoms for overweight individuals, these phantoms were applied in an interesting study of radiation dose received by patients undergoing CT examinations (Ding *et al* 2012).

Posture-specific phantom is relatively rare, but is important to more realistically model how people interact with radiation in real-world environments. Han *et al* (2010) reported a pair of walking phantoms to represent individuals walking on a contaminated ground. Using the same method, Su *et al* (2012) then changed the posture of these phantoms to sitting. These are some of the earliest effort to design posture-specific phantoms, but the deformation was based on simple and unrealistic postures, as depicted in Figure 19.

To improve the posture-specific phantoms reported earlier at RPI, Vazquez *et al* (2014a; 2014b) developed two phantoms, called CHAD, with adjusted postures defined by a motion capture system. They applied the phantoms to simulate unique human postures found in a criticality accident that took place in 1997 in Sarov, Russia (Vazquez et al 2014a) and then a criticality accident at a JCO facility in Tokai-mura, Japan (2014b). Figure 20 shows the process to use motion capture to create a realistic sequence of worker movements.

4.3.3. Work at the University of Florida—In a series of papers, the UF group led by Wesley Bolch reported their work on “hybrid” family phantoms of both genders and children at various ages (Lee *et al* 2007, 2008, 2010; Bolch *et al* 2010). They created the BREP phantom series, called UFH-NURBS phantoms using the following steps. First, they segmented patient-specific CT image data from which they then generated polygonal meshes. These meshes were then converted to the NURBS format using commercial software. They then extracted several contours from the polygonal meshes and generated the NURBS surfaces by a software tool called “lofting”. It was then in the NURBS geometrical domain they carried out organ adjustment to match the ICRP-89 reference values. In the final step, the NURBS–based phantoms were voxelized so that they could be implemented in Monte Carlo calculations. However, in order to voxelize the smooth NURBS models, they transferred the NURBS surfaces back to the polygonal meshes. In September 2008, ICRP established that its future reference phantoms for pediatric individuals would be based upon the UF series of hybrid phantoms. Recently, Geyer *et al* (2014) summarized their family phantoms and application to CT dose calculations at the Zurich workshop. Figure 21 shows the UF family phantoms developed using BREP methods (Bolch *et al* 2010).

In 2011, the UF group (Maynard *et al* 2011) reported a family of NURBS based fetal phantoms. The phantoms were based on CT and MR images of fetus specimens of various ages between 10 and 30 weeks and were modified to conform to reference values. Tissues and organs were segmented using the modeling software 3D-DOCTOR and turned into polygon mesh surfaces. The models were then imported into Rhinoceros® 3D modeling software to incorporate NURBS surfaces and correctly orient the models.

One important contribution to the literature by the UF group is in the area of bone marrow dosimetry. For radiation protection purposes, photon or neutron dose response functions can be used to report active marrow and endosteum dose by tallying photon or neutron fluence in spongiosa regions of the skeleton (Eckerman 1985). With anatomically realistic phantoms developed at UF, Johnson *et al.* (2011) reported information to use the 3-factor method as an alternative to the dose response function for photon skeletal dose. The approach was also applied to neutrons by Bahadori *et al*. (2011).

The UF phantoms have seen wide use. The UF hybrid adult male phantom was used in a study by Johnson *et al* (2009) to calculate the effects of patient size on dose conversion coefficients. A model of electron dosimetry on infants based on the UF hybrid newborn phantom and an earlier developed skeleton tissue model (Pafundi *et al* 2009) was released by Pafundi *et al* (2010) from the UF. Hough *et al* (2011) released a model for skeletal based electron dosimetry in the ICRP reference male. CT scans of a cadaver were implemented in the Rhinoceros® 3D software to modify the UF hybrid male reference phantom to include segmented skeletal tissue. Dimbylow *et al* (2010) published a study that used the UF's newborn NURBS based voxel phantom to calculate SAR for exposure to electromagnetic fields in the 20 MHz to 6 GHz region. Bahadori *et al* (2011) from the UF released a publication studying dose estimates from space radiation on astronauts. They modeled the astronauts by adapting the UF family of hybrid phantoms to the 5th, 50th, and 95th percentiles for 40 year old American Males and 40 year old Japanese females. Recently, a group led by Zaidi has used the UF phantoms for a number of nuclear medicine dose calculations (Xie *et al* 2013, Xie and Zaidi 2014).

4.3.4. Work at Vanderbilt University—The Vanderbilt group led by Michael Stabin, in collaboration with Segars from Duke University, reported a "family" of adult and pediatric phantoms by adapting the NURBS-based NCAT adult male and female phantoms (Stabin *et al* 2008; Stabin *et al* 2012). ICRP-89 reference body and organ values were used to adjust NURBS surfaces. The authors state several advantages of this approach: (1) NURBS-based phantoms can be developed much more quickly than working with voxels and manually segmenting individual patient image data sets; (2) The phantoms have a higher level of internal consistency; and (3) The phantoms are complete from head to toe, thus avoiding the problem of missing organs in some of the medical images. It should be noted that the groups at RPI, UF, and Vanderbilt (and Duke) developed these BREP phantoms as part of the joint Virtual Patients Project funded by the National Cancer Institute as well as other individual projects.

4.3.5 Work at the Federal University of Pernambuco—Led by Richard Kramer, a group at the Federal University of Pernambuco (UFPE) in Brazil has been active in developing BREP phantoms. Cassola *et al* (2010) reported two phantoms based on polygon mesh surfaces. The phantoms, FASH (Female Adult meSH) and MASH (Male Adult meSH), were constructed using software, including Blender, ImageJ, Binvox, and MakeHuman. The researchers based their phantoms on anatomical models and atlases, and showed that whole-body CT scans are unnecessary for phantom design. The organ masses were based on the values recommended for the male and female reference adult outlined in

ICRP-89. Cassola compared FASH and MASH to the RPI-AF and RPI-AM phantoms and noted significant differences in anatomy. The UFPE group (Kramer *et al* 2010) made a series of calculations on the FASH and MASH phantoms. Large differences were observed compared to calculations done on the RPI-AM and RPI -AF mesh phantoms. Cassola *et al* (2011) continued the work on the FASH and MASH phantoms and published a library of 18 phantoms in 2011. The phantoms were adjusted based on reference values for the 10th, 50th, and 90th height and mass percentiles for Caucasian members of each gender. The reference values were obtained from the PeopleSize software package, which obtained the values from over 100 publications in North America, Asia, Australia, and Europe. In 2011, the group published 5 and 10 year old pediatric phantoms based on the same methodology that created FASH and MASH (Lima 2011). The phantoms were developed with polygon mesh surfaces in the modeling programs BLENDER and MAKEHUMAN and were edited in the programs DIP (Digital Imaging Processing) and QtVoxel. The researchers used ICRP data for the 5- and 10-year old reference children. Figure 22 shows the MASH phantoms organized by weight and height at the 10^{th}, 50^{th}, and 90^{th} percentiles (Cassola *et al* 2011)

4.3.6. Work at IRSN—The group at IRSN developed a series of female torso phantoms in the Rhinoceros® 3D modeling software (Farah *et al* 2010a). A thoracic torso phantom was produced from mesh surfaces and NURBS, and was based on reference data from the ICRP adult female reference computational phantom. A series of 34 phantoms of differing girth, cup size, breast tissue composition, and internal organ volumes were created from the base phantom. They used the phantoms to ascertain the morphological dependence of counting efficiency curves from *in vivo* lung monitoring of workers (Farah *et al* 2010b). In 2011 they released a thoracic male phantom and a mesh equivalent to the physical Livermore phantom for the purposes of simulating *in vivo* measurements (Farah *et al* 2011). The phantoms were modeled with mesh and NURBS geometries. Data from CT and MRI scans were used to delineate organs. The data was then imported to Rhinoceros® 3D, where it was assembled into the two phantoms. Simulations of the two phantoms yielded comparable data to those done with voxel phantoms. The phantoms will be the basis for a new library of phantoms in a future study. A separate project at the IRSN produced a library of 25 whole body male phantoms in 2011 (Broggio *et al* 2011). The phantoms were produced from data in the CAESAR database, a compilation of male and female 3D models constructed from full body optical imaging. A total of 22 male Caucasian optical models were used as the basis for the phantoms. The phantom's organs were constructed from ICRP reference data and added to the optical models. The phantoms possess a total of 109 segmented organs. The phantoms occupy a range of different body types, organ masses, and organ volumes. Figure 23 are the IRSN male phantoms with different body types from the CAESAR database, a compilation of surface models from full body optical images (Broggio *et al* 2011).

4.4. Non-ionizing radiation applications

Although not the focus of this article, voxel phantoms have also been used for non-ionizing radiation applications are listed in Table 2. Most of this work was neglected in the previous review articles by Caon (2004) and by Zaidi and Xu (2007), although the methods and approaches to phantom design are very similar. In fact, some phantoms, such as the NORMAN phantom, have been used for both ionizing and non-ionizing radiation

applications. Table 2 clearly specifies whether the voxel phantoms that have been used for non-ionizing applications: the Visible Man from the VHP color photographs by the Brooks Air Force (Mason *et al* 2000, Wang *et al* 2004), the DAM adult male phantom from MR images by a group in Italy (Mazzurana *et al* 2003), the SILVY 30-week pregnant woman phantom from hybrid CT (originally obtained by RPI) and MR images by the Graz University of Technology, Austria (Cech *et al* 2007, Cech *et al* 2008), the MEET Man from VHP color photographs by University of Karlsruhe, Germany (Doerfel and Heide 2007, Sachse *et al* 1997), and the Anatomically Based Model from MR images by University of Utah (Tinniswood *et al* 1998).

Findlay and Dimbylow (2009) reported the specific absorption rate (SAR) for exposure to electromagnetic fields using the NORMAN phantom. Findlay and Dimbylow (2010) continued their work on SAR measurements and conducted a study of SAR in children due to Wi-Fi. He rescaled the sitting posture NORMAN phantom so that it matched ICRP reference values for a 10 year old child. The effects of electromagnetic fields from Wi-Fi devices operating at 2.4 and 5 GHz were modeled using a FDTD method.

Uusitupa *et al* (2010) measured SAR in the 300 to 5000 MHz region utilizing 15 voxel phantoms, including NORMAN, the Japan MALE/FEMALE, the VHP Male, and the VF series. The simulations were run with FDTD code on a HP supercluster at the Helsinki University of Technology in Finland. This study modeled the effects of different postures, human body models, and incoming direction of the electromagnetic field.

4.4.1. Work at IT'IS—Christ *et al* (2010) and Gosselin *et al* (2014) report the Virtual Family—a series of BREP-based phantoms developed for electromagnetic exposure calculations by the Foundation for Research on Information Technologies in Society (IT'IS). As shown in Figure 24, the Virtual Family consists of a 34-year old adult male, 26-year old adult female, 11-year old girl, and a 6-year old boy (Christ *et al* 2010). MRI images from volunteers were analyzed and segmented into 80 different tissues and organs using the imaging processing software iSEG. The boundaries between the tissues and organs were then remodeled using the software tool Amira. The Virtual Family is a part of the larger Virtual Population project at IT'IS. The Virtual Population project has developed 6 additional anatomic models using the same methods that were used with the Virtual Family (Gosselin 2014). The additional models consist of the Virtual Classroom, a series of four child models, and two individually developed models: an obese 37-year old male model, and an aged 84-year old male model.

The second to last item in Table 3 is a series of 9 phantoms representing a pregnant female in each gestational month developed by a group led by Ji Chen from the University of Houston in collaboration with Wolfgang Kaine of the U.S. Food Drug Administration (FDA) (who was previously with IT'IS) for studying the effects of radiofrequencies emitted from various electronic devices (Wu *et al* 2006). These phantoms only include a limited number of organs such as the body, placenta, embryonic fluid, bladder, bone, fetus and the uterus. They used patient-specific MRI images and CAD software to specify the organ shapes.

Researchers do not consider the heart models in current phantoms to have enough clinical details. Gu *et al* (2011) of the Center for Devices and Radiological Health (CDRH) developed a series of high resolution heart phantoms for the purposes of accurate dosimetric calculations. The computational heart models were generated through a nearly automated algorithm created by the researchers that will allow the creation of new heart phantoms. The heart phantoms were inserted into the mesh based Virtual Family of phantoms for simulation. Aubert *et al* (2013) also built new hybrid computational phantoms (HCPs) with an inserted detailed heart model. The use of a detailed heart model eliminates the problem of identifying the coronaries on the patient's CT.

4.4.2. Work at Hanyang University—Current permutations of hybrid phantoms must be voxelized so that they may be used in Monte Carlo dose calculations. Voxelizing a BREP phantom reintroduces the majority of the limitations of the voxel phantoms. Researchers at Hanyang University in Korea have converted the voxel phantom VKH-Man into a polygon surface phantom using 3D-DOCTOR and directly implemented the phantom into Geant4 code in order to circumvent this limitation (Kim *et al* 2011). Calculational speed and accuracy on their new phantom, PSRK-Man (Polygon Surface Reference Korean Man) have been compared to the HDRK-Man phantom, which was also based on VKH-Man. The PSRK-Man phantom has overcome many of the limitations of a voxel phantom; however, the calculation speed for the phantom is 70–150 times slower than for its voxel counterpart HDRK-Man. The speed was significantly improved later when this group developed a method to calculate polygon-mesh geometry in GEANT4 code directly (Han *et al* 2013).

5. Physical Phantoms

Table 4 summarizes selected physical phantoms that are often used to benchmark calculations performed on computational phantoms. These phantoms are typically used for three different applications: external radiation dosimetry, internal radiation dosimetry, and imaging quality assurance. For external radiation dosimetry, a physical phantom is designed so that small thermoluminescent dosimeters (TLDs) (or ion chambers or solid-state detectors) can be inserted in different locations of the phantom to measure doses from external irradiation. Examples of this type of phantom include the RANDO® phantom by the Phantom Laboratory and the ATOM® phantom by the CIRS Inc., which contain tissue equivalent slices that have anatomical maps and cavities for organ dose measurements (Anderson *et al* 1962, CIRS 2013, Phantom Laboratory 2013). Phantoms for calibrating radiobioassay detectors or nuclear medicine imaging equipment are designed to contain either removable organs that are doped with long-lived radioactive materials or hollow body regions that are filled with short-lived radioactive liquids.

These designs allow the phantoms to mimic internally contaminated individuals. The physical torso phantom by Lawrence Livermore National Laboratory (LLNL) and the Bottle Manikin Absorption (BOMAB) phantom family by the Radiation Protection Bureau, Canada are important examples of radiobioassay calibration phantoms. There are many phantoms that are used for medical image quality assurance purposes. Most of these phantoms, such as the NEMA image quality phantom, cover only partial body and some are anatomically very simple. Table 4 lists examples of several such phantoms by the CIRS and Kyoto Kagaku Co.

that are used for image analysis. With anatomically realistic computational phantoms, the UF group led by David Hintenlang has fabricated several physical phantoms representing a newborn, 1-year old, and adult male (Hintenlang *et al* 2009). Rapid prototyping processes were also used to quickly produce physical phantoms from patient-specific data (Mille and Xu 2008). A detailed review of physical phantoms can be found in a newly released book edited by DeWerd and Kissick (2014).

6. Examples of Computational Phantom Applications by Students at RPI

A potential benefit of this review article is the opportunity to illustrate how computational phantoms have been used for radiation dosimetry. For expedience, projects carried out by my students at RPI since 2000 are used as examples here. The topics cover health physics, diagnostic imaging and radiotherapy. Collaborative projects involving non-radiation related research such as surgical planning is not included (Jin *et al* 2005).

6.1. Health Physics

Health physics dosimetry typically involves organ dose and effective dose quantities for external and internal sources under standard irradiation conditions. The VIP-Man model was used to compare dosimetry data from VIP-Man — a large sized individual of 40 years old — with other voxel phantoms including the ICRP Computational Phantoms. Details of these studies have been reported for different radiation types including photons (Chao *et al* 2001a, Xu *et al* 2005), electrons (Chao and Xu 2001, Chao *et al* 2001b), neutrons (Bozkurt *et al* 2000, Bozkurt *et al* 2001) and protons (Bozkurt and Xu 2004).

6.1.1. External Photon Dosimetry—Using the VIP-Man phantom, Chao *et al* reported a new set of conversion coefficients from kerma free-in-air to absorbed dose and kerma free-in-air to “effective VIP-Man dose” for external monoenergetic photon beams from 10 keV to 10 MeV (Chao *et al* 2001a, and a later correction by Chao *et al* 2003). This study noted that kerma approximation, which assumes secondary electrons from photon interactions deposit their energies at an interaction site, could lead to potential uncertainty for high-energy photons incident on shallow tissues (such as breast, skin, eye lenses, or gonads). The study concluded that the size of the model, kerma approximation, and the anatomical difference were three main factors in causing dosimetric discrepancies. These comparisons also suggested possible ways to improve the stylized models. For example, the stomach is situated too close to the left side of the body when compared to VIP-Man.

Han *et al* (2010) used the walking phantoms to calculate environmental exposures involving parallel and isotropic planar sources of ^{137}Cs and ^{60}Co with concentrations of 30 kBq/m^2. For the parallel plane source case, the organ doses were found to be up to 78% greater for walking phantoms than those for the stationary phantoms with legs together. The dose difference is due to that fact that widely open legs during walking provide less shielding to several organs, especially the kidneys, ovaries, and liver, from parallel sources on the ground. The effective doses of the walking phantoms were on average 15% higher than standing phantoms. On the other hand, when isotropic surface contamination sources were considered, no significant dose difference was observed between phantoms with different postures. This study demonstrated the feasible to use deformable phantoms to represent

realistic postures for organ dose calculations in environmental dosimetry studies. Similar findings were reported by Su *et al* (2012) for sitting phantoms above a nuclear medicine clinic where positron emission tomography (PET) imaging is used.

6.1.2. External Electron Dosimetry—Chao *et al* (2001b) presented organ doses from the VIP-Man phantom from external electron beams using EGS4-VLSI Monte Carlo code and compared data with those reported for the ADAM phantom using MCNP4 code by Schultz and Zoetelief (1996), a hermaphrodite mathematical model using FLUKA by Ferrari *et al* (1997), and the MIRD-5 mathematical model using EGS4 by Katagiri *et al* (2000). These comparisons suggested, that at least for electron dosimetry, a single standard body model does a poor job in representing individuals of diverse anatomy. The study further concluded that a large number of voxel phantoms would need to be investigated before the degree of dose variation is understood.

6.1.3. External Neutron Dosimetry—Using the VIP-Man phantom, Bozkurt and his co-authors reported a new set of fluence-to-absorbed dose and fluence-to-effective dose conversion coefficients calculated for both low-energy (10^{-9} – 20 MeV) and high-energy (20 – 10000 MeV) neutrons (Bozkurt *et al* 2000, Bozkurt *et al* 2001). The absorbed dose for 24 major organs and effective dose results based on the realistic VIP-Man were presented and compared with those based on the simplified MIRD-based phantoms reported in literature. The authors noted discrepancies between the doses calculated on the two phantoms and concluded that several factors may have contributed to the discrepancies. The differences in anatomical models, which cause approximately a 10% difference in effective dose, are because the VIP-Man is heavier and taller and how the Monte Carlo codes treat the transport of high-energy particles, including the use of evaluated data and theoretical models.

6.1.4. External Proton Dosimetry—Bozkurt and Xu (2004) applied the VIP-Man phantom to calculate fluence-to-absorbed dose and fluence-to-effective dose conversion coefficients under high-energy proton environment. The absorbed dose results were presented for 24 major organs of VIP-Man, and the calculated data were compared with those based on mathematical phantoms reported in literature. Some discrepancies in organ dose and effective dose, within 40%, were observed due to the use of different transport models employed by different Monte Carlo codes. Taranenko and Xu (2009) used the RPI-P phantom series to calculate conversion coefficients for fetuses from whole body irradiation with monoenergetic proton beams. The simulation was run in MCNPX for 12 different source energies ranging from 100 MeV to 100 GeV, and for 6 different configurations.

6.1.5. External Dosimetry for Red Bone Marrow—Caracappa and co-workers used two sets of Visible Human images for the identical anatomy to gain insight to the external dose to the red bone marrow, which is the most radiosensitive tissue (Caracappa *et al* 2009). A Monte Carlo computational model was constructed in this study from the CT images of the Visible Human Project, and compared to the VIP-Man phantom derived from color photographs of the same individual (Xu *et al* 2000). These two data sets for the same individual offered interesting information that was not previously available. Dose to the red

bone marrow was calculated for the CT model using the uniform mixture assumptions and using the cellularity factors adopted by ICRP to test the previous assumptions and evaluate the accuracy of the computed dose to the red bone marrow in Monte Carlo simulations. Based on the newly developed algorithms, three dosimetry applications were investigated and tested. Broad beam photon irradiation in occupational exposure results in similar doses for high energies, but differences as great as 40% for low energies. An electron total-body irradiation procedure for treating skin cancer was also studied, with a 39% difference in red bone marrow dose between the existing method and the proposed revised method. These results demonstrate the advantage of the new algorithms by accounting for marrow cellularity and distribution various bone sites in the anatomical and dosimetry models.

6.1.6. Internal Electron Dosimetry—Based on the VIP-Man phantom, Chao and Xu calculated complete sets of specific absorbed fractions for internal electron emitters (Chao and Xu 2001). This was also the first report of internal electron data for walled organs such as the esophagus, lower large intestine, stomach, and upper large intestine. Although electrons are considered as weakly penetrating radiation and researchers have usually ignored the dose to organs other than the source organ, results from this study show that doses to neighbor organs and nearby organs can be too great to be neglected. This study provided convincing evidence that internal electrons do affect organs beyond the source organ.

6.1.7. Internal Photons Dosimetry for GI tract—In this study, the VIP-Man phantom was used to calculate SAFs for the gastrointestinal (GI) tract (Xu *et al* 2005). SAFs for sources in GI tract have been previously studied based on stylized phantoms. Using the VIP-Man phantom, the authors compared SAFs for stomach wall from VIP-Man to those previously published by Cristy and Eckerman for photon sources in the stomach content. The stylized models have been widely utilized by the nuclear medicine dosimetry community. However, SAFs derived from this phantom can have considerable uncertainties when compared to the realistic VIP-Man under certain conditions. This study clearly demonstrated the advantage of the VIP-Man phantom whose small voxel size allows the dosimetry to be performed on small tissues structures such as the mucosal layer in the GI tract.

6.1.8. Dynamic phantoms for criticality accident dose reconstruction—Using the CHAD phantoms developed motion-capture data, Vazquez *et al* (2014a; 2014b) simulated how workers were fatally exposed to extremely high levels of radiation. Implementation of the emergent techniques produced more accurate and more detailed dose estimates for the workers than were reported in previous studies. In Vazquez *et al* (2014b), a total-body dose of 6.43 and 26.38 Gy was estimated for the two workers, who assumed a crouching and a standing posture, respectively. Additionally, organ-specific dose estimates were determined, including a 7.93 Gy dose to the thyroid and 6.11 Gy dose to the stomach for the crouching worker and a 41.71 Gy dose to the liver and a 37.26 Gy dose to the stomach for the standing worker. Implications for the medical prognosis of the workers are discussed, and the results of this study were found to correlate better with the patient outcome than previous estimates, suggesting potential future applications of such methods

for improved epidemiological studies involving next-generation computational phantom tools.

6.2. Radiological Imaging

6.2.1. Organ doses from SPECT and PET brain imaging—To estimate internal dosimetry for brain imaging, a head and brain portion of the VIP-Man was used to implement into the Monte Carlo code, EGS4-VLSI (Chao and Xu 2004). Fifteen sub-regions were modeled including caudate nucleus, cerebellum, cerebral cortex, cerebral white matter, corpus callosum, eyes, lateral ventricles, lenses, lentiform nucleus, optic chiasm, optic nerve, pons and middle cerebellar peduncle, skull CSF, thalamus, and thyroid. S-values were calculated for the most important sources and targets encountered in SPECT and PET brain imaging. These results were then compared to those from the stylized head/brain model recommended by the MIRD (Bouchet *et al* 1996). Although heavier individuals (e.g. VIP-Man) will usually receive lower radiation doses, the stylized head/brain model underestimates the S-values by 15% on average for a patient similar to the VIP-Man model. More tomographic head/brain models are needed in order to compare various brain sizes and anatomical variations. Before such an inter-comparison is performed, the results presented in this paper are useful for patients who are similar to VIP-Man in body size or weight.

6.2.2. Organ doses from X-ray Radiographs—VIP-Man was used by Mark Winslow, a Ph.D. student at RPI, in collaboration with Walter Huda from University of Syracuse, to calculate values of energy imparted (ε) and effective dose (E) for monoenergetic photons (30–150 keV) in radiographic examinations. Energy deposition in the organs and tissues of the human phantom were obtained using Monte Carlo simulations. These monoenergetic E/ε values can generate values of E/ε for any x-ray spectrum and can be used to convert values of energy imparted into effective dose for patients undergoing common head and body radiological examinations (Winslow *et al* 2005). Later, in his doctoral research, Mark Winslow, in collaboration with Birsen Yazici of RPI, also studied the image quality by analyzing approximately 2000 simulated chest x-ray images for the VIP-Man using the ROC/AUC analysis (Son *et al* 2006, Winslow *et al* 2006).

6.2.3. Organ Dose from CT—Gu *et al* (2009) used the RPI Pregnant Female phantoms to run dose calculations for multi detector CT (MDCT) scans. The MDCT scanner and the phantoms were implemented in MCNPX code. The dose profiles showed that there was little risk to the patient or the fetus from the MDCT scans. Ding *et al* (2012) developed 10 obese phantoms for the purpose of optimizing image quality and CT dose in obese patients. It was found that calculated dose for obese patients differed significantly from the dose calculated for normal weight phantoms.

6.3. Radiotherapy

6.3.1. Adjoint Monte Carlo method for external-beam prostate radiation treatment—The abdominal portion of the VIP-Man model was used in the doctoral research by Brian Wang, a Ph.D. student at RPI, to develop and demonstrate an Adjoint Monte Carlo (AMC) method for optimizing the external beam directions in the so-called 3D Conformal Radiation Treatment of prostate cancer (Wang *et al* 2005a). The AMC method

had been widely used in nuclear reactor physics research but was never demonstrated for treatment planning in realistic 3D patient anatomy. With the VIP-Man model, which was already implemented in the MCNP code with multi-group adjoint cross-sections, it was possible to test the theory in clinically relevant scenarios. This work was in collaboration with Moshe Goldstein, a nuclear engineer from Israel who first proposed the possibility during a sabbatical at ORNL, and Narayan Sahoo, who was a clinical therapeutic physicist at Albany Medical Center at the time. In this application, the adjoint fluxes for the prostate (PTV) and the rectum and bladder (OARs) in the VIP-Man phantom were calculated on a spherical surface of approximately 1-m radius, centered at the center of gravity of PTV (Wang *et al* 2005a). An "importance" ratio, defined as the PTV dose divided by the weighted OAR doses, was calculated for each of the available beamlets to select the best beam angles. Finally, the doses in PTV and OAR were calculated using the forward Monte Carlo method. This study demonstrated the feasibility of the AMC method in optimizing external beam directions based on anatomical information in a 3D and realistic patient anatomy. The study also identified issues to be further addressed before this method could become clinically useful (Wang *et al* 2005b).

6.3.2. Non-target organ doses from proton radiation treatments—In a separate study, doctoral student Brian Wang, worked with Harald Paganetti of Massachusetts General Hospital to adopt the VIP-Man phantom to assess organ doses and the associated risk for developing secondary cancer after proton radiation treatment (Jiang *et al* 2005).

6.3.3. Respiration management in IGRT—After graduating from RPI, Chengyu Shi worked with RPI doctoral student Juying Zhang, to apply the respiration-simulating 4D VIP-Man phantom for Image-Guide Radiotherapy (IGRT) of lung cancer (Zhang *et al* 2008). To extend the geometry-based modeling to physics-based modeling, Eom *et al* (2010) introduced the use of finite element analysis to develop patient-specific phantoms that simulate respiratory motions in a predictive manner.

6.3.4. Brachytherapy dosimetry—Using the RPI Adult Female phantom, graduate student Matt Mille collaborated with Mark Rivard of Tufts University (Mille *et al* 2010) to simulate patients undergoing balloon brachytherapy of the breast. Monte Carlo simulations were performed to compare doses from treatments involving ^{192}Ir or electronic sources using Monte Carlo simulations. This work helped demonstrate that the recently developed miniature x-ray sources may offer a more optimal treatment for the patient because of the lower radiation doses received by organs and tissues far from the treatment site.

6.3.5. Imaging doses in IGRT for Radiotherapy—Mr. Jianwei Gu and workers used the VIP-Man phantom to calculate organ doses from image-guided radiation treatment (IGRT) (Gu *et al* 2008b). Two imaging procedures were considered: kV Cone Beam CT and MV Cone Beam CT. The results indicate that thyroid received the highest dose in head and neck scans for both kV and MV CBCT, and the bladder receives the highest dose in prostate scan for both kV and MV CBCT. The effective doses for H&N scan and for prostate scan are at the same level in both kV CBCT and MV CBCT. This study provided a method to compute organ doses and effective dose that are useful in treatment planning and risk

assessment. A second study performed calculations on the prostate, simulating kV CBCT and MDCT (Ding *et al* 2010). The calculations indicated that the imaging dose from standard IGRT procedures is high enough to warrant modifications to the procedure.

6.3.6. Proton Radiography—In his Ph.D. work, Bin Han collaborated with George Chen from MGH to use Monte Carlo simulations to evaluate the performance of a time-resolved proton range telescope (TRRT) (Han et al. 2011). This was done by tracking 230-MeV protons as they passed through position detectors, a patient 4DCT phantom, and scintillation detectors. The proton water equivalent length (WEL) was deduced using a reconstruction algorithm that incorporated the linear proton track to improve image quality, and three patients' 4DCT images were used to measure WEL variations and tumor motions. The results from the simulations showed that the tumor trajectories from the WEL map agreed with direct 4DCT measurements within one millimeter.

7. Discussion

It is possible that Tables 1–3 do not include all phantoms ever reported in the literature. The grouping of these phantoms into three types may not be always accurate since it was done using author supplied descriptions. Nevertheless, these tables allow us to plot and analyze the trends, as plotted in Figure 25. It can be observed that, interestingly, only a total of 38 stylized phantoms were reported in the 50 years since the phantom was first developed in the 1960s. The work on stylized phantoms peaked in the 1980s with the publication of the so-called Cristy and Eckerman stylized family phantoms (Cristy and Eckerman 1987) which were widely adopted as the de facto standard in radiation protection dosimetry. The 2nd generation voxel phantoms surfaced in the late 1980s and gradually reached the peak in the middle of 2000s with a total of 85 voxel phantoms as of 2014. In comparison, the BREP phantoms did not emerge until early 2000s and, out of the total of 287 BREP phantoms as of 2014, the majority were reported within the past several years. When data for three phantom types were shown together in Figure 25, a surprising pattern of exponential growth in research activity becomes apparent. Given the fact that the radiation protection dosimetry community relied on a dozen stylized phantoms for decades, one might have probably predicted a similar trend for voxel or BREP phantoms. In this case, we are wrong about the phantoms as we are often wrong about the general trend for technology, according to Ray Kurzweil, the author of the best-seller "The Singularity Is Near: When Humans Transcend Biology."

An important question is: Why computational phantoms have evolved the way they did? Mathematical formulations of organs and tissues of the body used in the dosimetry of internally distributed radionuclides existed as early as the 1940s, although the first anthropomorphic phantom was not reported until the 1960s. In the 1970s and 1980s, the sophistication of these stylized phantoms was increased significantly. This evolution began with the specification of a single organ mass, followed by the use of simple shapes to simulate organs or the entire body of an adult human. The desire to model the entire body of the "Reference Man" and to specify the location, shape, volume and mass of organs in the body as realistically as possible has remained the same to this day. The climax for stylized phantoms was reached in the 1980s when the gender- and age-specific family phantoms

were systematically documented (Cristy and Eckerman 1987) and widely adopted for various studies in internal and external radiation dosimetry, as well as in medical imaging and radiotherapy. By that time, Monte Carlo codes and personal computers had become accessible to a large number of researchers. I did my PhD research at Texas A&M University using two dozen PCs with Intel 486 processors and MCNP Version 3 (Reece *et al* 1994, Xu *et al* 1995, Xu *et al* 1996, Reece and Xu 1997).

The research on stylized human models at ORNL up to the 1980s played an essential role in the history of computational phantoms. The sex-specific adult phantoms at GSF in the early 1980s were revisions of the MIRD-5 phantom originally developed at ORNL. Major extensions in the 1990s, on the pregnant women and brain/head models, were also closely tied to the earlier work at ORNL. The direct involvement of ORNL's scientists in the Society of Nuclear Medicine (SNM)'s MIRD Committee facilitated the necessary standardization process. It is clear that close collaborations between leading developers were a key factor contributing to the success of first-generation computational phantoms. Not all phantoms of this generation enjoyed the same recognition in the history, however. In fact, CAM and CAF phantoms were practically unknown to people outside the NASA community for decades. The early 1990s marks the beginning of an exciting new era of voxel phantoms. With easy access to rapidly advancing computers and medical imaging technologies, computational phantom research was no longer dominated by a few groups.

The shift from stylized phantoms to voxel phantoms in the late 1980s was initially motivated by the desire to improve upon anatomical realism. The advent of modern computers and medical imaging fueled the researcher-initiated efforts. During the 1990s, however, it was unclear to the research community what roles voxel phantoms would play. If voxel phantoms were to replace stylized phantoms as the standard in radiation protection, how much improvement in dose estimates should be expected? There were already strong indications that the methods used in voxel phantoms were not ideal, as observed by Caon (2004) and Zaidi and Xu (2007). For example, the segmentation of original images into organs and tissues often required a laborious and tedious manual process, requiring months or years to complete. Some of the voxel phantoms were based on relatively large image slice thickness, thus the anatomical accuracy of such phantoms was inevitably compromised. Even today, there is no consensus as to what constitutes a faithful segmentation procedure in creating these whole-body voxel phantoms because the process often required assumption about the anatomy during the image analysis. Certain organs in the stomach and GI tract have poor image contrast and, as a result, the segmentation is nearly impossible in CT without the use of contrast agent. Then, there is also a question of how small the voxel size should be. While voxels at 2 mm × 2 mm × 2 mm seem to do a good job representing most organs, they are not fine enough for some small and radiosensitive organs to be delineated. For this reason, the skin of most existing voxel phantoms is defined artificially as the outermost voxel layer in a phantom. The segmentation of two radiosensitive tissues—the red bone marrow and bone surface that are explicitly recommended for radiation protection dose calculations—is especially difficult. Consequently, doses to the red bone marrow and bone surface are always calculated using algorithms involving other parts of the bone. It is worth noting that phantoms based on cadaver images provided an opportunity to segment the red

bone marrow explicitly. For example, Xu *et al* (2000) reported for the first time the whole-body red bone marrow distribution by harvesting color pixels of 0.33 mm × 0.33 mm resolution. Later the method was adopted in the development of several cadaver-based phantoms (Zhang *et al* 2009).

The lack of standardized procedures contributed to the current situation that although many phantoms and dosimetry data are reported, the accuracy may be impossible to compare. Voxel phantoms were realistic in depicting the anatomy, but they are also tied to a specific individual (thus conceivably not representative for a large group of people). The degree of anatomical differences between two equally realistic voxel phantoms surprised many developers who were used to the idea that a single radiation protection phantom could represent the average population. The "Reference Man" methodology required a computational phantom to match the 50th percentile values in terms of body height and weight for a specific gender and age group. From the literature review, it was found that many developers later rushed to revise the original voxel phantoms by adjusting the organ sizes in the original image data to match with the ICRP-89 recommended anatomical data. In doing so, these voxel phantoms in fact lost their individual realism — a shortcoming that was associated previously with the stylized phantoms.

It is important to note the differences between "population-averaged" prospective dosimetry needed for radiological protection under the current ICRP radiation protection system and "individualized" retrospective dosimetry needed for accident dose reconstruction, medical dose tracking, or epidemiological study[1]. The ICRP system assumes that the workers and members of the public are adequately protected as long as the organ doses and effective doses estimated for the Reference Man — a hypothetical gender-averaged adult person whose relevant anatomical and physiological parameters are at the 50th percentile of the population defined by ICRP 89 — are kept below the ICRP dose limits. In other words, the ICRP system of radiological protection does not require the assessment of the "real dose" to every exposed person. To follow ICRP recommendations for radiation protection dosimetry, one would need to (1) assess external exposures (e.g., by measuring quantities that can be related to a physical quantity such as fluence) and internal intakes (e.g., by performing bioassay for the amount of radioactivity inside the body) and then (2) convert these quantifies using ICRP reference dose coefficients (e.g., effective dose per fluence or per Bq inhaled) to yield estimates of organ dose or effective dose (ICRP 2007). Similarly, the use of a personnel dosimeter would require the comparison of the "deep dose equivalent" measured at 1-cm in tissue equivalent materials with "effective dose". These dose coefficients, but design, should be calculated using only ICRP Computational Phantoms (e.g., 50th percentile reference phantoms) and reference biokinetic models (ICRP 2009). This means that non-reference phantoms reported in this review article should not be used to assign values of effective dose according to the design of the ICRP radiation protection system. So what is the usage of these phantoms reported in this article? To ICRP, these non-reference phantoms only helped to understand potential uncertainties in using the ICRP Computational Phantoms as the standard models. However, when the effective dose to the Reference

[1]This paragraph about the distinction between ICRP "population-averaged" prospective dosimetry and "individualized" retrospective dosimetry is based on extensive discussion with Prof Wesley Bolch.

Worker is deemed to be high compared to the dose limits such as in the case of an accident or in the case of assessing the dose-response functions during an epidemiological study, one should be encouraged to assess the actual and true organ doses to the exposed individual. At this point, any individual-specific computational phantoms representing an individual of both genders at different ages, heights, and weights can and should be used. Similarly, the ICRP radiation protection system does not apply to medical radiation exposures. A good example is the need to report CT doses to patients who are not subjected to the ICRP occupational dose limits. In that and other potential medical dosimetry applications, the researcher is no longer obligated to restrict their calculation to ICRP Computational Phantoms or reference biokinetic models. In fact, non-reference families of phantoms have been used for CT dose reporting (see www.virtualphantoms.com). Therefore, many voxel and BREP phantoms covered in this article are ideally suited for this type of "individualized" retrospective applications that benefit from person-specific information in the calculations.

Looking into the future, is it necessary or feasible to bring about a change in the ICRP radiation protection concept described above? If so, how should the research community participate? The BREP phantoms have demonstrated the feasibility to develop new-generation phantoms that represent a much broader range of individuals in terms of body height and weight, as well as organ topology—features that were impossible even 10 years ago. So, should we move beyond the "Reference Man" paradigm even for radiation protection purposes? Why cannot we adopt a method that quantifies "uncertainty" in every dose calculation using a range of phantoms? There is no doubt that we are at crossroads now, perhaps as we were 20 years ago when voxel phantoms were about to emerge. The diversity of computational human phantoms developed by various groups within the community reflects the true variations amongst people and, ultimately, the true underlying uncertainty in radiation dose estimates.

This review also revealed a human factor that we do not normally see in the scientific discourse. In the history of voxel phantom development, Zubal was one of the first to share the original image data freely with other users based on a mutual agreement. Heated debate continued for some time at workshops regarding the intellectual property associated with phantoms that are revised by phantom users. It is often a technical necessity for a researcher to name a phantom created by him or her. However, it is not clear who should own such a copyright because each of the four steps of developing a phantom can be carried out by a different group. One scenario is when the original images were acquired and segmented by one individual and a different individual performed additional image processing and modification before implementing the data into a specific Monte Carlo code. Such changes produce a practically unique phantom, and proper naming is often useful for research purposes, even though individuals involved in the process do not seem to always agree upon the ownership of such a product. Some have chosen not to share phantoms partially due to this concern. Others are afraid that sharing may cost an advantage in research in a time when too many voxel phantoms exist.

The history of computational phantom development has shown that it is the need for applications, not the need for policy-making, that determines the course of technological

advancement. The need for simulating organ motions for cardiac imaging, for example, resulted in the developments of MCAT phantom by Tsui *et al* (2004) using quadric and superquadric surface equations as well as more recently the NCAT models by Segars (2001) using the NURBS technology. Xu and Shi (2005) adopted "the geometry-based" respiration algorithm in the NCAT phantom for radiation treatment. Later Eom *et al* (2009) developed a "physics-based" respiration-simulating 4D phantoms for the need to understand and "predict" the effects of respiration on radiation treatment. Using the same approach, Lee *et al* (2007) developed the size-adjustable pediatric models. The BREP-based pregnant females by Xu *et al* (2007) and those by Stabin *et al* (2008) are also examples of application-driven research that will likely continue to dominate the research horizon in the future.

As shown in Figure 25, the BREP-based phantoms are clearly going to be the future. NURBS geometries are flexible and computationally efficient, but fine details may be lost on certain organs that have complex topology. On the other hand, polygonal models can be used to create very smooth surfaces with impressive anatomical detail by paying the price of having too many vertices. Geometrical modeling of the human body is a challenge for that it consists of organ surfaces of complex and unique shapes. For cardiac and respiratory motions at the frequency range of 10–100 cycles per second, the mesh models may still be acceptable. However, previous work has also shown that the NURBS primitives were easy to adopt for both real-time and non-real-time applications. Therefore, the specific strategy will likely be based on the applications and user preference. Regardless of the specific BREP data structure, there is currently an urgent need for application-based software that can streamline the process.

Looking forward, the following issues should be addressed by the research community in the next 5–10 years:

(1) Intercomparison of ICRP-89 compatible phantoms

More than a dozen groups worldwide have developed anatomically realistic and ICRP-89 compatible phantoms. However, organ locations and shapes differ from phantom to phantom. In particular, the dosimetric differences between these phantoms — some of which represent Asian populations instead of Caucasians —and the ICRP Reference Computational Phantoms are not well understood. What is needed is a systematic intercomparison of these phantoms and quantification of dosimetric differences related to variations in organ topology.

(2) A shift away from the Reference Man-based paradigm in radiation protection

Research on radiation protection phantoms has been influenced by the "Reference Man" paradigm. This approach required a computational phantom to match the 50^{th} percentile population-average values in terms of body height and weight. However, anatomical variations associated with body size and organ shape can cause as much as 100% difference in the estimated organ doses. So the use of ICRP Reference Computational Phantoms carries a very large uncertainty. Future radiation protection systems may require this uncertainty to be quantified and reduced (say, to a level of 30% or less). To achieve that future goal, a shift away from the ICRP "Reference Man" methodology must take place by expanding the 50^{th}-

percentile phantoms into a much larger set of phantoms ranging from the 10th percentile to the 90th percentile, as well as people who are overweight, in each of the gender and age groups. Anthropometric data from population surveys can be used to evaluate trends in body and organ distributions. Both body weight index and trunk height can be used to match a specific individual with this expanded library of reference phantoms. Such phantoms are already used today for retrospective patient dose tracking and accidental dose reconstruction. It is anticipated that ICRP will begin to consider adopting such phantoms for prospective dosimetry in the future.

(3) Physics-based methods for deformation modeling

Motion-simulating 4D computational phantoms will play an increasingly vital role in the understanding and management of organ motion in radiotherapy and medical imaging. Work has been done to model cardiac and respiratory motions using BREP-based methods. These phantoms contain patient-specific imaging data such as 4D CT and therefore provide a realistic simulation of the motion. A limitation to these models is that they provide only one realization of the motion, specifically that observed in the patient images. They do not have the ability to realistically predict motion variations that may occur inside the same individual. To model variations in motion, one would require accurate handling of the interactions at the organ interfaces. Finite element analysis methods have the advantage of being physics-based and can be used in single- and multiple-organ deformable registration. Furthermore, internal dose models are currently based on a static 3D lung anatomy. Phantoms that account for aerodynamic flow of radioactive particulates in various parts of a deformable respiratory system will be developed in the next decade.

(4) Monte Carlo simulations with advanced geometries

Monte Carlo codes for radiation transport simulations were originally designed for nuclear engineering and high-energy physics applications. Although these codes contain excellent radiation physics algorithms, they suffer from poor software engineering design and are only able to handle simple geometries. These deficiencies have resulted in three problems that compromise current efforts in phantom research: (1) The implementation of various anatomically complex phantoms in these codes requires cumbersome manual processes. (2) Currently the NURBS-based or mesh-based phantoms must be converted to voxels before using with Monte Carlo programs (but a few groups have begun to address this issue as discussed earlier in this article). (3) Existing Monte Carlo codes are unable to handle a “moving” target such as the dynamic heart or lung. Research to convert an object defined in CAD software to those acceptable by a Monte Carlo code has been on-going in the nuclear engineering community for years. Future research is needed to develop new and computationally efficient ray-tracing algorithms that can directly process NURBS- and mesh-based geometric objects for Monte Carlo radiation transport calculations. Open-source Monte Carlo codes will be widely adopted in the next decade. With new technologies such as cloud-computing and hardware accelerated Monte Carlo methods involving the GPUs and coprocessors, one expects that dose calculation involving a whole-body voxel and BREP phantom can be carried out in seconds in the near future (for examples, see our own work by Liu *et al* 2014 and Su *et al* 2014). Such near-real-time Monte Carlo methods will likely

further increase the rate of computational phantom research toward the 4th generation of "patient-specific" phantoms.

8. Conclusion

A paper which appeared in 2000 on the VIP-Man phantom predicted that the advantages afforded by both the voxels and BREP-type of surface geometries would be eventually combined (Xu *et al* 2000):

> "*For the purposes of setting radiation protection standards, it may be possible to eventually bridge these two types of models, leading to a new generation of hybrid "standard" model(s) that will be acceptable to the radiation protection community. Such a new generation of models for radiation protection should be realistic enough to accurately represent major radiosensitive tissues and organs, and flexible enough to represent different populations by scaling. Computers are going to be so powerful that very complex models can be handled without a problem*."

These so-called "hybrid" computational phantoms were indeed realized in less than a decade as shown in Figure 25. In the next 10 years and beyond, advances in computational phantom research will be once again exponential. Increasingly personalized whole-body computational phantoms will be developed and applied for various clinical applications. Such phantoms will contain deformable anatomies that are physics-based and are, therefore, biomechanically realistic in depicting real-time and multi-organ deformation associated with cardiac and respiratory motions. These phantoms will also possess physiological and functional information of the human body at the organ and cellular levels obtained from multiple scanners. Breakthroughs in computational radiobiology, in the context of cancer radiotherapy, are expected to bring a new horizon to the personalized radiation medicine by understanding and harnessing the massive power of genomic data. At the same time, the power of computers will reach the exascale by the end of 2020s owing to highly efficient hardware designs (such as NVIDIA GPUs and INTEL coprocessors), thus making real-time Monte Carlo calculations for next-generation computational phantoms possible. The 50-year history reviewed in this article shows clearly that coordinated and cooperative efforts among radiological engineers, computer scientists, biologists, and clinicians will always be the key to the success of future research endeavors.

Supplementary Material

Refer to Web version on PubMed Central for supplementary material.

Acknowledgments

This article benefitted from discussions in the past decade with many colleagues, especially Keith Eckerman, John Poston, Dan Reece, Wes Bolch, Mike Stabin, Randy Brill, Paul Segars, Ben Tsui, Harald Paganetti, Mike McNitt-Gray, George Zubal, Maria Zankl, Nina Petoussi-Henss, Richard Kramer, Qian Liu, Junli Li, Chan Kim, and Habib Zaidi. This article adopted several chapters of the *Handbook of Anatomical Models For Radiation Dosimetry for which I was a co-editor*. RPI research activities highlighted in the article were based on the following Ph.D. or M.S. projects (the year of graduation indicated): Ahmet Bozkurt (2000), TC Ephraim Chao (2001), Chengyu Shi (2004), Mark Winslow, (2005), Brian Wang (2005), Peter Caracappa (2006), Bryan Bednarz (2008), Juying Zhang (2009), Yong Hum Na (2009), Jianwei Gu (2010), Bin Han (2011), Aiping Ding (2012), Matthew Mille (2013), and Justin Vazquez (2013). Grants Funding for these projects include: National Science Foundation (BES-9875532), National

Library of Medicine (R03LM007964, R01LM009362, and R01LM009362-03S1), National Cancer Institute (R01CA116743 and R42CA115122), National Institute of Biomedical Imaging and Bioengineering (R42EB010404), and National Institute of Standards and Technology (70NANB9H9198). Several RPI students and postdoc researchers helped me with the preparation and submission of this article: Xining Du, Michael Pinkert, Ashley Rhodes, Tianyu Liu, Haikuan Liu, and Matthew Mille.

References

Akkurt H, Bekar KB, Eckerman KF. VOXMAT: Phantom model with combination of voxel and mathematical geometry. Health Phys. 2008; 95(1):S100.

Alderson SW, Lanzl LH, Rollins M, Spira J. An instrumented phantom system for analog computation of treatment plans. Am. J. Roentgenol. Radium. Ther. Nucl. Med. 1962; 87:185–195.

Allison J, et al. Geant4 developments and applications. IEEE Trans. Nucl. Sci. 2006; 53:270–278.

Alziar I, et al. Individual radiation therapy patient whole-body phantoms for peripheral dose evaluations: method and specific software. Phys. Med. Biol. 2009; 54:N375–N383. [PubMed: 19652292]

Andreo P. Monte Carlo techniques in medical radiation physics. Phys. Med. Biol. 1991; 36:861–920. [PubMed: 1886926]

Attix, FH. Introduction to Radiological Physics and Radiation Dosimetry. New York, NY: John Wiley & Sons, Inc.; 1986.

Bahadori AA, Johnson PB, Jokisch DW, Eckerman KF, Bolch WE. Response functions for computing absorbed dose to skeletal tissues from neutron irradiation. Phys. Med. Biol. 2011; 56:6873–6897. [PubMed: 21983525]

Bahadori AA, Van Baalen M, Shavers MR, Dodge C, Semones EJ, Bolch WE. The effect of anatomical modeling on space radiation dose estimates: A comparison of doses for NASA phantoms and the 5th, 50th, and 95th percentile male and female astronauts. Phys. Med. Biol. 2011; 56:1671–1694. [PubMed: 21346276]

Battistoni G, Cerutti F, Fassò A, Ferrari A, Muraroi S, Ranft J, Roesler S, Sala PR. The FLUKA code: Description and benchmarking. AIP Conf. Proc. 2007; 896:31–49.

Beck P, et al. MATSIM: Development of a voxel model of the MATROSHKA astronaut dosimetric phantom. IEEE Trans. Nuc. Sci. 2011; 58:1921–1926.

Becker J, Zankl M, Petoussi-Henss N. A software tool for modification of human voxel models used for application in radiation protection. Phys. Med. Biol. 2007; 52:N195–N205. [PubMed: 17440236]

Bento J, Barros S, Teles P, Neves M, Gonçalves I, Corisco J, Vaz P. Monte Carlo simulation of the movement and detection efficiency of a whole-body counting system using a BOMAB phantom. Radiat. Prot. Dosimetry. 2012; 148:403–413. [PubMed: 21525044]

Bhati S, Patni HK, Ghare VP, Singh IS, Nadar MY. Monte Carlo calculations for efficiency calibration of a whole-body monitor using BOMAB phantoms of different sizes. Radiat. Prot. Dosimetry. 2012; 148:414–419. [PubMed: 21531750]

Billings, MP.; Yucker, WR. The Computerized Anatomical Man (CAM) model. Houston, TX: National Aeronautics and Space Administration; 1973. NASA CR-134043

Bolch W, Lee C, Wayson M, Johnson P. Hybrid computational phantoms for medical dose reconstruction. Radiat Environ Biophys. 2010; 49(2):155–168. [PubMed: 20039051]

Bouchet LG, Bolch WE, Weber DA, Atkins HL, Poston JW Sr. A revised dosimetric model of the adult head and brain. J. Nucl. Med. 1996; 37:1226–1236. [PubMed: 8965203]

Bouchet LG, Bolch WE, Weber DA, Atkins HL, Poston JW Sr. MIRD Pamphlet No. 15: Radionuclide S values in a revised dosimetric model of the adult head and brain. J. Nucl. Med. 1999; 40:62S–101S. [PubMed: 10086719]

Bouchet LG, Bolch WE, Blanco HP, Rajon DA, Clairand I, Sgouros G, Wessels BW. MIRD Pamphlet No. 19: Absorbed fractions and radionuclide S values for six age-dependent multi-region models of the kidney. J. Nucl Med. 2003; 44(7):1113–1147. [PubMed: 12843230]

Bozkurt A, Chao TC, Xu XG. Fluence-to-dose conversion coefficients from monoenergetic neutron beams below 20 MeV based on the VIP-Man anatomical model. Phys. Med. Biol. 2000; 45:3059–3079. [PubMed: 11049188]

Bozkurt A, Chao TC, Xu XG. Fluence-to-dose conversion coefficients based on the VIP-Man anatomical model and MCNPX code for monoenergetic neutrons above 20 MeV. Health Phys. 2001; 81:184–202. [PubMed: 11480876]

Bozkurt A, Xu XG. Fluence-to-dose conversion coefficients for monoenergetic proton beams based on the VIP-Man anatomical model. Radiat. Prot. Dosimetry. 2004; 112:219–235. [PubMed: 15304668]

Bozkurt A, Bor D. Simultaneous determination of equivalent dose to organs and tissues of the patient and of the physician in interventional radiology using the Monte Carlo method. Phys. Med. Biol. 2007; 52:317–330. [PubMed: 17202617]

Broggio D, Beurrier J, Bremaud M, Desbrée A, Farah J, Huet C, Franck D. Construction of an extended library of adult male 3D models: rationale and results. Phys. Med. Biol. 2011; 56:7659–7692. [PubMed: 22086354]

Brown, FB., editor. Report LA-UR-03-1987. Los Alamos, NM: Los Alamos National Laboratory; 2003. MCNP—A general Monte Carlo N-Particle transport code, version 5.

Caon M, Bibbo G, Pattison J. Monte Carlo calculated effective dose to teenage girls from computed tomography examinations. Radiat. Prot. Dosimetry. 2000; 90:445–448.

Caon M. Voxel-based computational models of real human anatomy: A review. Radiat. Environ. Biophys. 2004; 42:229–235. [PubMed: 14730450]

Caon M, Bibbo G, Pattison J. An EGS4-ready tomographic computational model of a 14-year-old female torso for calculating organ doses from CT examinations. Phys. Med. Biol. 1999; 44:2213–2225. [PubMed: 10495116]

Caracappa, PF. Ph.D. Dissertation. Troy, NY: Rensselaer Polytechnic Institute; 2006. Development and evaluation of a new algorithm for determining radiation dose to the red bone marrow.

Caracappa PF, Chao TCE, Xu XG. A study of predicted bone marrow distribution on calculated marrow dose from external radiation exposures using two sets of image data for the same individual. Health Phys. 2009; 96:661–674. [PubMed: 19430219]

Cassola VF, Lima VJM, Kramer R, Khoury HJ. FASH and MASH: Female and male adult human phantoms based on polygon mesh surfaces: I. Development of the anatomy. Phys. Med. Biol. 2010; 55:133–162. [PubMed: 20009183]

Cassola VF, Milian FM, Kramer R, de Oliveira Lira CAB, Khoury HJ. Standing adult human phantoms based on 10th, 50th and 90th mass and height percentiles of male and female Caucasian populations. Phys. Med. Biol. 2011; 56:3749–3772. [PubMed: 21628776]

CCHP. Tomographic models for radiation protection dosimetry session in The Monte Carlo Method: Versatility Unbounded in a Dynamic Computing World; Proceedings of the Monte Carlo 2005 Topical Meeting held in Chattanooga; April 17–21; TN. LaGrange, Park IL: American Nuclear Society; 2005. on CD-ROM (ISBN:0-89448-695-0)

Cech R, Leitgeb N, Pediaditis M. Current densities in a pregnant woman model induced by simultaneous ELF electric and magnetic field exposure. Phys. Med. Biol. 2008; 53:177–186. [PubMed: 18182695]

Cech R, Leitgeb N, Pediaditis M. Fetal exposure to low frequency electric and magnetic fields. Phys. Med. Biol. 2007; 52:879–888. [PubMed: 17264358]

Chao TC, Bozkurt A, Xu XG. Conversion coefficients based on the VIP-Man anatomical model and EGS4-VLSI code for external monoenergetic photons from 10 keV to 10 MeV. Health Phys. 2001; 81:163–183. [PubMed: 11480875]

Chao TC, Bozkurt A, Xu XG. Organ dose conversion coefficients for 0.1–10 MeV electrons calculated for the VIP-Man tomographic model. Health Phys. 2001; 81:203–214. [PubMed: 11480877]

Chao TC, Xu XG. Specific absorbed fractions from the image-based VIP-Man body model and EGS4-VLSI Monte Carlo code: Internal electron emitters. Phys. Med. Biol. 2001; 46:901–927. [PubMed: 11324968]

Chao TC, Bozkurt A, Xu XG. (correction) Conversion coefficients based on the VIP-Man anatomical model and EGS4-VLSI code for external monoenergetic photons from 10 keV to 10 MeV. Health Phys. 2003; 84(3):390.

Chao TC, Xu XG. S-values calculated from a tomographic head/brain model for brain imaging. Phys. Med. Biol. 2004; 49:4971–4984. [PubMed: 15584531]

Chen J. Mathematical models of the embryo and fetus for use in radiological protection. Health Phys. 2004; 86:285–295. [PubMed: 14982229]

Choi SH, Lee C-S, Cho SK, Chung MS, Na SH, Kim CH. Construction of a high-definition 'Reference Korean' voxel phantom for organ and tissue radiation dose calculation. IFMBE Proc. 2006; 14:4204–4207.

Christ A, et al. The Virtual Family—development of surface-based anatomical models of two adults and two children for dosimetric simulations. Phys. Med. Biol. 2010; 55:N23–N38. [PubMed: 20019402]

CIRS. [last access 02/27/2014] Tissue Simulation and Phantom Technology. 2013. http://www.cirsinc.com

CMPWG. [last access 02/27/2014] Phantoms. 2013. http://cmpwg.ans.org/phantoms/camera.pdf

Courageot E, Huet C, Clairand I, Bottollier-Depois JF, Gourmelon P. Numerical dosimetric reconstruction of a radiological accident in South America in April 2009. Radiat. Prot. Dosimetry. 2011; 144:540–542. [PubMed: 21051432]

Courageot E, Sayah R, Huet C. Development of modified voxel phantoms for the numerical dosimetric reconstruction of radiological accidents involving external sources: Implementation in SESAME tool. Phys. Med. Biol. 2010; 55:N231–N241. [PubMed: 20371912]

Cristy, M. Mathematical phantoms representing children of various ages for use in estimates of internal dose. Oak Ridge, TN: Oak Ridge National Laboratory; 1980. U.S. Nuclear Regulatory Commission Report NUREG/CR-1159 http://web.ornl.gov/info/reports/1980/3445605812234.pdf [last access 02/27/2014]

Cristy, M.; Eckerman, KF. Specific absorbed fractions of energy at various ages from internal photon sources I: Methods. Oak Ridge, TN: Oak Ridge National Laboratory; 1987. Oak Ridge National Laboratory Report ORNL/TM-8381/V1 http://ordose.ornl.gov/documents/tm8381V1.pdf [last access 02/27/2014]

Dawson TW, Caputa K, Stuchly MA. A comparison of 60 Hz uniform magnetic and electric induction in the human body. Phys. Med. Biol. 1997; 42:2319–2329. [PubMed: 9434290]

Deus, SF.; Poston, JW. Proceedings of the Symposium on Radiopharmaceutical Dosimetry. Rockville, MD: U.S. Food and Drug Administration; 1976. The development of a mathematical phantom representing a 10-year-old for use in internal dose calculations. HEW Publication 76-8044

DeWerd, LA.; Kissick, M. The Phantoms of Medical and Health Physics. , editor. Berlin, Germany: Springer; 2014.

Dimbylow P. Development of pregnant female, hybrid voxel-mathematical models and their application to the dosimetry of applied magnetic and electric fields at 50 Hz. Phys. Med. Biol. 2006; 51:2383–2394. [PubMed: 16675859]

Dimbylow P. Development of the female voxel phantom, NAOMI, and its application to calculations of induced current densities and electric fields from applied low frequency magnetic and electric fields. Phys. Med. Biol. 2005a; 50:1047–1070. [PubMed: 15798308]

Dimbylow P. Resonance behaviour of whole-body averaged specific energy absorption rate (SAR) in the female voxel model, NAOMI. Phys. Med. Biol. 2005b; 50:4053–4063. [PubMed: 16177529]

Dimbylow, PJ. Proc. Workshop on Voxel Phantom Development. Chilton, UK: 1996. The development of realistic voxel phantoms for electromagnetic field dosimetry.

Dimbylow PJ. FDTD calculations of the whole-body averaged SAR in an anatomically realistic voxel model of the human body from 1 MHz to 1 GHz. Phys. Med. Biol. 1997; 42:479–490. [PubMed: 9080530]

Dimbylow P, Bolch W, Lee C. SAR calculations from 20 MHz to 6 GHz in the University of Florida newborn voxel phantom and their implications for dosimetry. Phys. Med. Biol. 2010; 55:1519–1530. [PubMed: 20157229]

Ding A, Gu J, Trofimov AV, Xu XG. Monte Carlo calculation of imaging doses from diagnostic multidetector CT and kilovoltage cone-beam CT as part of prostate treatment plans. Med. Phys. 2010; 37:6199–6204. [PubMed: 21302776]

Ding A, Mille MM, Liu T, Caracappa PF, Xu XG. Extension of RPI-adult male and female computational phantoms to obese patients and a Monte Carlo study on the effects on CT imaging dose. Phys. Med. Biol. 2012; 57:2441–2459. [PubMed: 22481470]

Doerfel H, Heide B. Calibration of a phoswich type partial body counter by Monte Carlo simulation of low-energy photon transport. Radiat. Prot. Dosimetry. 2007; 123:464–472. [PubMed: 17261536]

Eckerman, KF. Aspects of the dosimetry of radionuclides within the skeleton with particular emphasis on the active marrow Proc. In: Schlafke-Stelson, AT.; Watson, EE., editors. 4th Int. Radiopharmaceutical Dosimetry Symp. Oak Ridge, TN: Oak Ridge Associated Universities; 1985. p. 514-534.

Eckerman KF, Stabin MG. Electron absorbed fractions and dose conversion factors for marrow and bone by skeletal regions. Health Phys. 2000; 78:199–214. [PubMed: 10647986]

Eckerman, KF.; Poston, JW., Sr; Bolch, WE.; Xu, XG. Handbook of Anatomical Models for Radiation Dosimetry. New York, NY: Taylor & Francis; 2009. The stylized computational phantoms developed at ORNL and elsewhere; p. 43-64.

Eom J, Xu XG, De S, Shi C. Predictive modeling of lung motion over the entire respiratory cycle using measured pressure-volume data, 4DCT images, and finite element analysis. Med. Phys. 2010; 37:4389–4400. [PubMed: 20879598]

Farah J, Broggio D, Franck D. Creation and use of adjustable 3D phantoms: Application for the lung monitoring of female workers. Health Phys. 2010a; 99:649–661. [PubMed: 20938235]

Farah J, Broggio D, Franck D. Female workers and in vivo lung monitoring: A simple model for morphological dependence of counting efficiency curves. Phys. Med. Biol. 2010b; 55:7377–7395. [PubMed: 21081821]

Farah J, Broggio D, Franck D. Examples of Mesh and NURBS modelling for in vivo lung counting studies. Radiat. Prot. Dosimetry. 2011; 144:344–348. [PubMed: 21030397]

Ferrari A, Pelliccioni M, Pillon M. Fluence to effective dose and effective dose equivalent conversion coefficients for electrons from 5 MeV to 10 GeV. Radiat. Prot. Dosimetry. 1997; 69:97–104.

Ferrari P. Development of an integrated couple of anthropomorphic models for dosimetric studies. Radiat. Prot. Dosimetry. 2010; 142:191–200. [PubMed: 20696671]

Ferrari P, Gualdrini G. An improved MCNP version of the NORMAN voxel phantom for dosimetry studies. Phys. Med. Biol. 2005; 50:4299–4316. [PubMed: 16148395]

Fill UA, Zankl M, Petoussi-Henss N, Siebert M, Regulla D. Adult female voxel models of different stature and photon conversion coefficients for radiation protection. Health Phys. 2004; 86:253–272. [PubMed: 14982227]

Findlay RP, Dimbylow PJ. SAR in a child voxel phantom from exposure to wireless computer networks (Wi-Fi). Phys. Med. Biol. 2010; 55:N405–N411. [PubMed: 20647607]

Findlay RP, Dimbylow PJ. Spatial averaging of fields from half-wave dipole antennas and corresponding SAR calculations in the NORMAN human voxel model between 65 MHz and 2 GHz. Phys. Med. Biol. 2009; 54:2437–2447. [PubMed: 19336844]

Fisher, HLJ.; Snyder, WS. Health Physics Division Annual Progress Report for Period Ending July 31, 1966. Oak Ridge, TN: Oak Ridge National Laboratory; 1966. Variation of dose delivered by ^{137}Cs as a function of body size from infancy to adulthood; p. 221-228.Report ORNL-4007

Fisher, HLJ.; Snyder, WS. Health Physics Division Annual Progress report for Period Ending July 31, 1967. Oak Ridge, TN: Oak Ridge National Laboratory; 1967. Distribution of dose in the body from a source of gamma rays distributed uniformly in an organ. Report ORNL-4168

Fung GS, Segars WP, Gullberg GT, Tsui BM. Development of a model of the coronary arterial tree for the 4D XCAT phantom. Phys. Med. Biol. 2011; 56:5651–5663. [PubMed: 21828911]

Furler, M. M.S. Thesis. Troy, NY: Rensselaer Polytechnic Institute; 2007. Methods Of Converting Geometry In CAD To MCNP Code.

Gardumi A, Farah J, Desbrée A. Creation of ORNL NURBS-based phantoms: Evaluation of the voxel effect on absorbed doses from radiopharmaceuticals. Radiat. Prot. Dosimetry. 2013; 153:273–281. [PubMed: 22719045]

Geyer AM, O'Reilly S, Lee C, Long DJ, Bolch WE. The UF/NCI family of hybrid computational phantoms representing the current US population of male and female children and adolescents—applications to CT dosimetry. Phys. Med. Biol. 2014 (in press).

Gibbs SJ, Pujol A, Chen TS, Malcolm AW, James AE. Patient risk from interproximal radiography. Oral Surg. Oral Med. O. 1984; 58:347–354.

Gibbs SJ, Pujol A Jr, Chen TS, Carlton JC, Dosmann MA, Malcom AW, James AE Jr. Radiation doses to sensitive organs from intraoral dental radiography. Dentomaxillofac Radiol. 1987; 16:67–77. [PubMed: 3507322]

Gjonaj E, Bartsch M, Clemens M, Schupp S, Weiland T. High-resolution human anatomy models for advanced electromagnetic field computations. IEEE Trans. Magn. 2002; 38:357–360.

Goorley, JT., et al. Initial MCNP6 Release Overview - MCNP6 version 1.0. Los Alamos, NM: Los Alamos National Laboratory; 2013. Report LA-UR-13-22934

Gosselin M-C, et al. Development of a new generation of high-resolution anatomical models for medical device evaluation: The Virtual Population 3.0. Phys. Med. Biol. 2014 (in press).

Griffith, RV.; Dean, PN.; Anderson, AL.; Fisher, JC. Fabrication of a tissue-equivalent torso phantom for intercalibration of in-vivo transuranic-nuclide counting facilities. Proceedings of International Symposium on Advances in Radiation Protection Monitoring; International Atomic Energy Agency; Stockholm, Sweden. 1978. also as Lawrence Livermore National Laboratory Report UCRL-80343

Gu J, Dorgu A, Xu XG. Comparison of main software packages for CT dose reporting. Health Phys. 2008a; 95(1):S50.

Gu J, Bednarz B, Xu XG, Jiang SB. Assessment of patient organ doses and effective doses using the VIP-Man adult male phantom for selected cone-beam CT imaging procedures during image guided radiation therapy. Radiat. Prot. Dosimetry. 2008b; 131:431–443. [PubMed: 18667400]

Gu J, Bednarz B, Caracappa PF, Xu XG. The development, validation and application of a multi-detector CT (MDCT) scanner model for assessing organ doses to the pregnant patient and the fetus using Monte Carlo simulations. Phys. Med. Biol. 2009; 54:2699–2717. [PubMed: 19351983]

Gu, J. Ph.D. Dissertation. Troy, NY: Rensselaer Polytechnic Institute; 2010. Development of CT scanner models for patient organ dose calculations using Monte Carlo methods.

Gu S, Gupta R, Kyprianou I. Computational high-resolution heart phantoms for medical imaging and dosimetry simulations. Phys. Med. Biol. 2011; 56:5845–5864. [PubMed: 21852725]

Hammersley, JM.; Handscomb, DC. Monte Carlo Methods. London, U.K: Metheun & Co. Ltd.; 1964.

Han B, Zhang J, Na YH, Caracappa PF, Xu XG. Modeling and Monte Carlo organ dose calculations for workers walking on ground contaminated with Cs-137 and Co-60 gamma sources. Radiation Prot. Dosimetry. 2010; 141:299–304.

Han B, Xu XG, Chen GTY. Proton radiography and fluoroscopy of lung tumors: A Monte Carlo study using patient-specific 4DCT phantoms. Med. Phys. 2011; 38:1903–1911. [PubMed: 21626923]

Han MC, Kim CH, Jeong JH, Yeom YS, Kim S, Wilson PH, Apostolakis J. DagSolid: a new Geant4 solid class for fast simulation in polygon-mesh geometry. Phys. Med. Biol. 2013; 58(13):4595–4609. [PubMed: 23771063]

Hegenbart L, Na YH, Zhang JY, Urban M, Xu XG. A Monte Carlo study of lung counting efficiency for female workers of different breast sizes using deformable phantoms. Phys. Med. Biol. 2008; 53:5527–5538. [PubMed: 18780959]

Hintenlang, D.; Moloney, W.; Winslow, J. Handbook of Anatomical Models for Radiation Dosimetry. New York, NY: Taylor & Francis; 2009. Physical Phantoms for Experimental Radiation Dosimetry.

Hirata A, Ito N, Fujiwara O, Nagaoka T, Watanabe S. Conservative estimation of whole-body-averaged SARs in infants with a homogeneous and simple-shaped phantom in the GHz region. Phys. Med. Biol. 2008; 53:7215–7223. [PubMed: 19043178]

Hough M, Johnson P, Rajon D, Jokisch D, Lee C, Bolch W. An image-based skeletal dosimetry model for the ICRP reference adult male—internal electron sources. Phys. Med. Biol. 2011; 56:2309–2346. [PubMed: 21427487]

Hubbell, JH. Photon Cross Sections, Attenuation Coefficients and Energy Absorption Coefficients from 10 keV to 100 GeV. Washington, DC: National Bureau of Standards; 1969. Report NSRDS-NBS 29

Hwang, JML.; Shoup, RL.; Poston, JW. Mathematical description of a newborn human for use in dosimetry calculations. Oak Ridge, TN: Oak Ridge National Laboratory; 1976. Report ORNL/TM-5453

ICRP. Report of Committee II on Permissible Dose for Internal Radiation. Oxford, UK: Pergamon Press Ltd.; 1959.

ICRP. Report of the Task Group on Reference Man. Oxford, UK: Pergamon Press Ltd.; 1975. *ICRP Publication 23*

ICRP. Basic anatomical and physiological data for use in radiological protection reference values. Oxford, UK: Pergamon Press Ltd.; 2002a. ICRP Publication 89

ICRP. [last access 03/02/14] 2002 Annual Report of the International Commission on Radiological Protection. 2002b. http://www.icrp.org/docs/2002_ann_rep_52_429_03.pdf

ICRP. Recommendations of the International Commission on Radiological Protection. Oxford, UK: Pergamon Press Ltd.; 2007. ICRP Publication 103

ICRP. Adult reference computational phantoms. Oxford, UK: Pergamon Press Ltd.; 2009. ICRP Publication 110

ICRU. Phantoms and computational models in therapy, diagnosis and protection. Bethesda, MD: International Commission on Radiation Units and Measurements; 1992. ICRU Report 48

Jiang H, Wang B, Xu XG, Suit HD, Paganetti H. Simulation of organ-specific patient effective dose due to secondary neutrons in proton radiation treatment. Phys. Med. Biol. 2005; 50:4337–4353. [PubMed: 16148397]

Jin, W.; Lim, Y-J.; Xu, XG.; Singh, TP.; De, S. Improving the visual realism of virtual surgery. In: Westood, JD., et al., editors. Proceedings of Medicine Meets Virtual Reality 13: The Magical Next Becomes the Medical Now. Amsterdam, Netherlands: IOS Press Inc.; 2005. p. 227-233.

Johnson P, Lee C, Johnson K, Siragusa D, Bolch WE. The influence of patient size on dose conversion coefficients: A hybrid phantom study for adult cardiac catheterization. Phys. Med. Biol. 2009; 54:3613–3629. [PubMed: 19458408]

Johnson PB, Bahadori AA, Eckerman KF, Lee C, Bolch WE. Response functions for computing absorbed dose to skeletal tissues from photon irradiation – an update. Phys Med Biol. 2011; 56:2347–2366. [PubMed: 21427484]

Jones AK, Simon TA, Bolch WE, Holman MM, Hintenlang DE. Tomographic physical phantom of the newborn child with real-time dosimetry I. Methods and techniques for construction. Med. Phys. 2006; 33:3274–3282. [PubMed: 17022222]

Jones DG. A realistic anthropomorphic phantom for calculating organ doses arising from external photon irradiation. Radiat. Prot. Dosimetry. 1997; 72:21–29.

Jones, RM.; Poston, JW.; Hwang, JL.; Jones, TD.; Warner, GG. The development and use of a fifteen-year-old equivalent mathematical phantom for internal dose calculations. Oak Ridge, TN: Oak Ridge National Laboratory; 1976. Report ORNL/TM-5278

Katagiri M, Hikoji M, Kitaichi M, Sawamura S, Aoki Y. Effective dose and organ doses per unit fluence calculated for monoenergetic 0.1 MeV to 100 MeV electrons by the MIRD-5 phantom. Radiat. Prot. Dosimetry. 2000; 90(4):393–401.

Kereiakes JG, Seltzer RA, Blackburn B, Saenger EL. Radionuclide doses to infants and children: A plea for a standard child. Health Phys. 1965; 11:999–1004. [PubMed: 5867167]

Kim CH, Choi SH, Jeong JH, Lee C, Chung MS. HDRK-Man: A whole-body voxel model based on high-resolution color slice images of a Korean adult male cadaver. Phys. Med. Biol. 2008; 53:4093–4106. [PubMed: 18612173]

Kim CH, Jeong JH, Bolch WE, Cho K-W, Hwang SB. A polygon-surface reference Korean male phantom (PSRK-Man) and its direct implementation in Geant4 Monte Carlo simulation. Phys. Med. Biol. 2011; 56:3137–3161. [PubMed: 21521906]

Kim JH, Kim CS, Whang JH. Assessment of radiation dose for surrounding organs and persons approaching implanted patients upon brachytherapy of prostate cancer with Iridium-192. Radiat. Prot. Dosimetry. 2010; 141:283–288. [PubMed: 20643801]

Kim JI, Choi H, Lee BI, Lim YK, Kim CS, Lee JK, Lee C. Physical phantom of typical Korean male for radiation protection purpose. Radiat. Prot. Dosimetry. 2006; 118:131–136. [PubMed: 16410295]

Kim JS, Ha WH, Jeong JH, Cho K-W, Lee JK. Use of photographic images to construct voxel phantoms for use in whole-body counting. Radiat. Prot. Dosimetry. 2010; 138:119–122. [PubMed: 19951986]

Kramer GH, Burns L, Noel L. The BRMD BOMAB phantom family. Health Phys. 1991; 61:895–902. [PubMed: 1955336]

Kramer, R.; Zankl, M.; Williams, G.; Drexler, G. The male (ADAM) and female (EVA) adult mathematical phantoms. Neuherberg, Germany: Institut fuer Strahlenschutz, GSF-Forschungszentrum fuer Umwelt und Gesundheit; 1982. The calculation of dose from external photon exposures using reference human phantoms and Monte Carlo methods: Part I. GSF-Report S-885

Kramer R, Cassola VF, Khoury HJ, Vieira JW, Lima VJM, Brown KR. FASH and MASH: Female and male adult human phantoms based on polygon mesh surfaces: II. Dosimetric calculations. 2010; 55:163–189.

Kramer R, Khoury HJ, Vieira JW, Lima VJM. MAX06 and FAX06: Update of two adult human phantoms for radiation protection dosimetry. Phys. Med. Biol. 2006; 51:3331–3346. [PubMed: 16825733]

Kramer R, Khoury HJ, Vieira JW, Loureiro ECM, Lima VJM, Lima FRA, Hoff G. All about FAX: A Female Adult voXel phantom for Monte Carlo calculation in radiation protection dosimetry. Phys. Med. Biol. 2004; 49:5203–5216. [PubMed: 15656272]

Kramer R, Vieira JW, Khoury HJ, Lima FRA, Fuelle D. All about MAX: A male adult voxel phantom for Monte Carlo calculations in radiation protection dosimetry. Phys. Med. Biol. 2003; 48:1239–1262. [PubMed: 12812444]

Kyoto Kagaku co., LTD. [last access 02/28/14] Patient Simulators, Imaging Phantoms for Skill Training. 2013. http://www.kyotokagaku.com/

Lee C, Nagaoka T, Lee J-K. Implementation of Japanese male and female tomographic phantoms to multi-particle Monte Carlo mode for ionizing radiation dosimetry. J. Nucl. Sci. Technol. 2006; 43:937–945.

Lee B, et al. Dose evaluation of selective collimation effect in cephalography by measurement and Monte Carlo simulation. Radiat. Prot. Dosimetry. 2011; 148:58–64. [PubMed: 21335329]

Lee C, Lee C, Williams JL, Bolch WE. Whole-body voxel phantoms of paediatric patients—UF Series B. Phys. Med. Biol. 2006; 51:4649–4661. [PubMed: 16953048]

Lee C, Williams JL, Lee C, Bolch WE. The UF series of tomographic computational phantoms of pediatric patients. Med. Phys. 2005; 32:3537–3548. [PubMed: 16475752]

Lee C, Lee J, Lee C. Korean adult male voxel model KORMAN segmented from magnetic resonance images. Med. Phys. 2004; 31:1017–1022. [PubMed: 15191287]

Lee C, Lee C, Park SH, Lee JK. Development of the two Korean adult tomographic computational phantoms for organ dosimetry. Med. Phys. 2006; 33:380–390. [PubMed: 16532944]

Lee C, Lodwick D, Hasenauer D, Williams JL, Lee C, Bolch WE. Hybrid computational phantoms of the male and female newborn patient: NURBS-based whole-body models. Phys. Med. Biol. 2007; 52:3309–3333. [PubMed: 17664546]

Lee C, Lodwick D, Williams JL, Bolch WE. Hybrid computational phantoms of the 15-year male and female adolescent: Applications to CT organ dosimetry for patients of variable morphometry. Med. Phys. 2008; 35:2366–2382. [PubMed: 18649470]

Lee C, Lodwick D, Hurtado J, Pafundi D, Williams JL, Bolch WE. The UF family of reference hybrid phantoms for computational radiation dosimetry. Phys. Med. Biol. 2010; 55:339–363. [PubMed: 20019401]

Leyton, M. A Generative Theory of Shape. Berlin, Germany: Springer-Verlag; 2001.

Li J, Qiu R, Zhang Z, Liu L, Zeng Z, Bi L, Li W. Organ dose conversion coefficients for external photon irradiation using the Chinese voxel phantom (CVP). Radiat. Prot. Dosimetry. 2009; 135:33–42. [PubMed: 19457976]

Lim SM, DeNardo GL, DeNardo DA, Shen S, Yuan A, O'Donnell TO, DeNardo SJ. Prediction of myelotoxicity using radiation doses to marrow from body, blood, and marrow sources. J. Nucl. Med. 1997; 38:1374–1378. [PubMed: 9293790]

Lima VJM, Cassola VF, Kramer R, Lira CABO, Khoury HJ, Vieira JW. Development of 5- and 10-year-old pediatric phantoms based on polygon mesh surfaces. Med. Phys. 2011; 38:4723–4736. [PubMed: 21928646]

Liu T, Du X, Su L, Ji W, Carothers C, Shephard M, Liu B, Kalra MK, Brown FB, Fitzegerald P, Xu XG. ARCHER-CT, an extremely fast Monte Carlo code for patient-specific CT dose calculations using Nvidia GPU and Intel coprocessor technologies: Part I—software development and testing. Phys. Med. Biol. 2014 (submitted).

Loevinger, R.; Japha, EM.; Brownell, GL. Discrete radioisotope sources Radiation Dosimetry. Hine, GJ.; Brownell, GL., editors. New York, NY: Academic Press; 1965a. p. 693-799.

Loevinger, R.; Hiolt, JG.; Hine, GJ. Internally administered radionuclides Radiation Dosimetry. Hine, GJ.; Brownell, GL., editors. New York, NY: Academic Press; 1965b. p. 801-873.

Loevinger, R. Distributed radionuclide sources Radiation Dosimetry Volume III. 2nd Edition. Attix, FH.; Tochilin, editors. New York, NY: Academic Press; 1969. p. 51

Marinelli LD. Dosage determination with radioactive isotopes Am. J. Roentgenol. Rad. Therapy. 1942; 47:210–216.

Marinelli LD, Quimby EH, Hine GJ. Dosage determination with radioactive isotopes II. Practical considerations in therapy and protection. Am. J. Roentgenol. Rad. Therapy. 1948; 59:260–281.

Mason, PA.; Ziriax, JM.; Hurt, WD.; Walters, TJ.; Ryan, KL.; Nelson, DA.; Smith, KI.; D'andrea, JA. Recent advancements in dosimetry measurements and modeling. In: Klauenberg, BJ.; Miklavčič, D., editors. Radio Frequency Radiation Dosimetry and Its Relationship to the Biological Effects of Electromagnetic Fields. Dordrecht, Netherlands: Kluwer Academic Publishers; 2000. p. 141-155.

Maynard MR, Geyer JW, Aris JP, Shifrin RY, Bolch W. The UF family of hybrid phantoms of the developing human fetus for computational radiation dosimetry. Phys. Med. Biol. 2011; 56:4839–4879. [PubMed: 21765203]

Mazzurana M, Sandrini L, Vaccari A, Malacarne C, Cristoforetti L, Pontalti R. A semi-automatic method for developing an anthropomorphic numerical model of dielectric anatomy by MRI. Phys. Med. Biol. 2003; 48:3157–3170. [PubMed: 14579858]

McGurk R, Seco J, Riboldi M, Wolfgang J, Segars P, Paganetti H. Extension of the NCAT phantom for the investigation of intra-fraction respiratory motion in IMRT using 4D Monte Carlo. Phys. Med. Biol. 2010; 55:1475–1490. [PubMed: 20157230]

Mille M, Xu XG. Fabrication of Human Organs for Realistic Calibration Phantoms by Rapid Prototyping. Health Phys. 2008; 95(1):S11.

Mille M, Xu XG, Rivard M. Comparison of organ doses for patients undergoing balloon brachytherapy of the breast with HDR ^{192}Ir or electronic sources using Monte Carlo simulations in a heterogeneous human phantom. Med. Phys. 2010; 37:662–671. [PubMed: 20229875]

Mille, M. Ph.D. Dissertation. Troy, NY: Rensselaer Polytechnic Institute; 2013. A study of shape-dependent partial volume correction in PET imaging using ellipsoidal phantoms fabricated via rapid prototyping.

Mishra P, Li R, James SS, Mak RH, Williams CL, Yue Y, Berbeco RI, Lewis JH. Evaluation of 3D fluoroscopic image generation from a single planar treatment image on patient data with a modified XCAT phantom. Phys. Med. Biol. 2013; 58:841–858. [PubMed: 23337614]

Mofrad FB, Zoroofi RA, Tehrani-Fard AA, Akhlahpoor S, Hori M, Chen YW, Sato Y. Statistical construction of a Japanese male liver phantom for internal radionuclide dosimetry. Radiat. Prot. Dosimetry. 2010; 141:140–148. [PubMed: 20562118]

Moignier A, Derreumaux S, Broggio D, Beurrier J, Chea M, Boisserie G, Franck D, Aubert B, Mazeron JJ. Potential of hybrid computational phantoms for retrospective heart dosimetry after breast radiation therapy: A feasibility study. Int. J. Radiat. Oncol. Biol. Phys. 2013; 85:492–499. [PubMed: 22608886]

Na YH, Zhang B, Zhang JY, Caracappa PF, Xu XG. Deformable adult human phantoms for radiation protection dosimetry: Anthropometric data representing size distributions of adult worker

populations and software algorithms. Phys. Med. Biol. 2010; 55:3789–3811. [PubMed: 20551505]

Na, YH. Ph.D. Dissertation. Troy, NY: Rensselaer Polytechnic Institute; 2009. Deformable adult human phantoms for radiation protection dosimetry: methods for adjusting body and organ sizes to match population-based percentile data.

Nagaoka T, Togashi T, Saito K, Takahashi M, Ito K, Ueda T, Osada H, Ito H, Watanabe S. An anatomically realistic voxel model of the pregnant woman and numerical dosimetry for a whole-body exposure to RF electromagnetic fields. Conf. Proc. IEEE Eng. Med. Biol. Soc. 2006; 1:5463–5467. [PubMed: 17946307]

Nagaoka T, Kunieda E, Watanabe S. Proportion-corrected scaled voxel models for Japanese children and their application to the numerical dosimetry of specific absorption rate for frequencies from 30 MHz to 3 GHz. Phys. Med. Biol. 2008; 53:6695–6711. [PubMed: 18997264]

Nagaoka T, Togashi T, Saito K, Takahashi M, Ito K, Watanabe S. An anatomically realistic whole-body pregnant-woman model and specific absorption rates for pregnant-woman exposure to electromagnetic plane waves from 10 MHz to 2 GHz. Phys. Med. Biol. 2007; 52:6731–6745. [PubMed: 17975294]

Nagaoka T, Watanabe S, Sakurai K, Kunieda E, Watanabe S, Taki M, Yamanaka Y. Development of realistic high-resolution whole-body voxel models of Japanese adult males and females of average height and weight, and application of models to radio-frequency electromagnetic-field dosimetry. Phys. Med. Biol. 2004; 49:1–15. [PubMed: 14971769]

NCRP. The experimental basis for absorbed-dose calculations in medical uses of radionuclides. Besthesda, MD: National Council on Radiation Protection and Measurements; 1985. NCRP Report No. 83

Nipper JC, Williams JL, Bolch WE. Creation of two tomographic voxel models of paediatric patients in the first year of life. Phys. Med. Biol. 2002; 47:3143–3164. [PubMed: 12361215]

Niu X, Yang Y, Jin M, Wernick MN, King MA. Regularized fully 5D reconstruction of cardiac gated dynamic SPECT images. IEEE Trans. Nucl. Sci. 2010; 57:1085–1095. [PubMed: 24049191]

NRC. [last access 03/02/14] EGSnrc. 2013. http://irs.inms.nrc.ca/software/egsnrc/

Pafundi D, Lee C, Watchman C, Bourke V, Aris J, Shagina N, Harrison J, Fell T, Bolch W. An image-based skeletal tissue model for the ICRP reference newborn. Phys. Med. Biol. 2009; 54:4497–4531. [PubMed: 19556686]

Pafundi D, Rajon D, Jokisch D, Lee C, Bolch W. An image-based skeletal dosimetry model for the ICRP reference newborn—internal electron sources. Phys. Med. Biol. 2010; 55:1785–1814. [PubMed: 20208096]

Park S, Lee JK, Lee C. Development of a Korean adult male computational phantom for internal dosimetry calculation. Radiat. Prot. Dosimetry. 2006; 121:257–264. [PubMed: 16632585]

Patni HK, Nadar MY, Akar DK, Bhati S, Sarkar PK. Selected organ dose conversion coefficients for external photons calculated using ICRP adult voxel phantoms and Monte Carlo code Fluka. Radiat. Prot. Dosimetry. 2011; 147:406–416. [PubMed: 21147784]

Pelowitz, DB., editor. MCNPX User's Manual Version 2.5.0. Los Alamos, NM: Los Alamos National Laboratory; 2005. Report LA-CP-05-0369

Petoussi-Henss N, Zankl M, Fill U, Regulla D. The GSF family of voxel phantoms. Phys. Med. Biol. 2002; 47:89–106. [PubMed: 11814230]

Phantom Laboratory. [last access 03/02/14] RANDO Phantoms. 2013. http://www.phantomlab.com/rando.html

Pretorius PH, Xia W, King MA, Tsui BM, Pan TS, Villegas BJ. Evaluation of right and left ventricular volume and ejection fraction using a mathematical cardiac torso phantom. J. Nucl. Med. 1997; 38:1528–1535. [PubMed: 9379187]

Pretorius PH, King MA, Tsui BM, LaCroix KJ, Xia W. A mathematical model of motion of the heart for use in generating source and attenuation maps for simulating emission imaging. Med. Phys. 1999; 26:2323–2332. [PubMed: 10587213]

Pujol A, Gibbs SJ. A Monte Carlo method for patient dosimetry from dental x-ray. Dentomaxillofac Radiol. 1982; 11:25–33. [PubMed: 6954117]

Qiu R, Li J, Zhang Z, Wu Z, Zeng Z, Fan J. Photon SAF calculation based on the Chinese mathematical phantom and comparison with the ORNL phantoms. Health Phys. 2008; 95:716–724. [PubMed: 19001898]

Quimby, EH. The development of radiation dosimetry in nuclear medicine. In: Cloutier, RJ.; Edwards, CL.; Snyder, WS., editors. Medical Radionuclides: Radiation Dose and Effects; Proceedings of AEC Symposium Series 20 (CONF-691212); Washington, DC: U.S. Atomic Energy Commission; 1970. p. 7-15.

Raeside DE. Monte Carlo principles and applications. Phys. Med. Biol. 1976; 21:181–197. [PubMed: 768998]

Reece WD, Poston JW Sr, Xu XG. Determining the effective dose equivalent for external photon radiation: Calculational results for beam and point source geometries. Radiat. Prot. Dosimetry. 1994; 55:5–21.

Reece WD, Xu XG. Determining the effective dose equivalent for external photon radiation: Assessing effective dose equivalent from personal dosemeter readings. Radiat. Prot. Dosimetry. 1997; 69:167–178.

Rogers DW. Fifty years of Monte Carlo simulations for medical physics. Phys. Med Biol. 2006; 51:R287–R301. [PubMed: 16790908]

Sachse, FB., et al. MEET Man–Models for Simulation of Electromagnetic, Elastomechanic and Thermic Behavior of Man. Karlsruhe, Germany: Universität Karlsruhe; 1997. available online http://www.ibt.kit.edu/english/973.php [last access 03/02/14]

Saito K, Wittmann A, Koga S, Ida Y, Kamei T, Funabiki J, Zankl M. Construction of a computed tomographic phantom for a Japanese male adult and dose calculation system. Radiat. Environ. Biophys. 2001; 40:69–75. [PubMed: 11357713]

Saito K, Koga S, Ida Y, Kamei T, Funabiki J. Construction of a voxel phantom based on CT data for a Japanese female adult and its use for calculation of organ doses from external electrons. Jpn. J. Health Phys. 2008; 43:122–130.

Salvat, F.; Fernández-Varea, JM.; Sempau, J. [last access 03/02/14] PENELOPE—A code system for Monte Carlo simulation of electron and photon transport. 2003. ISBN: 92-64-02145-0, available online http://www2.cose.isu.edu/~tforest/Classes/NucSim/penelope-2003.pdf

Sato K, Noguchi H, Emoto Y, Koga S, Saito K. Japanese adult male voxel phantom constructed on the basis of CT images. Radiat. Prot. Dosimetry. 2007; 123:337–344. [PubMed: 16905760]

Sato K, Noguchi H, Endo A, Emoto Y, Koga S, Saito K. Development of a voxel phantom of Japanese adult male in upright posture. Radiat. Prot. Dosimetry. 2007; 127:205–208. [PubMed: 17553860]

Sato K, Noguchi H, Emoto Y, Koga S, Saito K. Development of a Japanese adult female voxel phantom. J. Nucl. Sci. Technol. 2009; 46:907–913.

Schlattl H, Zankl M, Petoussi-Henss N. Organ dose conversion coefficients for voxel models of the reference male and female from idealized photon exposures. Phys. Med. Biol. 2007; 52:2123–2145. [PubMed: 17404459]

Schultz FW, Zoetelief J. Organ and effective doses in the male phantom Adam exposed in AP direction to broad unidirectional beams of monoenergetic electrons. Health Phys. 1996; 70:498–504. [PubMed: 8617589]

Segars, WP. Ph.D. Dissertation. Chapel Hill, NC: University of North Carolina; 2001. Development and application of the new dynamic NURBS-based cardiac-torso (NCAT) phantom.

Segars WP, Tsui BMW, Frey EC, Johnson GA, Berr SS. Development of a 4-D digital mouse phantom for molecular imaging research. Mol. Imaging Biol. 2004; 6:149–159. [PubMed: 15193249]

Segars WP, Tsui B. 4D MOBY and NCAT phantoms for medical imaging simulation of mice and men. J. Nucl. Med. 2007; 48(Suppl. 2):203P.

Segars WP, Lalush DS, Frey EC, Manocha D, King M, Tsui BMW. Improved dynamic cardiac phantom based on 4D NURBS and tagged MRI. IEEE Trans. Nucl. Sci. 2009; 56:2728–2738. [PubMed: 20711514]

Segars, WP.; Tsui, BMW. The MCAT, NCAT, XCAT, and MOBY computational human and mouse phantoms. In: Xu, XG.; EckermanK, F., editors. Handbook of Anatomical Models for Radiation Dosimetry. Boca Raton, FL: Taylor & Francis; 2009. p. 105-134.

Segars WP, Sturgeon GM, Ward DJ, Ratnanather JT, Miller MI, Tsui BMW. The new XCAT series of digital phantoms for multi-modality imaging. IEEE Nucl. Sci. Symp. & Med. Imaging Conf. 2010:2392–2395.

Segars WP, et al. Population of anatomically variable 4D XCAT adult phantoms for imaging research and optimization. Med. Phys. 2013; 40:043701. [PubMed: 23556927]

Shi C, Xu XG. Development of a 30-week-pregnant female tomographic model from computed tomography (CT) images for Monte Carlo organ dose calculations. Med. Phys. 2004; 31:2491–2497. [PubMed: 15487729]

Shi C, Xu XG, Stabin MG. SAF values for internal photon emitters calculated for the RPI-P pregnant-female models using Monte Carlo methods. Med. Phys. 2008; 35:3215–3224. [PubMed: 18697546]

Shi, CY. Ph.D. Dissertation. Troy, NY: Rensselaer Polytechnic Institute; 2004. Development and application of a tomographic model from CT images for calculating internal dose to a pregnant woman.

Sjögreen K, Ljungberg M, Wingårdh K, Erlandsson K, Strand SE. Registration of emission and transmission whole-body scintillation-camera images. J. Nucl. Med. 2001; 42:1563–1570. [PubMed: 11585874]

Smans K, Tapiovaara M, Cannie M, Struelens L, Vanhavere F, Smet M, Bosmans H. Calculation of organ doses in x-ray examinations of premature babies. Med. Phys. 2008; 35:556–568. [PubMed: 18383677]

Smith TJ, Petouissi N, Zankl M. Comparison of internal radiation doses estimated by MIRD and voxel techniques for a “family” of phantoms. Eur. J. Nucl. Med. 2000; 27:1387–1398. [PubMed: 11007522]

Snyder, WS. Health Physics Division Annual Progress report for Period Ending July 31, 1967. Oak Rdige, TN: Oak Ridge National Laboratory; 1967. Variation of dose in man from exposure to a point source of gamma rays; p. 257Report ORNL-4168

Snyder WS, Ford MR, Warner GG, Fisher HL Jr. Estimates of absorbed fractions for monoenergetic photon sources uniformly distributed in various organs of a heterogeneous phantom. J. Nucl. Med. 1969; 10(Suppl 3):5–52.

Snyder, WS.; Ford, MR.; Warner, GG. Estimates of specific absorbed fractions for monoenergetic photon sources uniformly distributed in various organs of a heterogeneous phantom. Oak Ridge, TN: Oak Ridge National Laboratory; 1978. MIRD Pamphlet 5, Revised

Son IY, Winslow M, Yazici B, Xu XG. X-ray imaging optimization using virtual phantoms and computerized observer modelling. Phys. Med. Biol. 2006; 51:4289–4310. [PubMed: 16912382]

Spitzer, VM.; Whitlock, DG. Atlas of the Visible Human Male: Reverse Engineering of the Human Body. Sudbury, MA: Jones and Bartlett Publishers; 1998.

Stabin, MG.; Watson, EE.; Cristy, M.; Ryman, JC.; Eckerman, KF.; Davis, JL.; Marshall, D.; Gehlen, MK. Mathematical models and specific absorbed fractions of photon energy in the nonpregnant adult female and at the end of each trimester of pregnancy. Oak Ridge, TN: Oak Ridge National Laboratory; 1995. Report ORNL/TM-12907

Stabin M, Emmons MA, Segars WP, Fernald M, Brill AB. ICRP-89 based adult and pediatric phantom series. J. Nucl. Med. 2008; 49(Supp. 1):14P.

Stabin MG, Xu XG, Emmons MA, Segars WP, Shi C, Fernald MJ. RADAR reference adult, pediatric and pregnant female phantom series for internal and external dosimetry. J. Nucl. Med. 2012; 53:1807–1813. [PubMed: 22967805]

Staton RJ, Jones A Kyle, Lee C, Hintenlang David E, Arreola MM, Williams Jonathon L, Bolch Wesley E. A tomographic physical phantom of the newborn child with real-time dosimetry II. Scaling factors for calculation of mean organ dose in pediatric radiography. Med. Phys. 2006; 33:3283–3289. [PubMed: 17022223]

Storm L, Israel HI. Photon cross sections from 1 keV to 100 MeV for elements Z=1 to Z=100. Atomic Data and Nuclear Data Tables 7. 1970:565–681.

Stovall M, Smith SA, Rosenstein M. Tissue doses from radiotherapy of cancer of the uterine cervix. Med. Phys. 1989; 16:726–733. [PubMed: 2509867]

Stroud, I. Boundary Representation Modeling Techniques. London, UK: Springer-Verlag; 2006.

Su L, Han B, Xu XG. Calculated organ doses for individuals in a sitting posture above a contaminated ground and a PET imaging room. Radiat. Prot. Dosimetry. 2012; 148:439–443. [PubMed: 21515624]

Su L, Yang YM, Bednarz B, Sterpin E, Du X, Liu T, Ji W, Xu XG. ARCHER—A photon-electron coupled Monte Carlo dose computing engine for GPU: software development and application to helical tomotherapy. Med. Phys. 2014 (submitted).

Sun W, Jia X, Xie T, Xu F, Liu Q. Construction of boundary-surface-based Chinese female astronaut computational phantom and proton dose estimation. J. Radiat. Res. 2013; 54:383–397. [PubMed: 23135158]

Tabary, J.; Marache-Francisco, S.; Valette, S.; Segars, WP.; Lartizien, C. Realistic x-ray CT simulation of the XCAT phantom with SINDBAD; 2009 IEEE Nuclear Science Symposium Conference Record (NSS/MIC); 2009. p. 3980-3983.

Taddei PJ, Mirkovic D, Fontenot JD, Giebeler A, Zheng Y, Kornguth D, Mohan R, Newhauser WD. Stray radiation dose and second cancer risk for a pediatric patient receiving craniospinal irradiation with proton beams. Phys. Med. Biol. 2009; 54:2259–2275. [PubMed: 19305045]

Takahashi M, Kinase S, Kramer R. Evaluation of counting efficiencies of a whole-body counter using Monte Carlo simulation with voxel phantoms. Radiat. Prot. Dosimetry. 2011; 144:407–410. [PubMed: 21131662]

Taranenko V, Xu XG. Foetal dose conversion coefficients for ICRP-compliant pregnant models from idealised proton exposures. Radiat. Prot. Dosimetry. 2009; 133:65–72. [PubMed: 19246483]

Tinniswood AD, Furse CM, Gandhi OP. Power deposition in the head and neck of an anatomically based human body model for plane wave exposures. Phys. Med. Biol. 1998; 43:2361–2378. [PubMed: 9725610]

Tresser MA, Hintenlang DE. Construction of a newborn dosimetry phantom for measurement of effective dose. Health Phys. 1999; 76:S190.

Tsui BMW, Zhao XD, Gregoriou GK, Lalush DS, Frey EC, Johnston RE, Mccartney WH. Quantitative cardiac SPECT reconstruction with reduced image degradation due to patient anatomy. IEEE Trans. Nucl. Sci. 1994; 41:2838–2844.

Tsui BM, Terry JA, Gullberg GT. Evaluation of cardiac cone-beam single photon emission computed tomography using observer performance experiments and receiver operating characteristic analysis. Inv. Radiol. 1993; 28:1101–1112.

Tung CJ, Tsai SF, Tsai HY, Chen IJ. Determination of voxel phantom for reference Taiwanese adult from CT image analyses. Radiat. Prot. Dosimetry. 2011; 146:186–190. [PubMed: 21511723]

Turner JE, Wright HA, Hamm RN. A Monte Carlo primer for health physicists. Health Phys. 1985; 48:717–733. [PubMed: 3997524]

Tward, DJ.; Ceritoglu, C.; Sturgeon, G.; Segars, WP.; Miller, MI.; Ratnanather, JT. Generating patient-specific dosimetry phantoms with whole-body diffeomorphic image registration; 2011 IEEE 37th Annual Northeast Bioengineering Conference (NEBEC); 2011. p. 1-2.

Uusitupa T, Laakso I, Ilvonen S, Nikoskinen K. SAR variation study from 300 to 5000 MHz for 15 voxel models including different postures. Phys. Med. Biol. 2010; 55:1157–1176. [PubMed: 20107250]

Vazquez JA, Ding A, Haley T, Caracappa PF, Xu XG. Development of a dynamic computational human phantom for animated dosimetry simulation using motion capture data and a dose-reconstruction demonstration considering the 1997 Sarov criticality accident. Health Phys. 2014a (in press).

Vazquez JA, Caracappa PF, Xu XG. Development of posture-specific computational phantoms using motion capture technology and application to radiation dose reconstruction for the 1999 Tokaimura Nuclear Criticality Accident. Phys. Med. Biol. 2014b (in press).

Veress AI, Segars WP, Tsui BMW, Gullberg GT. Incorporation of a left ventricle finite element model defining infarction into the XCAT imaging phantom. IEEE Trans. Med. Imaging. 2011; 30:915–927. [PubMed: 21041157]

Wang B, Xu XG, Kim CH. A Monte Carlo CT model of the Rando Phantom. Trans. Am. Nucl. Soc. 2004; 90:473–474.

Wang J, Fujiwara O, Watanabe S, Yamanaka Y. Computation with a parallel FDTD system of human-body effect on electromagnetic absorption for portable telephones. IEEE Trans. Microw. Theory Tech. 2004; 52:53–58.

Wang, B.; Xu, XG.; Goorley, JT.; Bozkurt, A. The use Of MCNP code for an extremely large voxel model VIP-Man. The Monte Carlo Method: Versatility 43 Unbounded In A Dynamic Computing World; Proceedings of the Monte Carlo 2005 Topical Meeting; April 17–21; Chattanooga, TN. LaGrange, Park IL: American Nuclear Society; 2005a. on CD-ROM (ISBN:0-89448-695-0) also available online http://mathematicsandcomputation.cowhosting.net/MonteCarlo05/FullPapers/usr-georgexu-3-paper.pdf

Wang B, Xu XG, Goldstein M, Sahoo N. Adjoint Monte Carlo method for prostate external photon beam treatment planning: An application to 3-D patient anatomy. Phys. Med. Biol. 2005b; 50:923–935. [PubMed: 15798265]

Williams G, Zankl M, Abmayr W, Veit R, Drexler G. The calculation of dose from external photon exposures using reference and realistic human phantoms and Monte Carlo methods. Phys. Med. Biol. 1986; 31:449–452. [PubMed: 3737684]

Winslow M, Huda W, Xu XG, Chao TC, Shi CY, Ogden KM, Scalzetti EM. Use of the VIP-Man model to calculate energy imparted and effective dose for x-ray examinations. Health Phys. 2004; 86:174–182. [PubMed: 14744051]

Winslow M, Xu XG, Yazici B. Development of a simulator for radiographic image optimization. Comput. Methods Programs Biomed. 2005; 78:179–190. [PubMed: 15899304]

Wu D, Shamsi S, Chen J, Kainz W. Evaluations of specific absorption rate and temperature increase within pregnant female models in magnetic resonance imaging birdcage coils. IEEE Trans. Microw. Theory Tech. 2006; 54:4472–4478.

Xie T, Zaidi H. Evaluation of radiation dose to anthropomorphic paediatric models from positron-emitting labelled tracers. Phys. Med. Biol. 2014; 59:1165–1187. [PubMed: 24557029]

Xie T, Bolch WE, Lee C, Zaidi H. Pediatric radiation dosimetry for positron-emitting radionuclides using anthropomorphic phantoms. Med. Phys. 2013; 40:102502–102514. [PubMed: 24089923]

Xie T, Zhang G, Li Y, et al. Comparison of absorbed fractions of electrons and photons using three kinds of computational phantoms of rat. Applied Physics Letters. 2010; 97(3)

Xu XG, Reece WD, Poston JW. A Study of the angular dependence problem in effective dose equivalent assessment. Health Phys. 1995; 68:214–224. [PubMed: 7814255]

Xu XG, Reece WD. Sex-specific tissue weighting factors for effective dose equivalent calculations. Health Phys. 1996; 70:81–86. [PubMed: 7499157]

Xu XG, Chao TC, Bozkurt A. VIP-Man: An image-based whole-body adult male model constructed from color photographs of the Visible Human Project for multi-particle Monte Carlo calculations. Health Phys. 2000; 78:476–486. [PubMed: 10772019]

Xu XG, Chao TC, Bozkurt A. Comparison of effective doses from various monoenergetic particles based on the stylised and the VIP-Man tomographic models. Radiat. Prot. Dosimetry. 2005; 115:530–535. [PubMed: 16381780]

Xu XG, Taranenko V, Zhang J, Shi C. A boundary-representation method for designing whole-body radiation dosimetry models: pregnant females at the ends of three gestational periods—RPI-P3, -P6 and -P9. Phys. Med. Biol. 2007; 52:7023–7044. [PubMed: 18029991]

Xu, XG. Computational phantoms for radiation dosimetry: A 40-year history of evolution. In: Xu, XG.; Eckerman, KF., editors. Handbook of Anatomical Models for Radiation Dosimetry. Boca Raton, FL: Taylor & Francis; 2009. p. 3-42.

Xu, XG.; Eckerman, KF. Handbook of Anatomical Models for Radiation Dosimetry. Boca Raton, FL: Taylor & Francis; 2009.

Yeom YS, Han MC, Kim CH, Jeong JH. Conversion of ICRP male reference phantom to polygon-surface phantom. Phys. Med. Biol. 2013; 58:6985–7007. [PubMed: 24029733]

Zaidi H. Relevance of accurate Monte Carlo modeling in nuclear medical imaging. Med. Phys. 1999; 26:574–608. [PubMed: 10227362]

Zaidi, H.; Sgouros, G., editors. Therapeutic Applications of Monte Carlo Calculations in Nuclear Medicine. London, UK: IOP Publishing; 2003.

Zaidi H, Xu XG. Computational anthropomorphic models of the human anatomy: the path to realistic Monte Carlo modeling in radiological sciences. Annu. Rev. Biomed. Eng. 2007; 9:471–500. [PubMed: 17298237]

Zaidi H, Tsui BMW. Review of computational anthropomorphic anatomical and physiological models. Proc. IEEE. 2009; 97:1938–1953.

Zankl M, Fill U, Petoussi-Henss N, Regulla D. Organ dose conversion coefficients for external photon irradiation of male and female voxel models. Phys. Med. Biol. 2002; 47:2367–2385. [PubMed: 12171328]

Zankl M, Veit R, Williams G, Schneider K, Fendel H, Petoussi N, Drexler G. The construction of computer tomographic phantoms and their application in radiology and radiation protection. Radiat. Environ. Biophys. 1988; 27:153–164. [PubMed: 3393623]

Zankl, M.; Becker, J.; Fill, U.; Petoussi-Henss, N.; Eckerman, KF. GSF male and female adult voxel models representing ICRP Reference Man—the present status. The Monte Carlo Method: Versatility Unbounded in a Dynamic Computing World; Proceedings of the Monte Carlo 2005 Topical Meeting held; April 17–21; Chattanooga, TN. LaGrange, Park IL: American Nuclear Society; 2005. on CD-ROM (ISBN:0-89448-695-0) also available online http://mathematicsandcomputation.cowhosting.net/MonteCarlo05/FullPapers/usr-zankl-1-paper.pdf

Zeng Z, Li J, Qiu R. Dose assessment for space radiation using a proton differential dose spectrum. Journal of Tsinghua University (Science and Technology). 2006; 46:374–376.

Zhang B, Ma J, Liu L, Cheng J. CNMAN: A Chinese adult male voxel phantom constructed from color photographs of a visible anatomical data set. Radiat. Prot. Dosimetry. 2007a; 124:130–136. [PubMed: 17526909]

Zhang G, Liu Q, Luo Q. Monte Carlo simulations for external neutron dosimetry based on the visible Chinese human phantom. Phys. Med. Biol. 2007b; 52:7367–7383. [PubMed: 18065844]

Zhang G, Liu Q, Zeng S, Luo Q. Organ dose calculations by Monte Carlo modeling of the updated VCH adult male phantom against idealized external proton exposure. Phys. Med. Biol. 2008a; 53:3697–3722. [PubMed: 18574316]

Zhang G, Luo Q, Zeng S, Liu Q. The development and application of the visible Chinese human model for Monte Carlo dose calculations. Health Phys. 2008b; 94:118–125. [PubMed: 18188046]

Zhang JY, Xu XG, Shi C, Fuss M. Development of a geometry-based respiratory motion-simulating patient model for radiation treatment dosimetry. J. Appl. Clin. Med. Phys. 2008c; 9:2700. [PubMed: 18449164]

Zhang, B.; Ma, J.; Zhang, G.; Liu, Q.; Qiu, R.; Li, J. The Chinese computational phantoms: CNMAN, VCH, and CVP. In: Xu, XG.; Eckerman, KF., editors. Handbook of Anatomical Models for Radiation Dosimetry. Boca Raton, FL: Taylor & Francis; 2009a. p. 279-304.

Zhang J, Na YH, Caracappa PF, Xu XG. RPI-AM and RPI-AF, a pair of mesh-based, size-adjustable adult male and female computational phantoms using ICRP-89 parameters and their calculations for organ doses from monoenergetic photon beams. Phys. Med. Biol. 2009b; 54:5885–5908. [PubMed: 19759412]

Ziriax JM, Smith KI, Nelson DA, Ryan KL, Gajsek P, D'Andrea JA, Walters TJ, Hurt WD, Mason PA. Effects of frequency, permittivity, and voxel size on predicted specific absorption rate values in biological tissue during electromagnetic-field exposure. IEEE Trans. Microw. Theory Tech. 2000; 48:2050–2058.

Zubal IG, Harrell CR, Smith EO, Rattner Z, Gindi G, Hoffer PB. Computerized three-dimensional segmented human anatomy. Med. Phys. 1994; 21:299–302. [PubMed: 8177164]

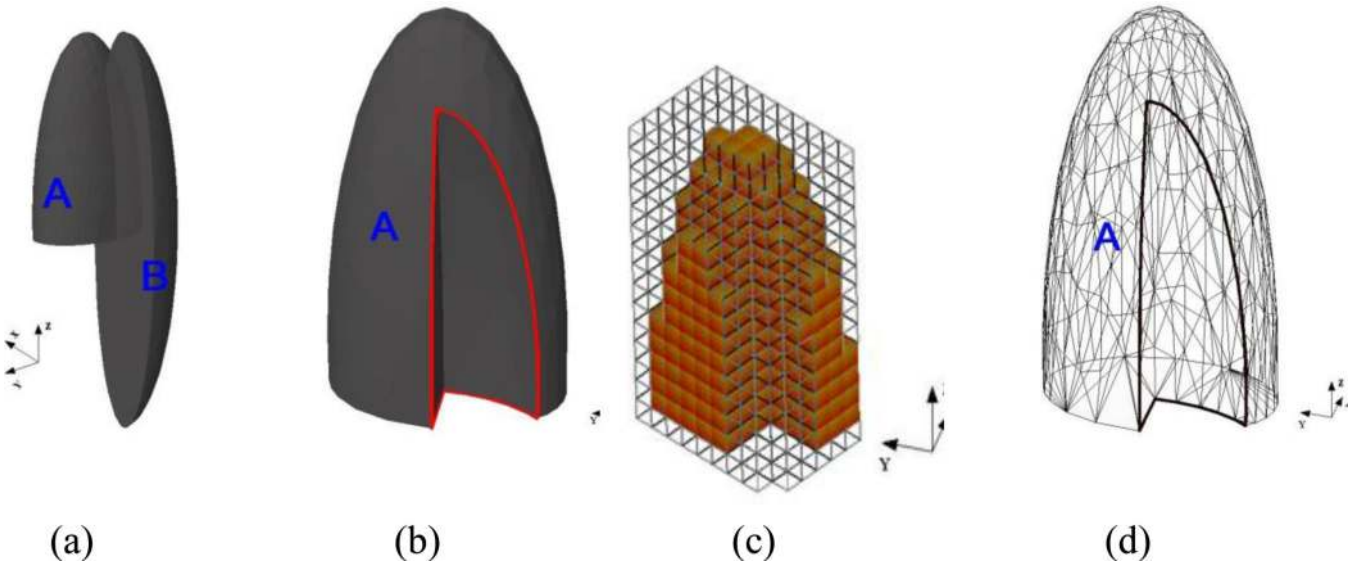

Figure 1.

A model of the left lung defined by different modeling methods. (a) The CSG-type modeling before the Boolean operation (subtraction) is performed involving two ellipsoids A and B. (b) After the subtraction of B from A. (c) A voxel representation of the lung. (d) A BREP-type of modeling of the same lung using polygon mesh.

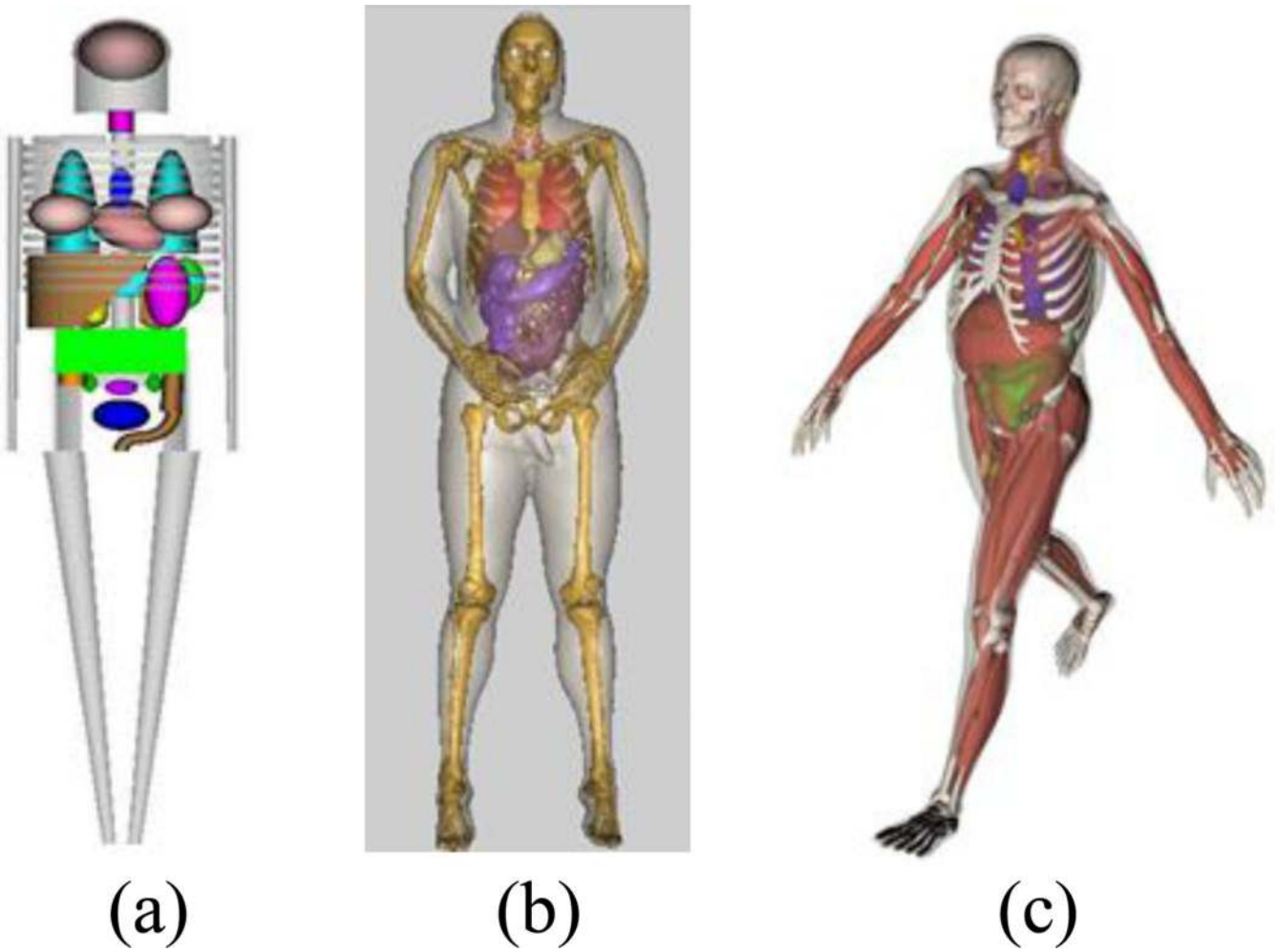

Figure 2.
Three phantom generations: (1) Stylized phantom; (2) Voxel phantom (but displayed in smooth surfaces); (3) BREP phantom.

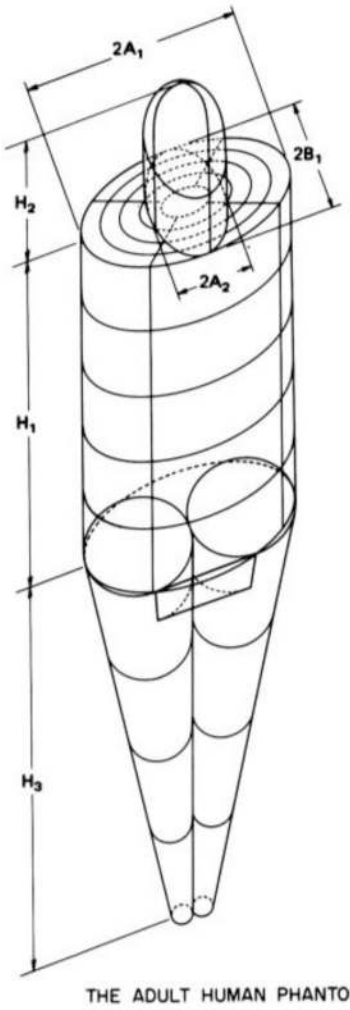

ORNL-DWG. 74-9373

PHANTOM DIMENSIONS AND DOSE REGIONS

Age (yr)	Weight (kg)	H_1 (cm)	H_2 (cm)	H_3 (cm)	A_1 (cm)	B_1 (cm)	A_2 (cm)
0	3.148	23	13	16	5.5	5	4.5
1	9.112	33	16	28.8	8	7	6.5
5	18.12	45	20	46	11	7.5	6.5
10	30.57	54	22	64	14	8	6.5
15	53.95	65	23	78	18	9	7
Adult	69.88	70	24	80	20	10	7

Figure 3.

The adult male phantom and its dimensions. Similar descriptions and diagrams were purposely followed in a series of ORNL technical reports by Snyder *et al* (1978), Cristy (1980), and Cristy and Eckerman (1987).

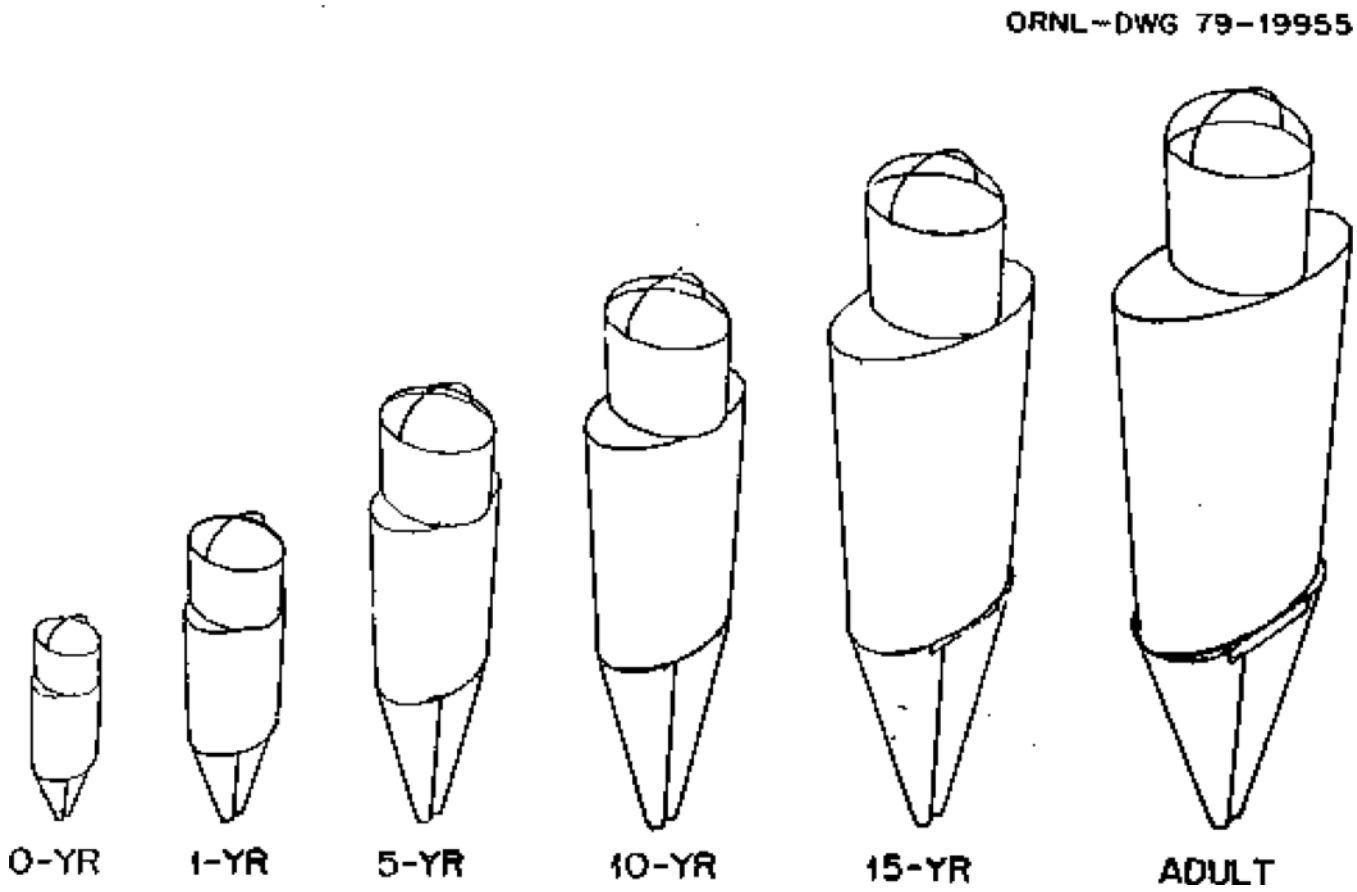

Figure 4.

External views of the age-specific phantom phantoms representing an adult male and children at 15-year old (adult female), 10-year old, 5-year old, 1-year old, and 0-year old (newborn) (From Cristy and Eckerman 1987). When used for an adult female, the 15-year old phantom has breasts appropriate for a reference adult female, which are not shown.

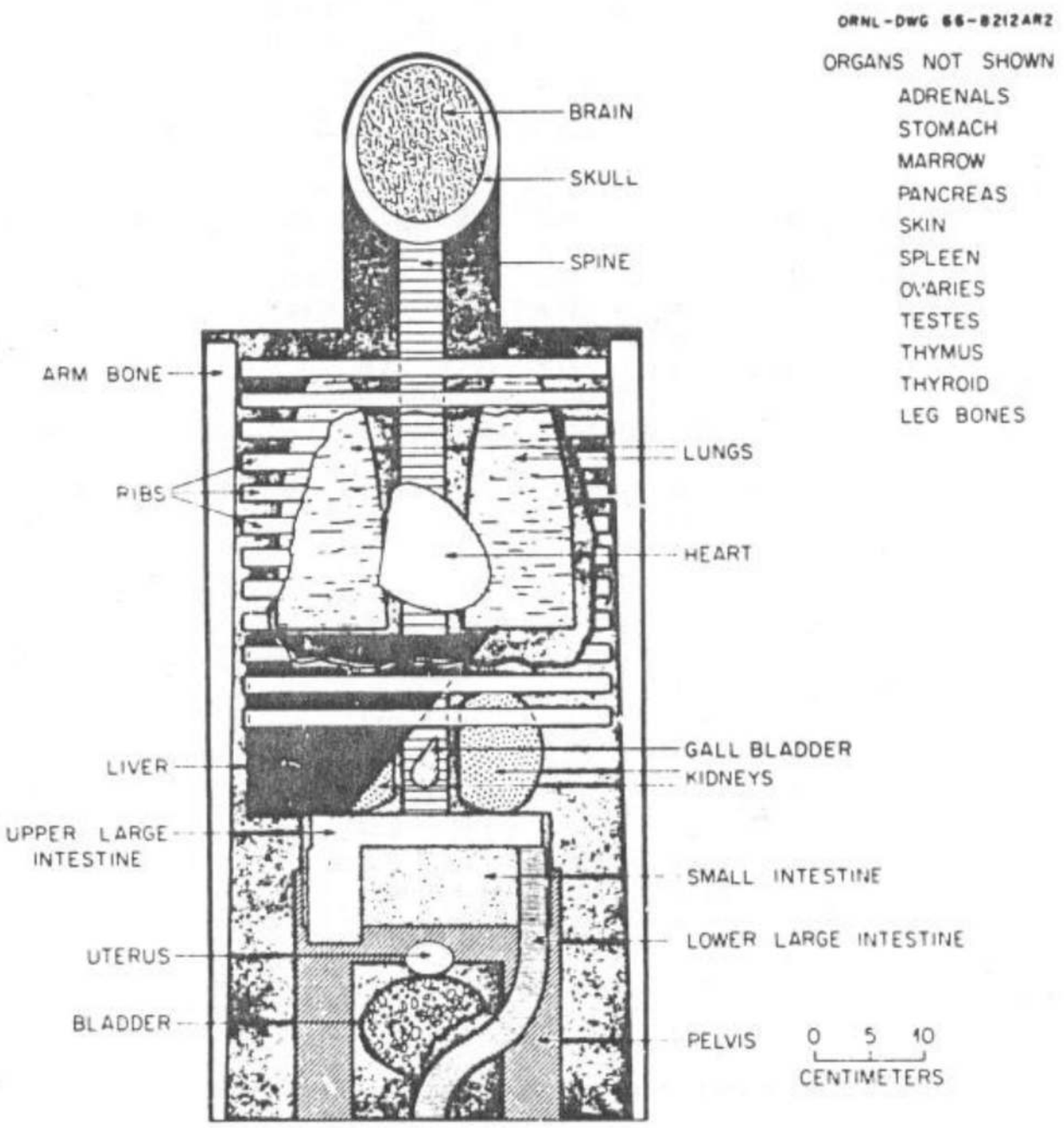

Figure 5.

Anterior view of the principal organs in the head and trunk of the adult phantom developed by Snyder *et al* (1978). Although the heart and head have been modified, this schematic illustrates the crude nature of the geometric modeling by today's standards. At the time, however, this was important work represented the state of the science.

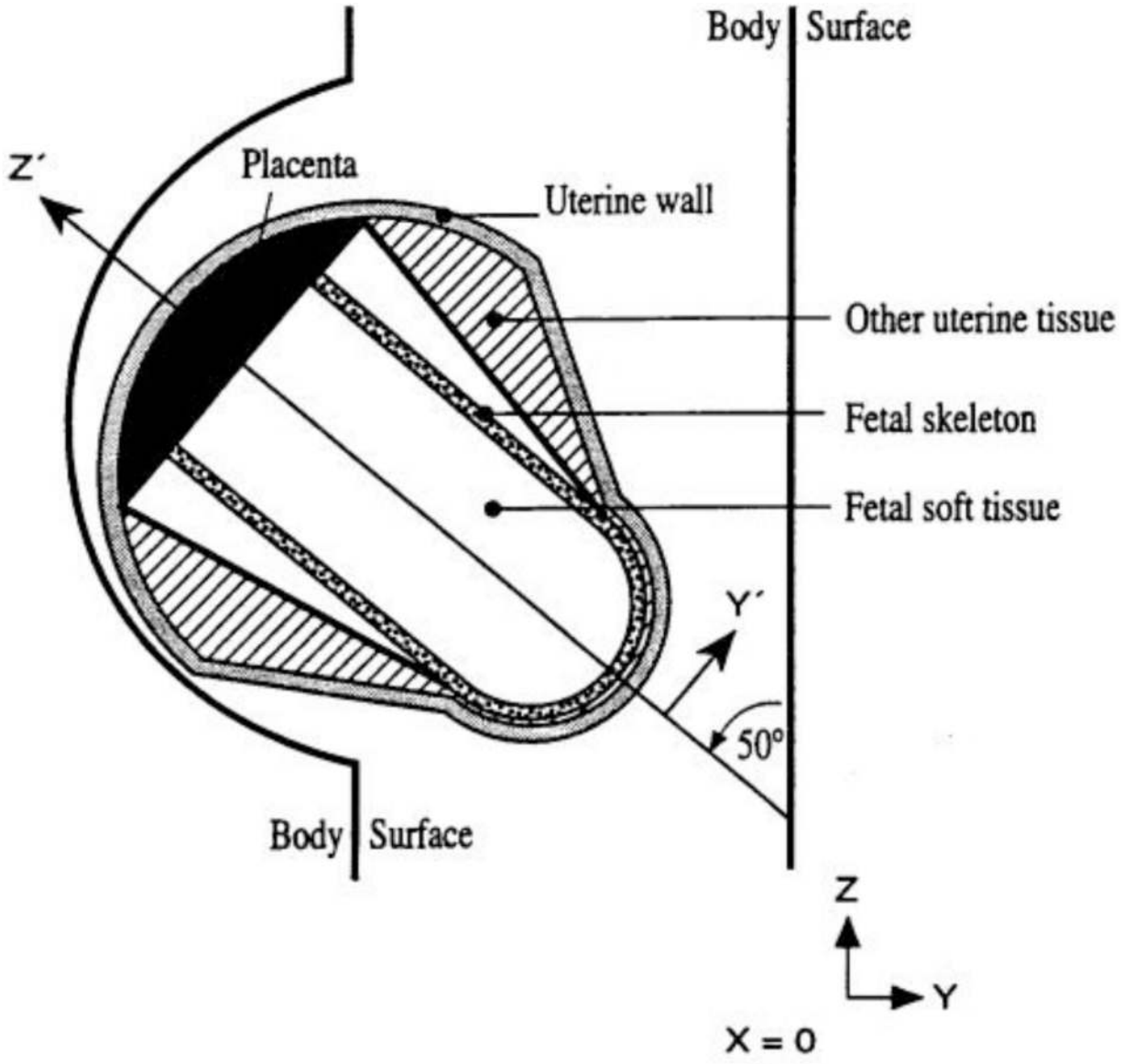

Figure 6.
Diagram of the uterus of the 9-month gestation model in the Stabin *et al* (1995) pregnant female phantom series.

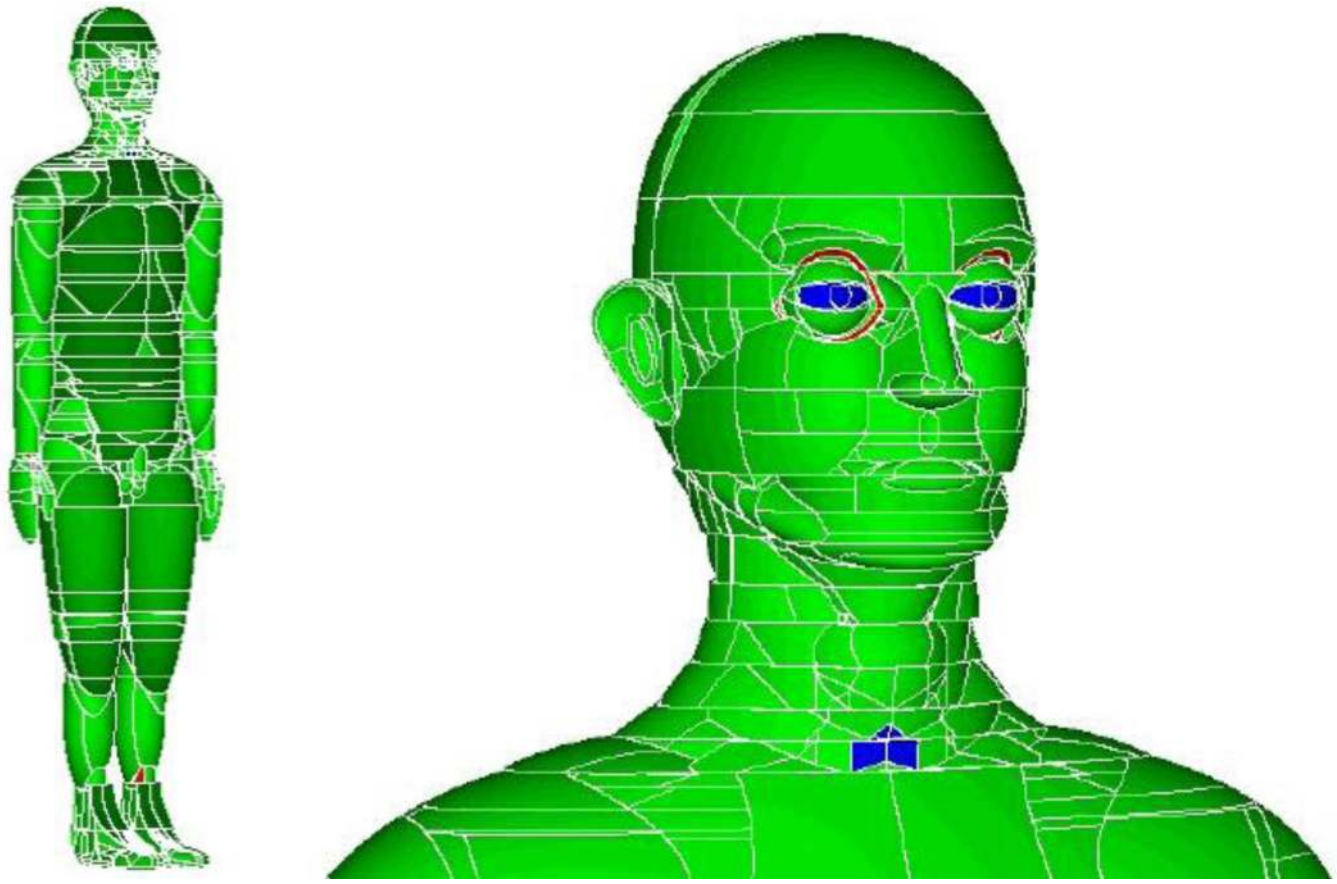

Figure 7.
The CAM phantom. (Left) The whole body view showing arms separated from the trunk. (Right)The close-up view of the facial details (http://cmpwg.ans.org).

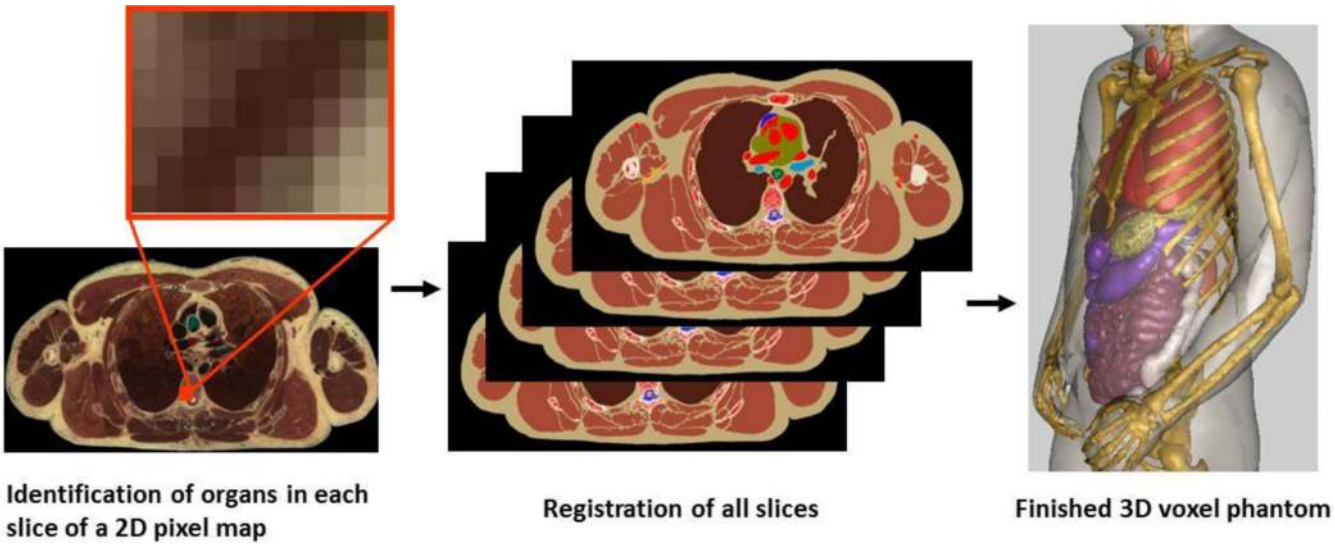

Figure 8.
Steps to create a voxel phantom using the Visible Human cadaver image dataset as an example.

Figure 9.
ICRP adult Reference Male and Female that are based on earlier work at the GSF (ICRP 2009).

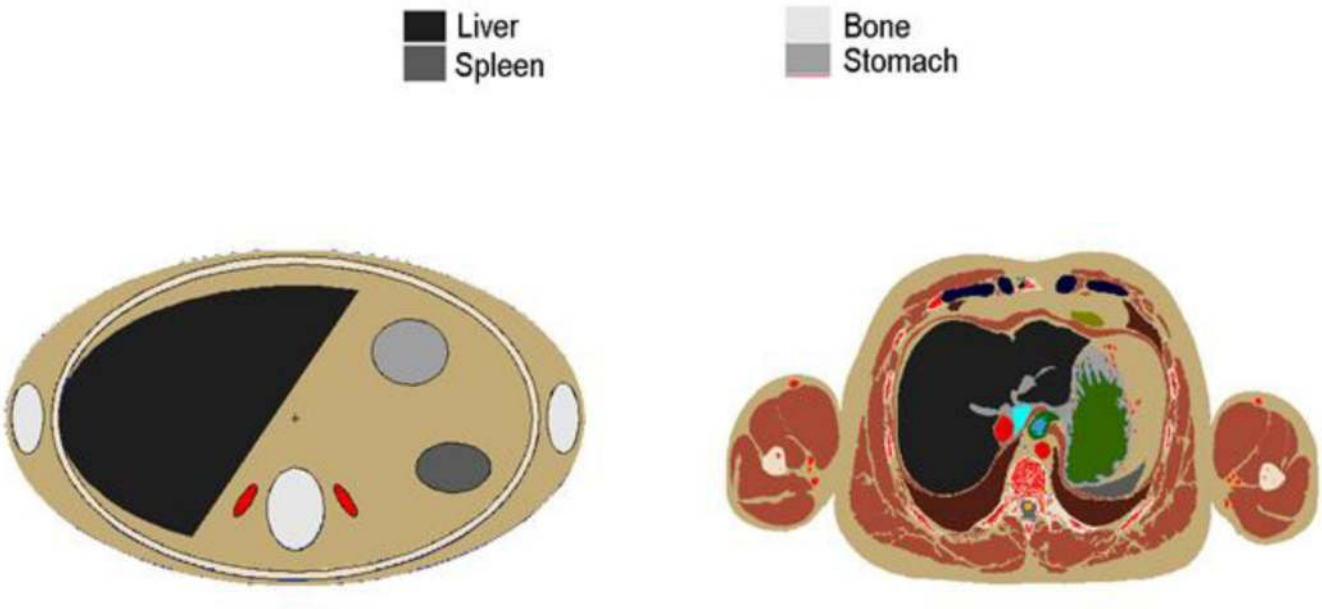

Figure 10.
Comparison of stylized adult phantom (left) and VIP-Man phantom (Xu *et al* 2000) (right) showing profound differecnes in anatomical detail. Such anatomical differences were believed effect the accuracy of radiation dose estimates.

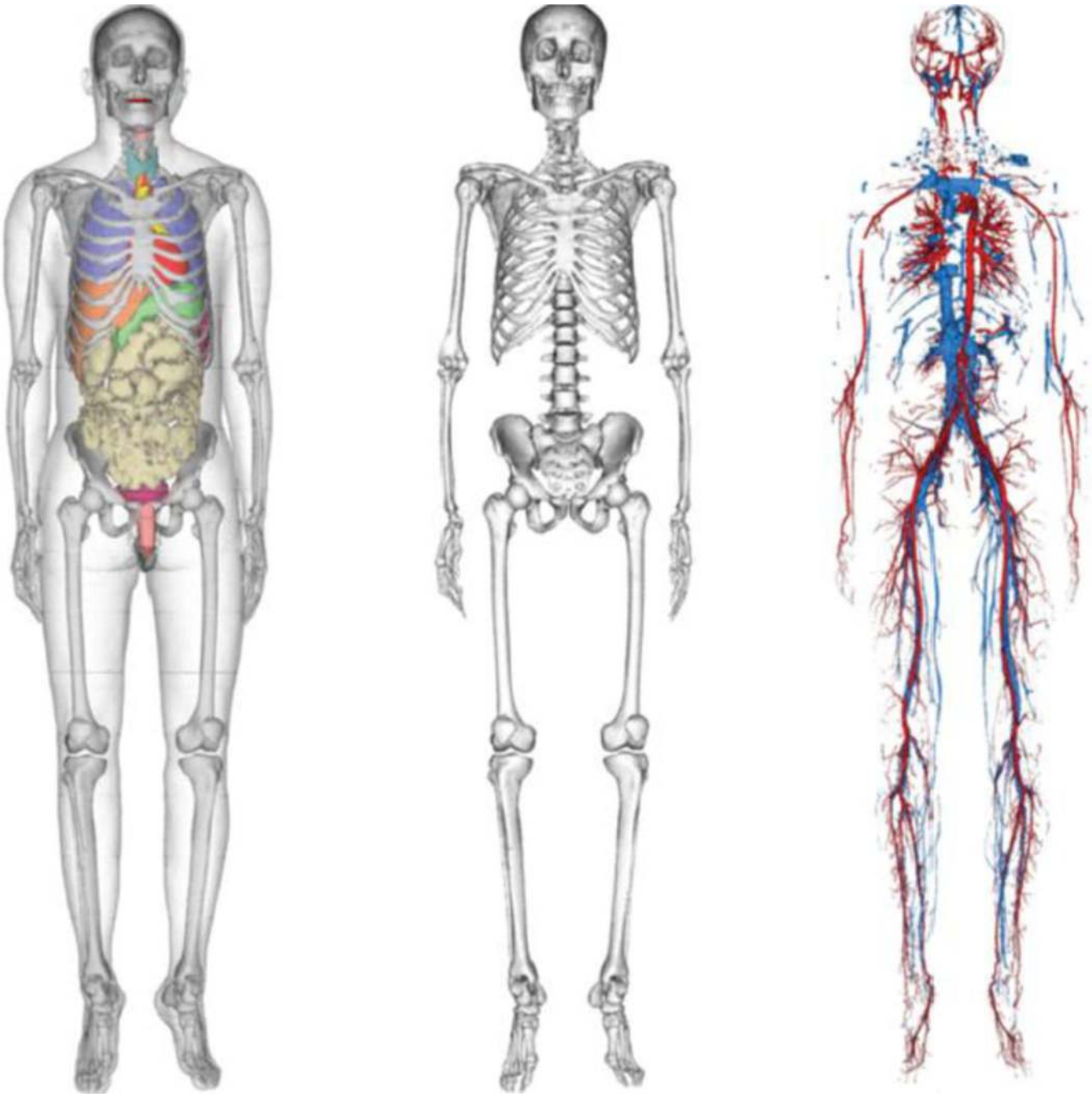

Figure 11.
One of the Chinese phantoms—VCH phantom showing (left) internal organs, (middle) whole-body skeleton, and (right) vascular system (Zhang *et al* 2008b).

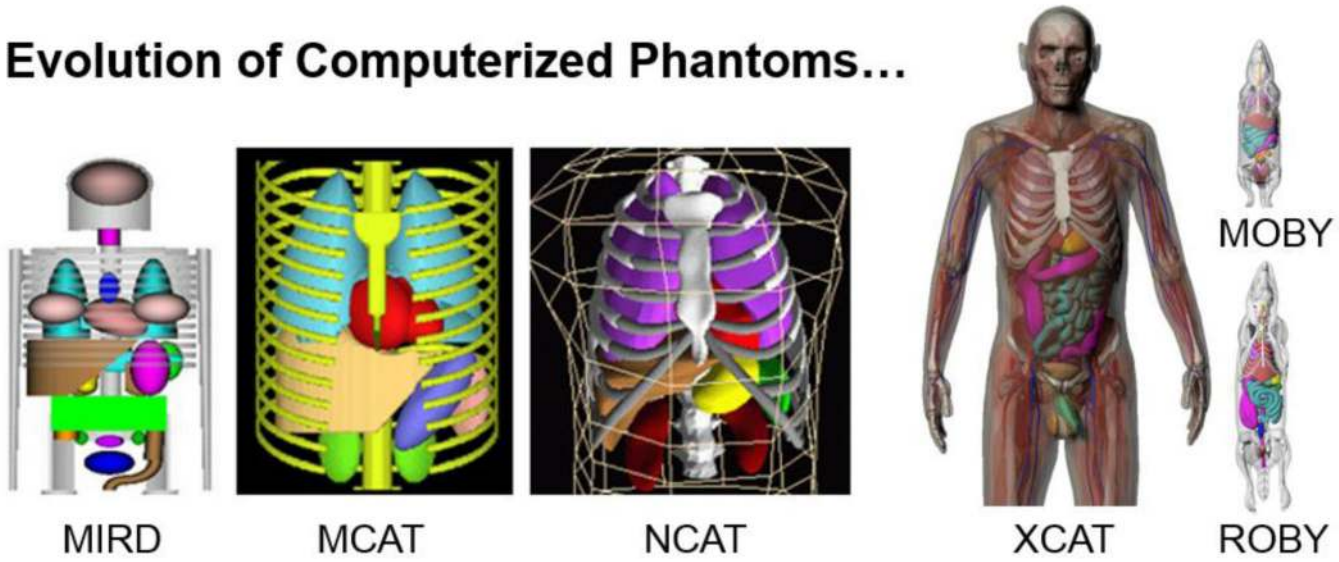

Figure 12.
Original MIRD phantom is shown with MCAT, NCAT, XCAT, MOBY and ROBY phantoms (Courtesy of Paul Segars).

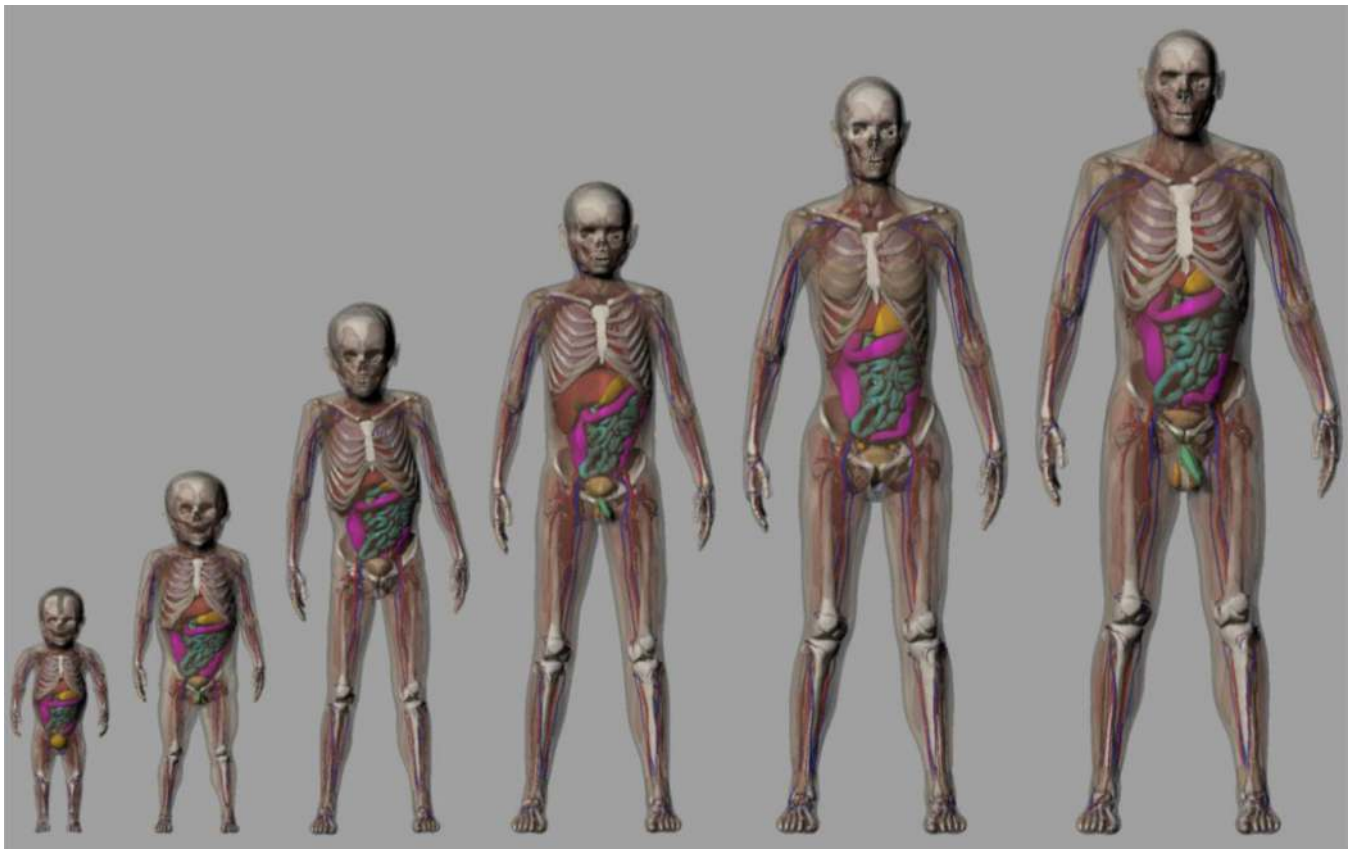

Figure 13.

A portion of the XCAT Phantom Family representing ages between newborn and 12 years-old. The phantoms can be adjusted to patient-specific information (Courtesy of Paul Segars).

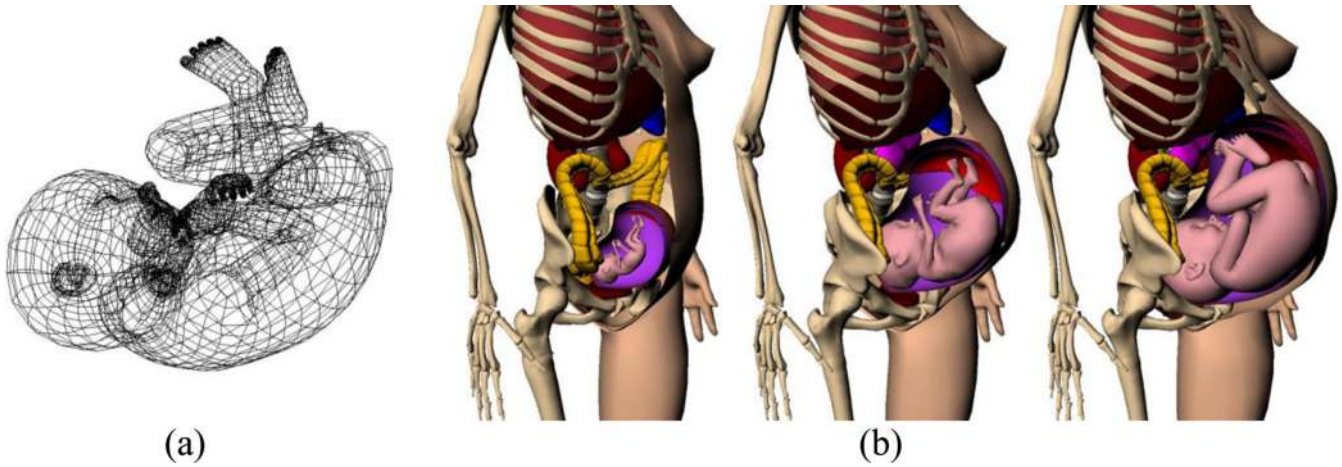

Figure 14.
RPI-P phantoms for pregnant women. (a) BREP-type geometry of a 9-month old fetus in mesh format. (b) The mother and fetus after assembly showing the 3-, 6- and 9-month gestational periods (from left to right).

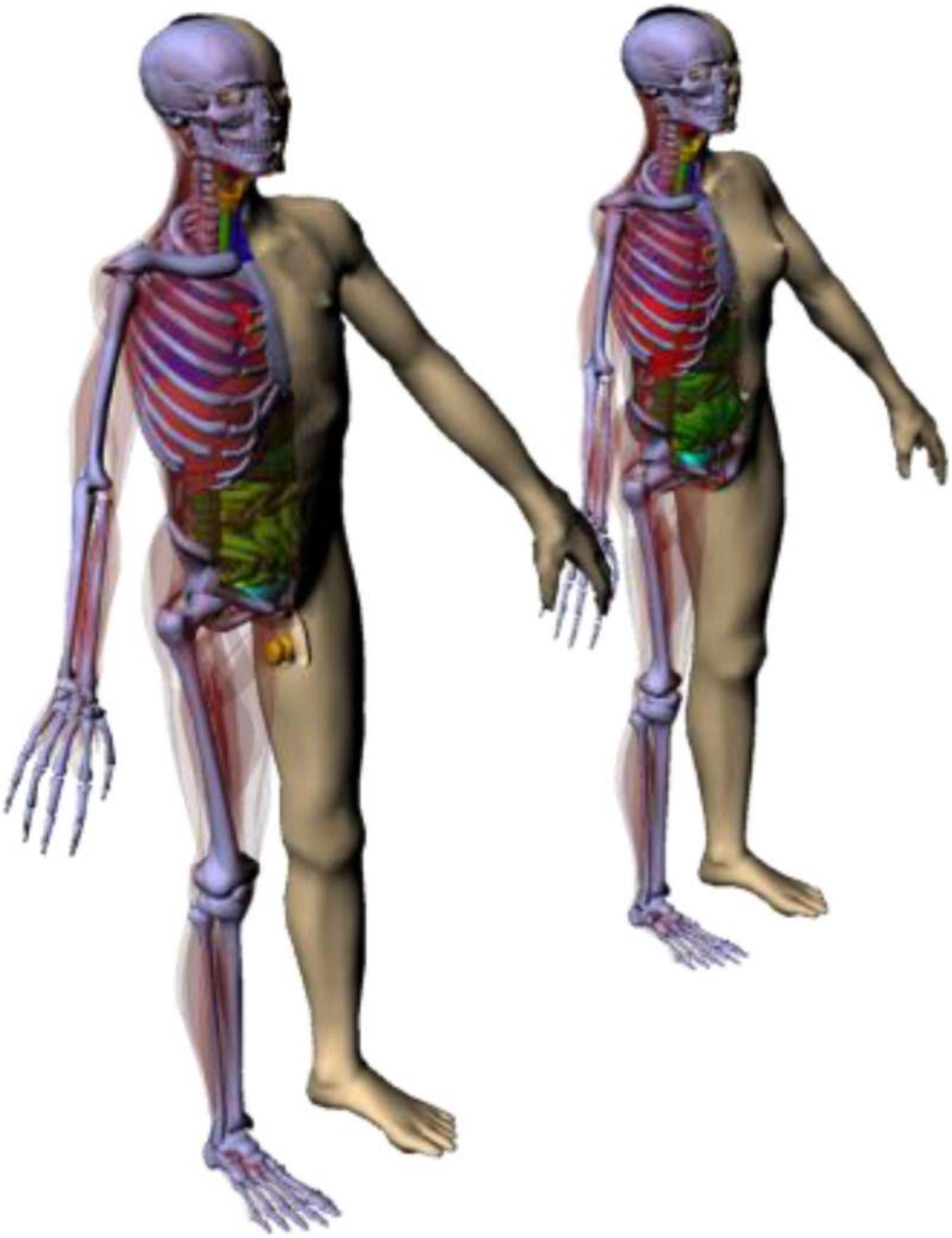

Figure 15.
The triangle mesh based RPI Adult Male and Adult Female phantoms (A supplementary file "3DPhantoms.pdf" to this figure is available for download that will allow a reader to interactively visualize the phantoms in 3D).

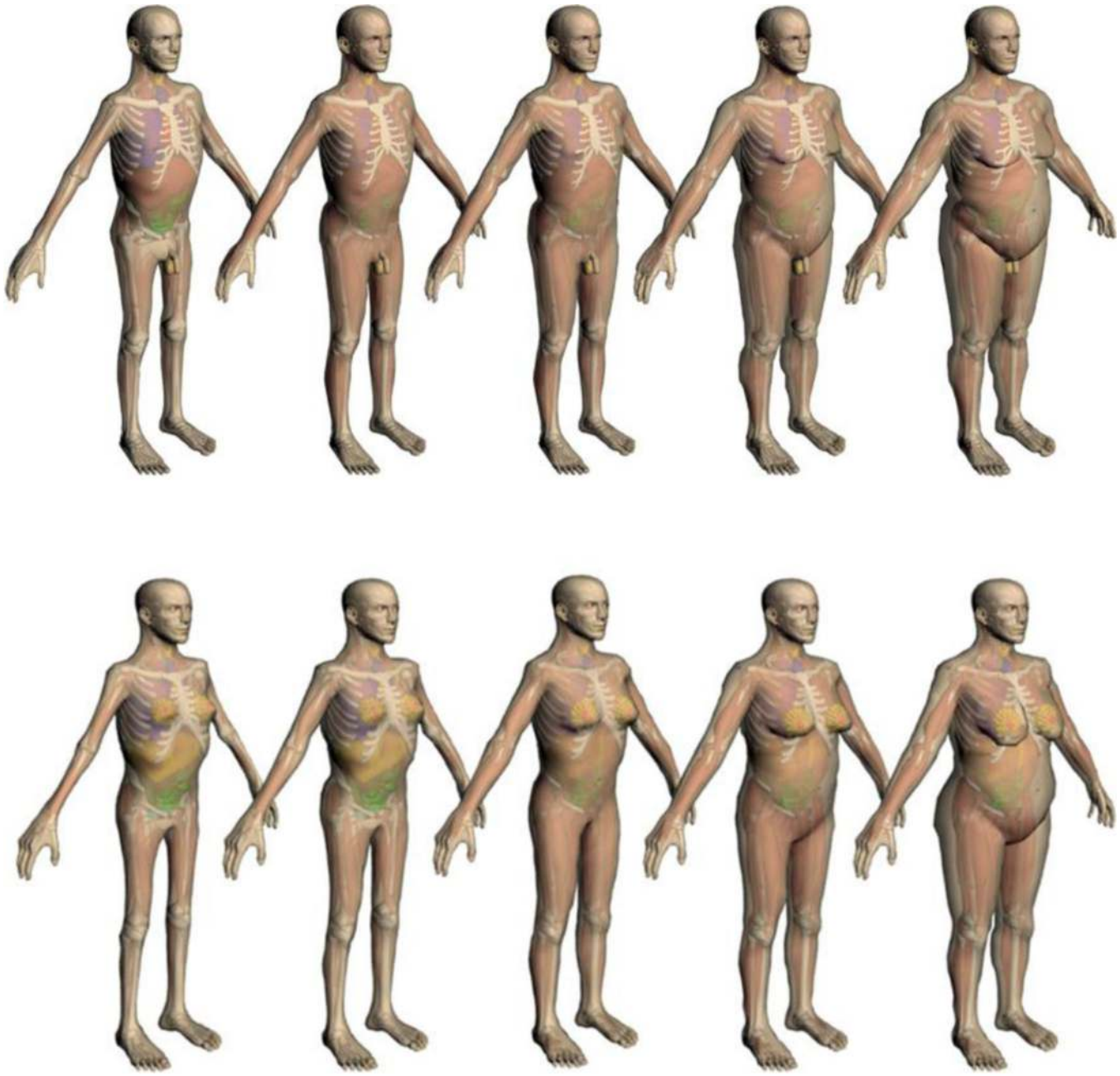

Figure 16.
The RPI Adult Male (top) and Adult Female (bottom) phantoms representing the 5th, 25th, 50th, 75th, and 95th weight percentiles (from left to right) (Na *et al* 2010).

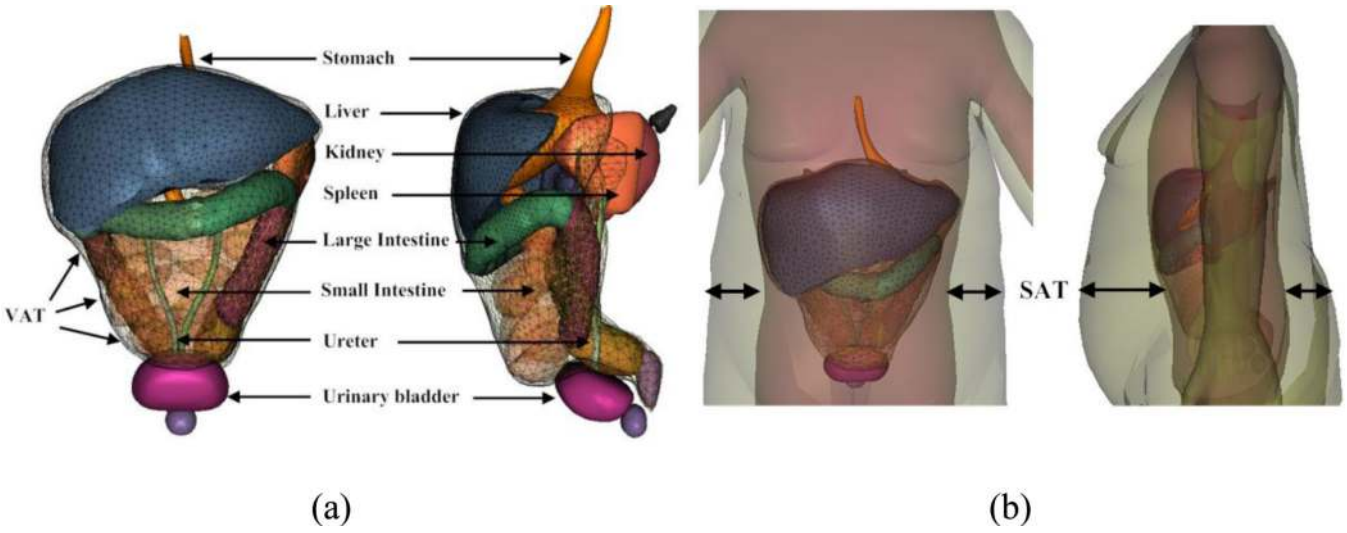

Figure 17.

Illustration of the method to develop overweight and obese individuals by adding adipose tissues: (a) abdominal organs (surface rendering mode) and VAT (wireframe rendering mode) which surrounds the abdominal organs, (b) SAT layer beneath the skin, defined as the region between the body surface and internal body cavity.

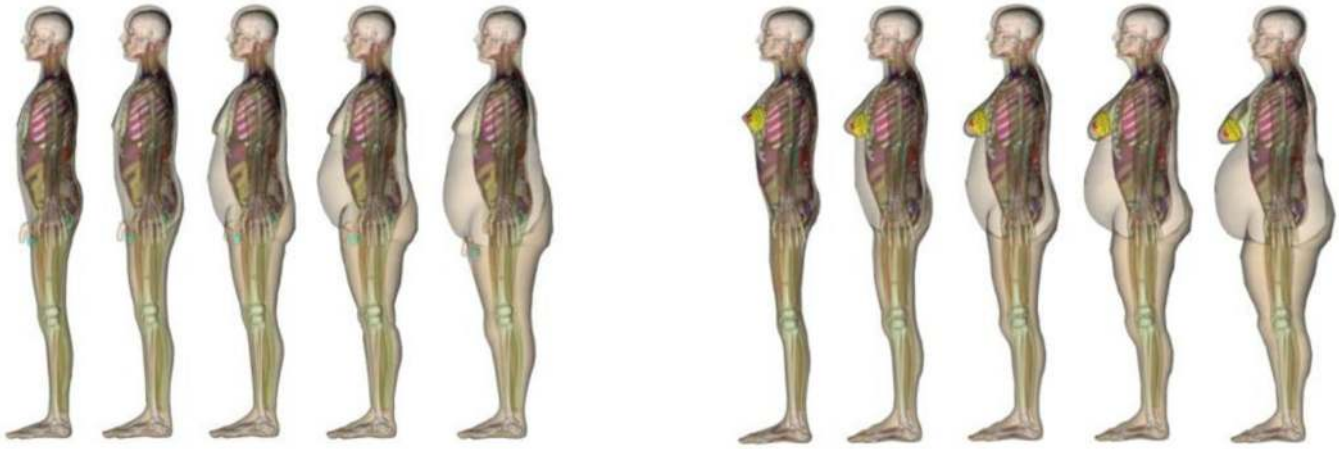

Figure 18.
Phantoms for overweight and obese individuals. (Left) males, and (right) females. The phantoms have the same height (1.76 m for the male and 1.63 m for the female) but differ in weight. From left to right, the weight classifications are, normal-weight, overweight, obese level-I, obese level-II and morbidly obese (Ding *et al* 2012).

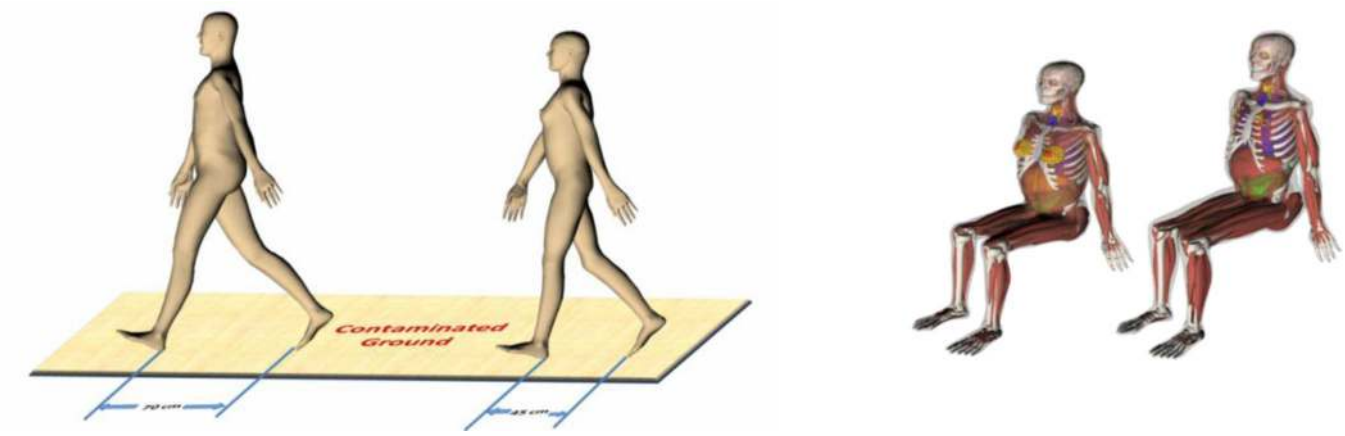

Figure 19.

(Left) Walking adult male and adult female phantoms on contaminated ground with a step size of 70 cm and 45 cm, respectively. (Right) Sitting phantoms on a floor above nuclear medicine clinic.

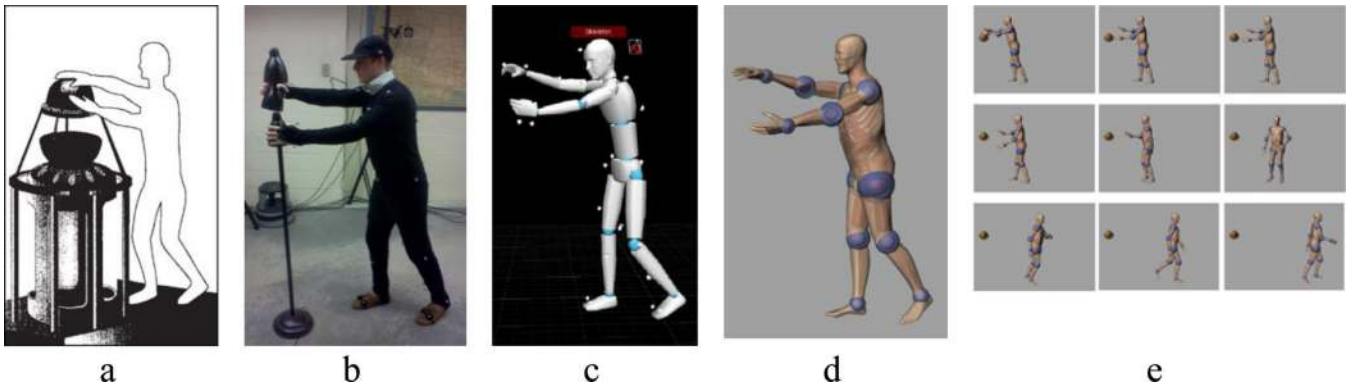

Figure 20.

Motion capture technology was used to develop realistic posture sequence for a criticality accident. (a) A worker was exposed to criticality excursion and died 66 hours later. (b) An actor reconstructs the postures using motion capture. (c) The postures are recorded sequentially. (d) The CHAD phantom recreates the same sequential postures. (e) A total of 9 postures used for Monte Carlo dose calculations.

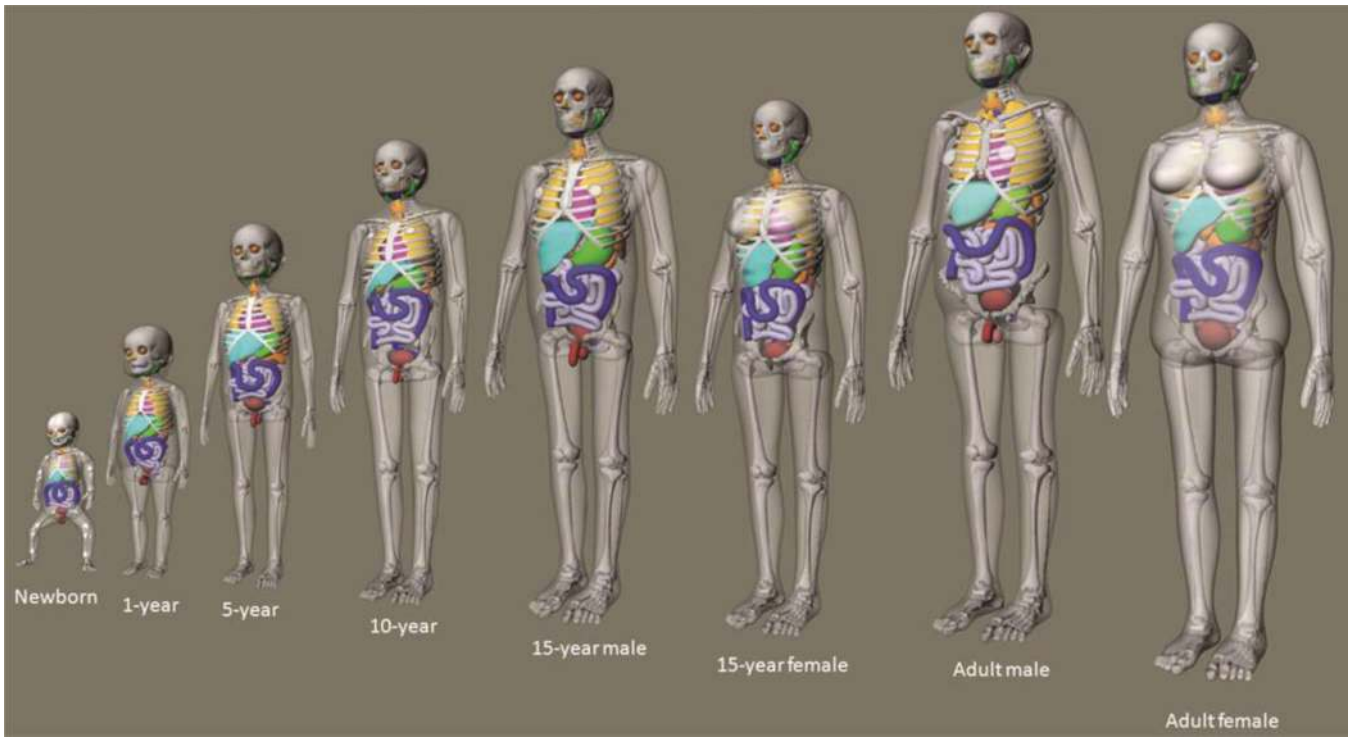

Figure 21.
UF family phantoms developed from the BREP methods (Bolch *et al* 2010).

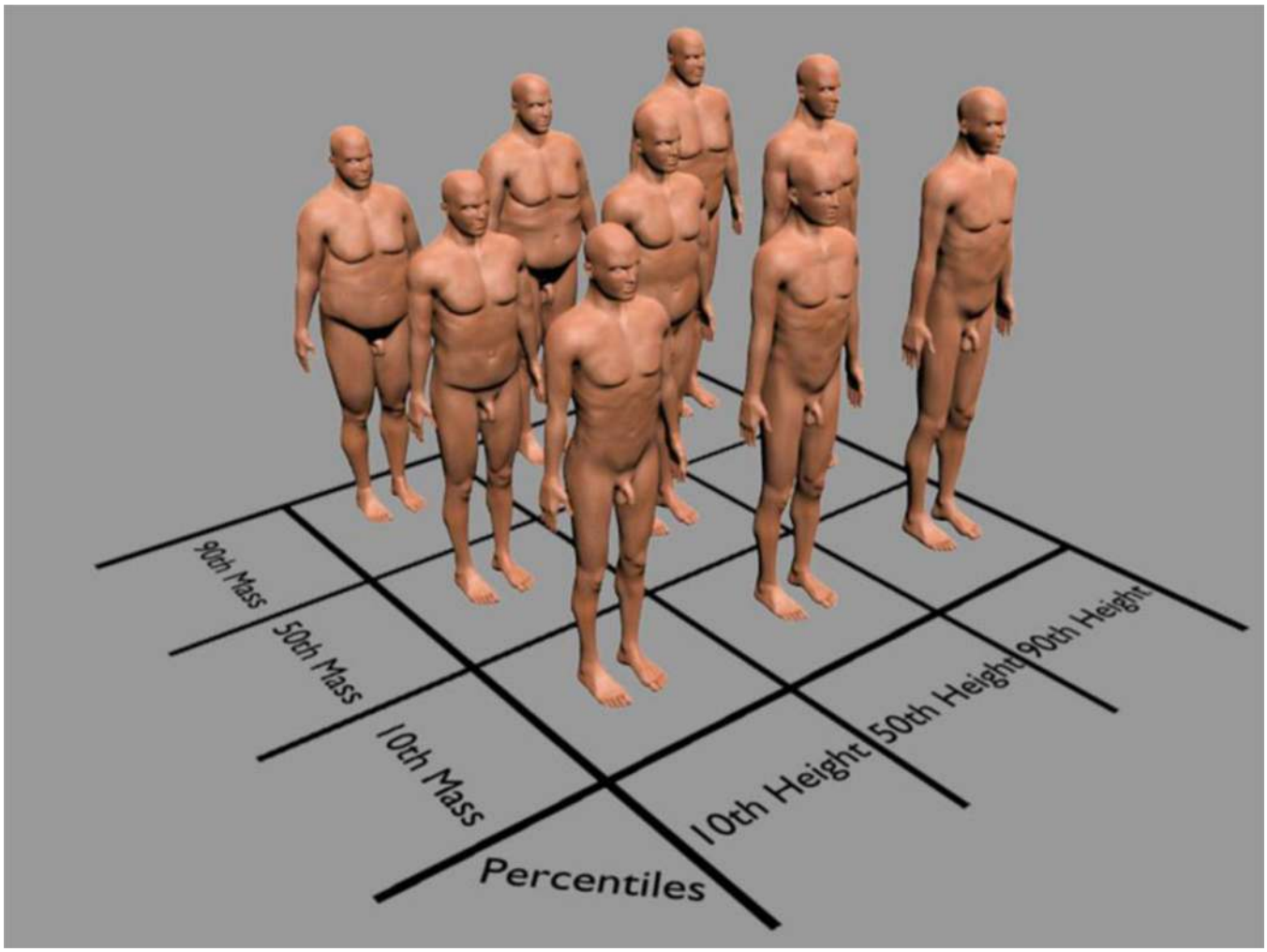

Figure 22.
The anthropomorphic MASH phantom organized by weight and height percentiles (Cassola *et al* 2011)

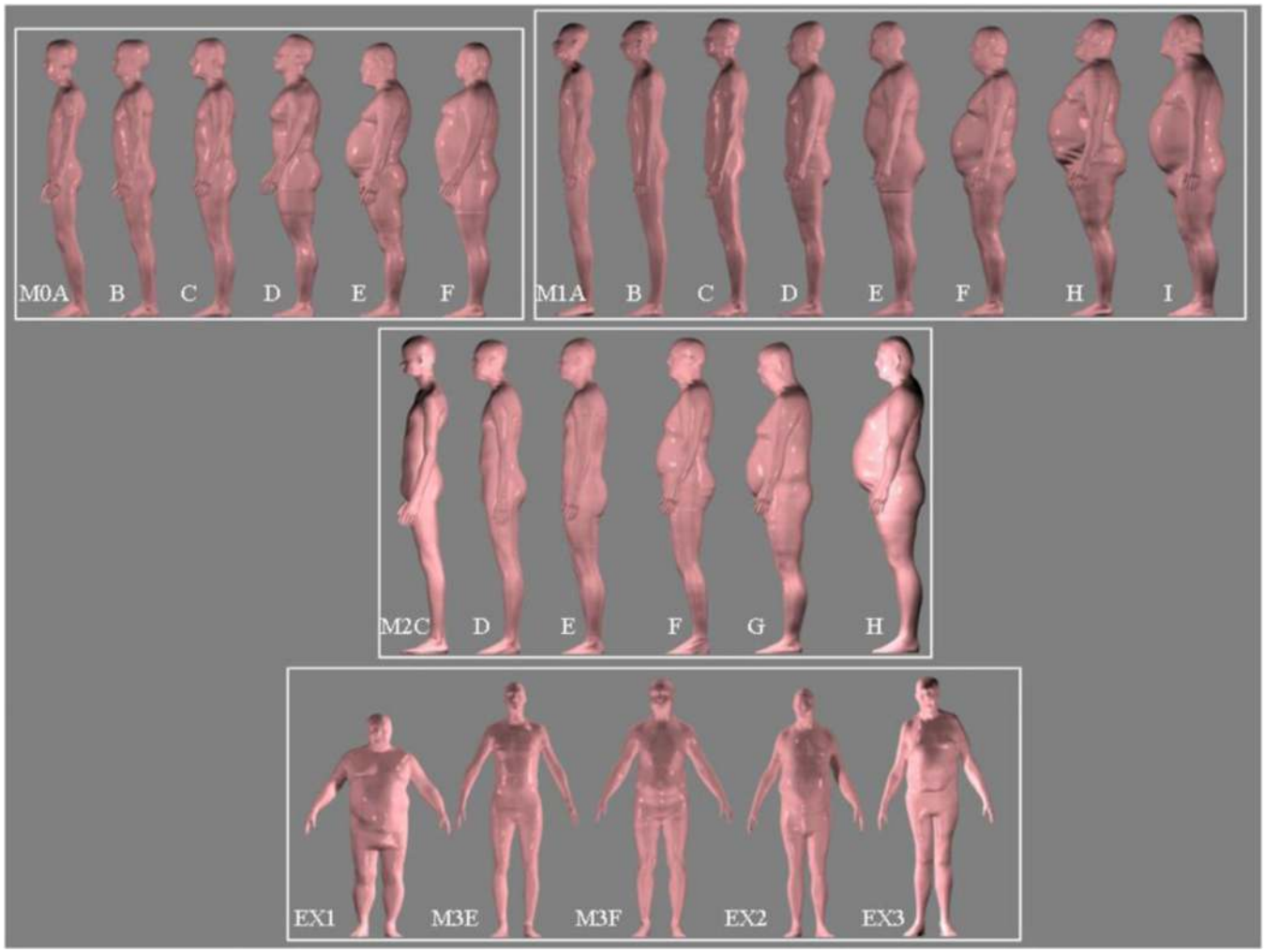

Figure 23.
Male phantoms of different body types based on the CAESAR database (Broggio *et al* 2011).

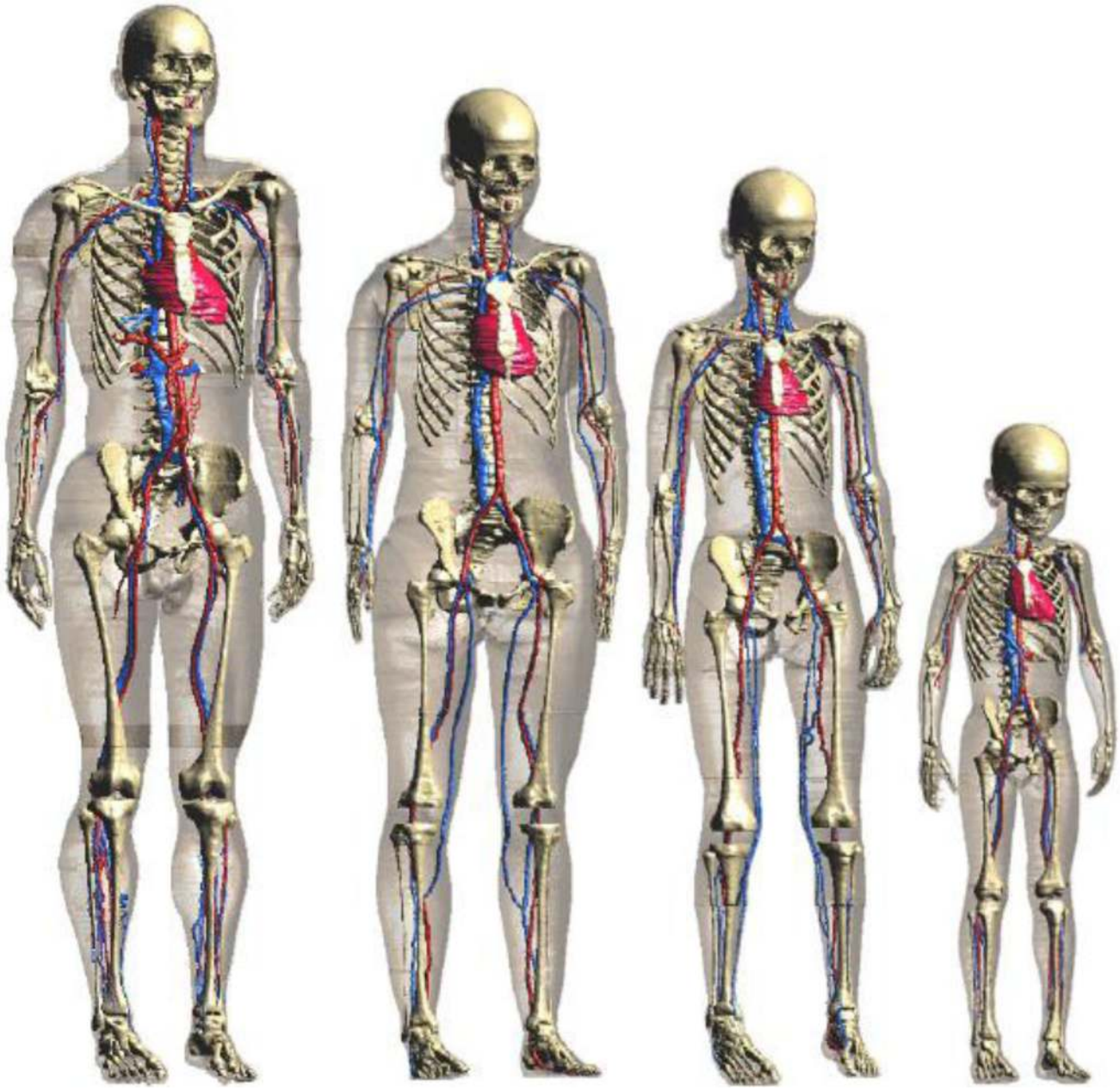

Figure 24.
The Virtual Family: Duke, Ella, Billie, Thelonious (from left to right) by IT'IS (Christ *et al* 2010).

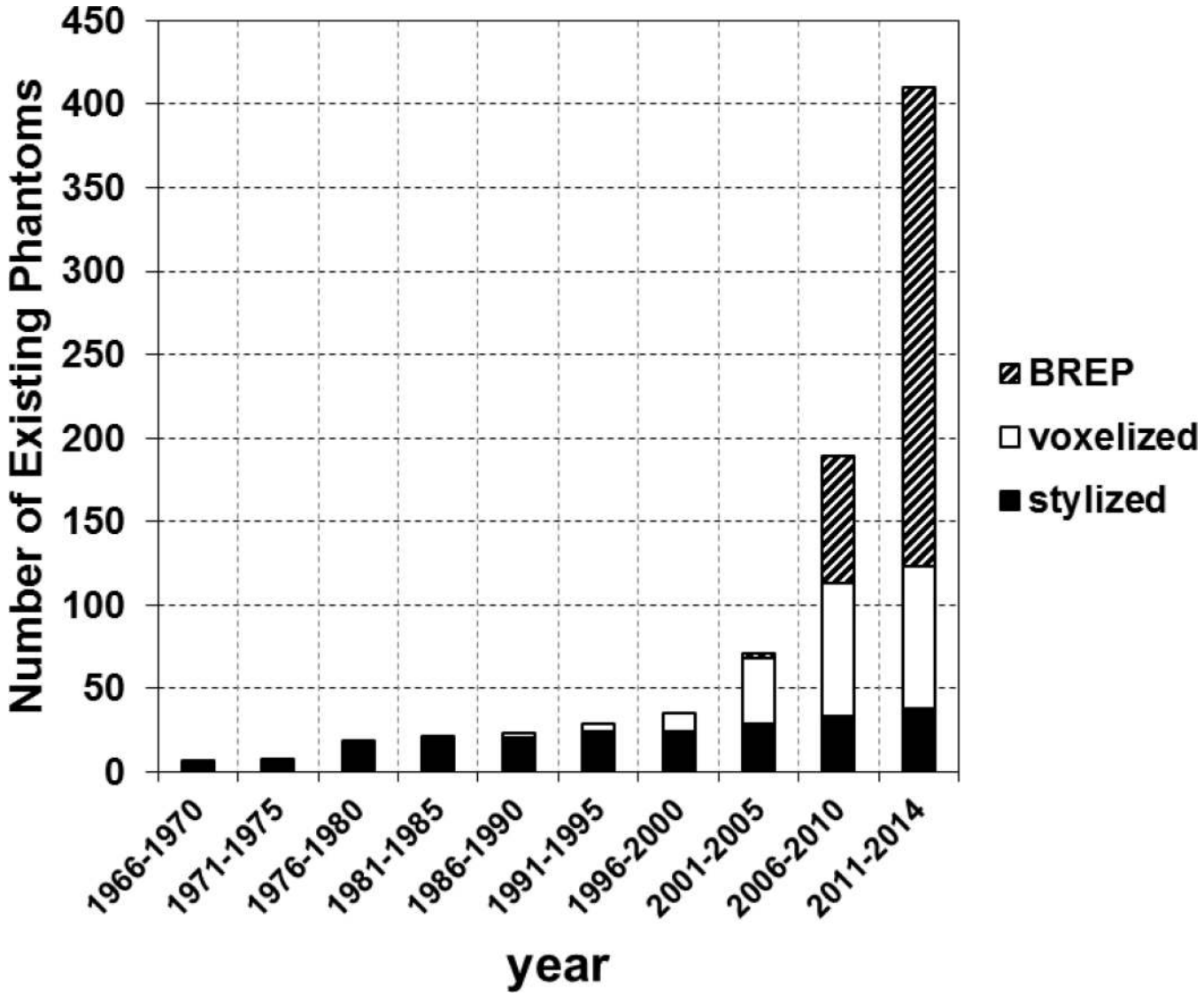

Figure 25.

The number of phantoms in existence since 1966, showing a somewhat surprising exponential growth due to the rapid increase in voxel and BREP phantoms in recent decades (Note: once a phantom is reported in the literature, it is counted in subsequent years when plotting this figure).

Table 1

Alphabetical listing of developers of stylized computational phantoms including information on the phantom names, phantom data types, the anatomical features modeled, the human subjects they mimic, whether they were designed for ionizing or non-ionizing radiation applications, and literature references.

Developers	Phantom Names	Data Types	Human Subjects	Anatomical Features	Ionizing (I) or Non-ionizing radiation (N)	References
Bhaba Atomic Research Centre, India	BARC WBC Phantoms (4 phantoms)	Quadric equations	Indian Adult Male	Phantoms representing the BOMAB phantoms BARC Reference Phantom and a scaled version of the ICRP Reference phantom	I	Bhati *et al* 2011
Catholic University of Pusan, Bugok	Korean Male	Quadric equations	Korean Male	MIRD type phantom with outer body and internal organs modified according to reference values from the Korean Ministry of Science and Technology	I	Kim *et al* 2010
GSF, Germany	ADAM and EVA	Quadric equations	Caucasian adult male and female	Gender-specific phantoms revised from the ORNL MIRD-5 Phantom for external dose assessment. Several minor anatomical changes including the breast size.	I	Kramer *et al* 1982
Hanyang University, Korea	KMIRD	Quadric equations	Korean adult male	Outer body and internal organs of the ORNL adult male phantom modified according to Korean anthropometric data.	I	Park *et al* 2006
ITN, Portugal	ITN WBC Phantom	Quadric equations	Caucasian adult male	A mathematical simulation of the reference male BOMAB phantom.	I	Bento *et al* 2012
Johns Hopkins University, USA (formerly with the University of North Carolina)	MCAT	Quadric equations	Caucasian adult male	3D and 4D cardiac torso phantom with gated patient organ motion information for imaging applications.	I	Pretorius *et al* 1997, Tsui *et al* 1993, 1994
Key Laboratory of Particle & Radiation Imaging, Beijing	CMP	Quadric equations	Chinese adult male	An anthropomorphic phantom constructed from the Reference Asian Man and the Chinese Reference Man	I	Qiu *et al* 2008
NASA, USA	CAM	Quadric equations	Caucasian adult male	A standing U.S. air force adult male representing 50th-percentile height and weight. More than 1000 geometric surfaces and 2450 solid regions.	I	Billings and Yucker 1973

Developers	Phantom Names	Data Types	Human Subjects	Anatomical Features	Ionizing (I) or Non-ionizing radiation (N)	References
ORNL, USA	Fisher-Snyder Phantom (MIRD-5) and others (6 phantoms)	Quadric equations	Caucasian newborn,1-, 5-, 10-, 15-year-old and the adult	The first anthropomorphic phantom representing a hermaphrodite adult for internal dosimetry. Organ masses, body weight and body height correspond to 50th-percentile data recommended in ICRP 23. Later, age-specific phantoms were developed by others.	I	Fisher and Snyder 1966, Fisher and Snyder 1967
	Pediatric Phantoms	Quadric Equations	Caucasian newborn, 1-year, 5-year, 10-year, and 150-year old	Individual phantoms based on the literature for each age.	I	Deus and Poston 1976, Hwang *et al* 1976, Jones *et al* 1976
	Cristy-Eckerman Family Phantoms (6 phantoms)	Quadric equations	Caucasian adult	Based on MIRD-5 Phantom and others from ORNL, including a 15-year male/female phantom	I	Cristy 1980, Cristy and Eckerman 1987
	Pregnant Women (3 phantoms)	Quadric equations	Caucasian pregnant women at three, six and nine months of gestation	The stylized adult female was modified by adding uterine contents including the fetus, fetal skeleton and placenta at three different gestational stages.	I	Stabin *et al* 1995
Nagoya Institute of Technology, Japan	Japanese Infants (2 phantoms)	Quadric equations	Japanese 3-year-old child	Infant represented by a homogenous spherical model, and an ellipsoidal model with three separate muscle tissues.	N	Hirata *et al* 2008
Radiation Protection Bureau, Canada	Mathematical Models of the Embryo and Fetus (4 phantoms)	Quadric equations	Caucasian pregnant women at 8, 13, 26,38 weeks of gestation	Phantoms include an embryo and fetus at different gestational periods not included in the ORNL Pregnant Women Phantoms. Designed for dosimetry studies involving commercial flights.	I	Chen 2004

Table 2

Alphabetical listing of developers of voxel computational phantoms including information on the phantom names, phantom data types, the anatomical features modeled, the human subjects they mimic, whether they were designed for ionizing or non-ionizing radiation applications, and literature references.

Developers	Phantom Names	Data Types	Human Subjects	Anatomical Features	Ionizing (I) or Non-ionizing radiation (N)	References
Austrian Institute of Technology, Austria	MATSIM head MATSIM torso	CT	International Space Station Astronaut	Based on the MATROSHKA RANDO phantom	I	Beck *et al* 2011
Brooks Air Force Base, USA	Visible Man	Color photos	Caucasian 39-year old male cadaver	Visible Human Project. More than 40 tissues were identified.	N	Mason *et al* 2000, Wang *et al* 2004
Chang Gung University, Taiwan	Taiwanese Adult	CT	30 Taiwanese adults	Whole body phantom (152 cm, 50 kg, Female)	I	Tung *et al* 2011
China Institute for Radiation Protection, China	CNMAN	Color Photos	Chinese adult male cadaver	Chinese Visible Human Project	I	Zhang *et al* 2007a
Darmstadt University of Technology, Germany	HUGO	Color photos	Caucasian 39-year old male cadaver	Visible Human Project. A total of 32 tissues were identified.	N	Gjonaj *et al* 2002
ENEA, Italy	NUDEL	CT	Caucasian Male	Based on a reconditioned physical phantom named AMOS	I	Ferrari 2010
FCS Department, Italy	DAM	MRI	34-year old male volunteer	Dielectric anatomical phantom.	N	Mazzurana *et al* 2003
Federal University of Pernambuco, Brazil	MAX	CT	Caucasian adult male patient	Based on VOXTISS8 phantom and adjusted to ICRP-89 Reference Man.	I	Kramer *et al* 2003
	FAX	CT	Caucasian adult female patient	Images of the trunk, the neck and the lower part of the head were from CT scan of a 37-year-old female. Images of the legs and feet were from CT scan of a 62-year-old woman. The head and arms were from MAX phantom.	I	Kramer *et al* 2004
	MAX06 and FAX06	CT	Caucasian adult male and female patient	Extension of MAX and FAX phantoms by adding more details in the skeleton to better match the ICRP-89 Reference Man values.	I	Kramer *et al* 2006

Phys Med Biol. Author manuscript; available in PMC 2015 September 21.

Developers	Phantom Names	Data Types	Human Subjects	Anatomical Features	Ionizing (I) or Non-ionizing radiation (N)	References
Flinders University, Australia	ADELAIDE	CT	Caucasian 14-year old female patient	Torso phantom, without head and arms.	I	Caon *et al* 1999, Caon *et al* 2000
Graz University of Technology, Austria	SILVY	MRI, CT	Caucasian pregnant woman patient at 30 weeks gestation	Trunk was based on MR images of a pregnant women and on modified CT images of a woman in the 30th week of pregnancy developed by RPI. The brain and spinal cord were from NORMAN and fitted into SILVY.	N	Cech *et al* 2007, Cech *et al* 2008
GSF-National Research Center for Environment and Health, Germany	BABY	CT	Caucasian 8-week old female cadaver	57 cm in height and weighed 4.2 kg.	I	Williams *et al* 1986, Zankl *et al* 1988
	CHILD	CT	Caucasian 7-year old female leukemia patient	115 cm in height and weighed 21.7 kg.	I	Williams *et al* 1986, Zankl *et al* 1988
	DONNA	CT	Caucasian 40-year old female patient	Whole body phantom (176 cm, 79 kg)	I	Fill *et al* 2004, Petoussi *et al* 2002
	FRANK	CT	Caucasian 48-year old male patient	Head and torso	I	Petoussi *et al* 2002
	HELGA	CT	Caucasian 26-year old female patient	From mid-thigh upwards	I	Fill *et al* 2004, Petoussi *et al* 2002
	IRENE	CT	Caucasian 32-year old female patient	Whole body phantom (163 cm, 51 kg)	I	Fill *et al* 2004, Zankl *et al* 2002
	GOLEM	CT	Caucasian 38-year old male patient	The weight and height are similar to those of ICRP 23 reference man.	I	Zankl *et al* 2002
	GODWIN	CT	Caucasian 38-year old male patient	Modification of Golem phantom to agree with the ICRP 89 reference values.	I	Zankl *et al* 2005
	VISIBLE HUMAN	CT	Caucasian 39-year old male cadaver	Head to knee. CT data from the Visible Human Project.	I	Zankl *et al* 2002
	LAURA	CT	Caucasian 43-year old female patient	167 cm height and a weight of 59 kg.	I	Zankl *et al* 2005
	KLARA	CT	Caucasian 43-year old female patient	The modification of Laura to agree with ICRP 89 reference values.	I	Zankl *et al* 2005
	KATJA	MRI	Caucasian pregnant woman patient in her 24th week of pregnancy	A woman in her 24th week of pregnancy. Based on the modified REGINA phantom and patient MRI	I	Becker *et al* 2007

Developers	Phantom Names	Data Types	Human Subjects	Anatomical Features	Ionizing (I) or Non-ionizing radiation (N)	References
				images of the abdominal and pelvic regions.		
	REGINA (ICRP Reference Phantom)	CT	Caucasian 43-year-old female patient	An adjusted LAURA phantom according to ICRP 89 reference values.	I	ICRP 2007, Schlattl *et al* 2007
	REX (ICRP Reference Phantom)	CT	Caucasian 38-year-old male leukemia patient	An adjusted GOLEM phantom according ICRP 89 reference values	I	ICRP 2007, Schlattl *et al* 2007
Hanyang University, South Korea	KORMAN	MRI	Korean 30-year-old healthy male	Korean male of average height and weight.	I	Lee *et al* 2004
	KORWOMAN	MRI	Korean 35-year-old female	Korean female of average height and weight. Legs were modeled from the Visible Human Project data.	I	Lee *et al* 2005
	KTMAN-1	MRI	Korean 25-year-old male volunteer	Korean Typical Man (172 cm, 65 kg, without arms)	I	Lee *et al* 2006
	KTMAN-2	PET and CT	Korean 35-year-old male volunteer	Korean Typical Man-2 (172 cm, 68 kg)	I	Lee *et al* 2006
	HDRK-Man	Color photos	Korean 33-year-old adult male cadaver	High-Definition Reference Korean Male phantom from the Visible Korean Human data.	I	Choi *et al* 2006, Kim *et al* 2008
Health Protection Agency, UK (formerly National Radiological Protection Board)	NORMAN	MRI	Caucasian adult male	Normalized man. Only 10 sets of ribs rather the traditional 12.	N, I	Dimbylow 1996, Dimbylow 1997, Jones 1997
	NAOMI	MRI	Caucasian healthy adult female volunteer	Weight and height were scaled to the values by ICRP 89.	N	Dimbylow 2005a, Dimbylow 2005b
	NORMAN-05	MRI	Caucasian adult male	Based on NORMAN with new tissues recommended by ICRP.	I	Ferrari and Gualdrini 2005
	Pregnant female, hybrid phantoms (4 phantoms)	Quadric equations and MRI	Pregnant woman at 8, 13, 26, 38 weeks of gestation	Based on NAOMI and Chen's stylized fetal phantoms	N	Dimbylow 2006
Huazhong University of Science and Technology, China	VCH	Color Photos	Chinese adult male cadaver	Visible Chinese Human Project	I	Zhang *et al* 2008a, Zhang *et al* 2008b, Zhang *et al* 2008c

Developers	Phantom Names	Data Types	Human Subjects	Anatomical Features	Ionizing (I) or Non-ionizing radiation (N)	References
	VCH-FA	VCH phantom	Chinese female astronauts	Based on cryosection images, the VCH phantom was constructed via NURBS so the models could deform to match the body parameters of Chinese female astronauts.	I	Sun *et.al 2013*
Institut National de la Santé et de la Recherché Médicale (INSERM), France	WBPM (4 Phantoms)	CT	27-year-old male, 52-year-old-female, two 3-year-old-boys	4 phantoms of different age and gender for radiotherapy treatment. Based on CT images of 4 volunteers	I	Alziar *et al* 2009
Institut de Radioprotection et de Sûreté Nucléaire (IRSN), France	Personalized Voxel Phantom	CT	Hispanic Male	Male victim of a radiological accident in South America	I	Courageot *et al* 2011
Japan Atomic Energy Agency (JAEA), Japan	OTOKO	CT	Japanese adult male volunteer	Japanese adult male voxel phantom (170cm, 65kg)	I	Saito *et al* 2001
	JM	CT	Japanese 54-year-old male volunteer	Japanese adult male voxel phantom using a CT scan in supine posture	I	Sato *et al* 2007a
	JM2	CT	Japanese 54-year-old male volunteer	The male subject recruited for the construction of JM was selected to obtain CT scan in upright posture.	I	Sato *et al* 2007b
	ONAGO	CT	Japanese adult female Volunteer	Japanese adult female phantom (162cm, 57kg)	I	Saito *et al* 2008
	JF	CT	Japanese adult female volunteer	Japanese adult female phantom (152cm, 44kg)	I	Sato *et al* 2009
Korea Atomic Energy Research Institute, South Korea	Photographic voxel phantom	Color Photos	Korean adult volunteers	A phantom was constructed from photographic images of subjects. Phantoms were modeled as homogenous	N	Kim *et al* 2010
National Institute of Information and Communications Technology (NIICT), Japan	TARO	MRI	Japanese 22-year-old male volunteer	Adult male phantom (171.4cm, 65.0kg) representing average anatomical values of Japanese 18-year-old male	N, I	Lee *et al* 2006
	HANAKO	MRI	Japanese 22-year-old female volunteer	Adult female phantom (159.1cm, 52.6kg) representing average anatomical values of	N, I	Lee *et al* 2006, Nagaoka *et al* 2004

Developers	Phantom Names	Data Types	Human Subjects	Anatomical Features	Ionizing (I) or Non-ionizing radiation (N)	References
				Japanese 30-year-old female.		
	Pregnant woman	MRI	Japanese 26-week-pregnant woman volunteer	Based on the HANAKO phantom and the abdominal phantom of a 26-week pregnant woman.	N	Nagaoka *et al* 2006, Nagaoka *et al* 2007
	Deformed Children (3 phantoms)	MRI/FFD	Japanese 3-, 5-, and 7-year children	Transformed from the TARO phantom into children models using the FFD algorithm.	N	Nagaoka *et al* 2008
Oak Ridge National Laboratory (ORNL), USA	VOXMAT	CT and quadric equations	Caucasian adult male	Voxelized head and torso phantom with stylized arms and legs.	I	Akkurt 2008
Rensselaer Polytechnic Institute (RPI), USA	VIP-Man	Color photos	Caucasian 39-year-old male cadaver	High resolution images from Visible Human Project	I	Xu *et al* 2000
	Pregnant Woman	CT	30-week pregnant woman patient	A pregnant woman phantom covering the abdominal region	I	Shi and Xu 2004
	RANDO CT Phantom	CT	Adult male	A whole-body model of the RANDO physical phantom	I	Wang *et al* 2004
Tsinghua University, China	CVP	MRI	Chinese adult male volunteer	Chinese Voxel Phantom (170cm, 70kg).	I	Li *et al* 2008, Zeng *et al* 2006
University Hospitals of Leuven, Belgium	Phantom 1	MRI	33-week old stillborn male baby cadaver	Baby phantom (50cm, 1.91kg)	I	Smans *et al* 2008
	Phantom 2	CT	22-week old stillborn male baby cadavers	Baby phantom (30.4cm, 0.59kg)	I	Smans *et al* 2008
University of Florida, USA	UF 2 month	CT	Caucasian 6-month old male cadaver	A voxel phantom equivalent to a 2 month old male newborn, representing a critically ill child.	I	Nipper *et al* 2002
	UF Newborn	CT	Caucasian 6-day old female newborn cadaver	A normal 6-day female newborn phantom; The lungs were created using CT images of a 1-month old patient and the adrenal glands created using CT images of a 2-month old male patient.	I	Nipper *et al* 2002
	UF Series A (5 phantoms)	CT	9-month, 11-, and 14-year old males; 4- and 8-year	UF pediatric phantom series without arms and	I	Lee *et al* 2005

Developers	Phantom Names	Data Types	Human Subjects	Anatomical Features	Ionizing (I) or Non-ionizing radiation (N)	References
			old females patients	legs.		
	UF Series B (5 phantoms)	CT	9-month, 11-, and 14-year males; 4- and 8-year female patients	Based on the UF Series A phantoms with arms and legs from CT images of a healthy Korean adult attached. The organ masses were adjusted to ICRP 89 reference values.	I	Lee *et al* 2006
University of Houston, USA	10 Year Old Boy	CT	10-year old male	Pediatric phantom developed for craniospinal proton irradiation.	I	Taddei *et al* 2009
University of Karlsruhe, Germany	MEET Man	Color photos	Caucasian 38-year-old adult male cadaver	Models for simulation of Electromagnetic, Elastomechanic and Thermic behavior of Man, developed from the Visible Human Project.	N, I	Doerfel *and Heide* 2007, Sachse *et al* 1997
University of Utah, USA	Anatomically based model	MRI	Caucasian adult male volunteer	Anatomic phantom. The outer parts of the arms are missing.	N	Tinniswood *et al* 1998
Vanderbilt University, USA	Gibbs Phantoms	Radiography	Caucasian representative female cadaver	Phantom includes head, trunk and proximal extremities developed from x-ray images	I	Pujol and Gibbs 1982, Gibbs *et al* 1987, Gibbs *et al* 1984
Yale University, USA	Zubal	CT	Caucasian adult male patient	Head and torso	I	Zubal *et al* 1994
	MANTISSUE3-6	CT	Caucasian adult male patient	Arms and legs from the Visible Human Project were attached to the Zubal phantom	N	Dawson *et al* 1997
	VOXTISS8	CT	Caucasian adult male patient	Arms and legs were attached to the Zubal phantom and the arms were straightened along the phantom side	I	Sjogreen *et al* 2001

Table 3

Alphabetical listing of developers of BREP computational phantoms including information on the phantom names, phantom data types, the anatomical features modeled, the human subjects they mimic, whether they were designed for ionizing or non-ionizing radiation applications, and literature references.

Developers	Phantom Names	Data Types	Human Subjects	Anatomical Features	Ionizing (I) or Non-ionizing radiation (N)	References
Duke University, USA	NCAT	NURBS	Caucasian 39-year-old male and 59-year-old female	NURBS-based Cardiac Torso phantom including organs from the Visible Human Project CT data of the male and female. Gated MRI dataset of a normal patient and 3D angiogram data are used for motion modeling.	I	Segars 2001
	XCAT (47 phantoms)	NURBS	Caucasian 39-year-old male and 59-year-old female	4D eXtended Cardiac Torso phantom based on the NCAT, including more detailed and realistic anatomy and physiology.	I	Fung *et al* 2011
	XCAT Library	NURBS	58 (35 male and 23 female) anatomically variable phantoms	extend the XCAT beyond reference anatomies by developing a series of anatomically variable 4D XCAT adult phantoms	I	Segars *et al* 2013
	MOBY	NURBS	16-week-old male C57bl/6 mouse	Mouse phantom from MR images	I	Segars and Tsui 2007, Segars *et al* 2004
Federal University of Pernambuco, Brazil	FASH and MASH	Polygon meshes	Anatomical atlases and models	Adult male and female phantoms based off of anatomical atlases and models. Organ masses were adjusted to ICRP89 reference values.	I	Cassola *et al* 2010 Kramer *et al* 2010
	FASH and MASH series (18 phantoms)	Polygon meshes	Anatomical atlases and models	Male and Female phantoms for the 10^{th}, 50^{th}, and 90^{th} mass and height percentiles from the ICRP89 reference values.	I	Cassola *et al* 2011
	5 and 10 year old Reference Males and Females	Polygon meshes	Anatomical Atlases and models	Produced by the same methodology as FASH and MASH. No patient images were used.	I	de Melo Lima *et al* 2011
Hanyang University, Korea	PSRK-Man	Polygon meshes	Korean Male	Polygon mesh phantom based on the VKH-MAN. Simulations can be run without voxelization	I	Kim *et al* 2011

Developers	Phantom Names	Data Types	Human Subjects	Anatomical Features	Ionizing (I) or Non-ionizing radiation (N)	References
Institut de Radioprotection et de Sûreté Nucléaire (IRSN), France	Thoracic Female Torsos (34 Phantoms)	Polygon meshes and NURBS	ICRP Reference Female Computational Phantom	34 phantoms of varying girth, cup size, breast tissue, and internal organ volume modified off of the ICRP Reference Female Computational Phantom	I	Farah *et al* 2010 Farah *et al* 2011
	Adult Male Whole Body (25 phantoms)	Polygon meshes and NURBS	CAESAR database	25 whole body male phantoms representing Caucasians of various body types.	I	Broggio et al. 2011
Foundation for Research on Information Technologies in Society (IT'IS), Switzerland	The Virtual Family (4 phantoms)	Polygon meshes	Caucasian volunteers of different gender and ages	Duke: 34-year-old male (174cm,70kg) Ella: 26-year-old female (160cm,58kg) Billie: 11-year-old female (148cm,34kg) Thelonious: 6-year-old male (107cm,17kg)	N	Christ *et al* 2010
	The Virtual Classroom (4 phantoms)	Polygon meshes	Caucasian volunteers of different gender and ages	Roberta: 5-year-old female (109 cm, 17.8 kg) Dizzy: 8-year-old male (140 cm, 26 kg) Eartha: 8-year-old female (136 cm, 30.7 kg) Louis 14-year-old male (169 cm, 50.4 kg)	N	IT'IS 2011
	Fats		Caucasian volunteers of different gender and ages	37-year-old male (182 cm, 120 kg)	N	IT'IS 2011
	Glen		Caucasian volunteers of different gender and ages	84-year-old male (173 cm, 65 kg)	N	IT'IS 2011
John Hopkins University, USA	Pediatric XCAT phantoms (24 phantoms)	NURBS	Caucasian 39-year-old male and 59-year-old female	Used large deformation diffeomorphic metric mapping to adjust the XCAT phantom to math pediatric reference data	I	Tward *et al* 2011
Rensselaer Polytechnic Institute (RPI), USA	4D VIP-Man Chest	NURBS	Caucasian 39-year-old male cadaver	Organ surfaces were extracted from the VIP-Man phantom and then extended to 4D by adding the respiration of the NCAT phantom.	I	Xu and Shi 2005, Zhang *et al* 2008
	RPI-Pregnant Females (3-, 6- and 9-month)	Polygon meshes	3-, 6-, and 9- month pregnant female	Based on a mixture of anatomical data. Organs of the mother and fetus were adjusted to match ICRP-89 references	I	Xu *et al* 2007

Developers	Phantom Names	Data Types	Human Subjects	Anatomical Features	Ionizing (I) or Non-ionizing radiation (N)	References
	RPI-AM and RPI-AF (2 phantoms)	Polygon meshes	Adult Male and Female	Based on mesh anatomical models that are adjusted to match with ICRP-89 references. Software supports deformation and posture change.	I	Zhang 2009, Na *et al* 2010
	Adult deformable Female breast phantoms (8 phantoms)	Polygon meshes	Adult deformable female breast phantoms	Deformable phantoms based on the RPI-AF phantom. Modified according to ICRP reference data.	I	Hegenbart *et al* 2008
	Obese Phantoms (10 phantoms)	Polygon meshes		Based on population surveys for class 1, 2, and 3 obese patients.	I	Ding *et al* 2012
University of Florida, USA	UFH-NURBS phantoms (4 phantoms)	NURBS	Caucasian 6-day-old female newborn cadaver, 14-year male patient and two 14-year female patients.	UF Hybrid NURBS based on previous voxel phantoms, add 16 sites of lymphatic nodes in 8 hybrid phantoms.	I	Lee *et al* 2007, Lee *et al* 2008 Lee *et al* 2013
	UFH-NURBS fetal phantoms (18 phantoms)	NURBS	11 week and 21.5 week fetal specimens	18 fetal phantoms of varying age and weight with detailed soft tissue orga and developing skeletons ns	I	Maynard *et al* 2011
University of Houston, USA	Pregnant Female (9 phantoms)	BREP/STL formatted CAD	A pregnant woman in the 34th gestational week and a non-pregnant female	Nine phantoms of limited organs covering 1- to 9-month pregnant females from MRI of a non-pregnant female and pregnant woman.	N	Wu *et al* 2006
Vanderbilt University, USA	adult and pediatric phantom series (7 phantoms)	NURBS	Caucasian adult male and female, newborn, 1-, 5-, 10- and 15-year-old	Derived from the NCAT phantom with organ and body masses adjusted to match ICRP-89 references.	I	Stabin *et al* 2008

Table 4

Alphabetical listing of developers of physical phantoms including information on the phantom names, phantom data types, the anatomical features modeled, the human subjects they mimic, whether they were designed for ionizing or non-ionizing radiation applications, and literature references.

Developers	Phantom Names	Anatomical Features	Human Subjects	Ionizing (I) or Non-ionizing radiation (N)	References
Alderson Research Laboratories (acquired by the Phantom Laboratory), USA	RANDO®	Lungs, soft tissue and breasts are included; Natural human skeletons were used.	Caucasian adult male and female	I	Anderson *et al* 1962 Phantom Laboratory 2013)
Computerized Imaging Reference Systems, Inc. (CIRS), USA	ATOM®	Bone, lung and soft tissue are included. Standard phantom includes head, torso, upper femur and genitalia. Legs and arms are included with the newborn and 1 year pediatric phantoms. Breasts can be added.	Caucasian newborn, 1-, 5-, and 10-year-old children, adult male and female	I	CIRS 2013
	3D Sectional Torso Phantom	Removable lungs, heart, liver, pancreas, kidney and spleen are included.	Caucasian adult male torso	I	CIRS 2013
Kyoto Kagaku Co. LTD, Japan	PBU-50	The skeleton, lungs, liver, mediastinum and kidney models are embedded in soft tissue substitute.	Japanese adult male	I	Kyoto Kagaku 2013
	CTU-41	One-piece anthropomorphic torso phantom with anatomical structures.	Japanese adult male	I	Kyoto Kagaku 2013
	Chest phantom N1 “lungman”	The inner components consists of mediastinum, pulmonary vasculature and an abdomen block	Japanese	I	Kyoto Kagaku 2013
Lawrence Livermore National Laboratory (LLNL), USA	LLNL (commercially available through Radiology Support Devices)	Removable organs such as the lungs, heart, liver, kidneys, spleen, tracheo-bronchial lymph nodes are included. Chest plates simulate different chest wall thicknesses. The first generation of LLNL phantom contains a real human male rib cage.	Caucasian adult male	I	Griffith *et al* 1978
Radiation Health Research Institute of Korea Hydro and Nuclear Power, South Korea	Typical Korean Male	Based on CT images of a human subject. The phantom contains bone, lungs and soft tissue without arms and legs. The rapid prototyping and manufacturing technique were used.	Korean adult male	I	Kim *et al* 2006
Radiation Protection Bureau, Canada	BOMAB phantom family	Each phantom is composed of 10 elliptical containers representing head, neck, chest, gut, arm, thigh, and calf.	Canada 5- and 10-year-old, reference man, reference woman, 5 and 95 percentile men	I	Kramer *et al* 1991
University of Florida, USA	MIRD stylized Newborn	Based on stylized computational phantom.	Newborn	I	Tresser and Hintenlang 1999
	UF 1-year old	CT images	1-year-old child	I	Tresser and Hintenlang 1999

Developers	Phantom Names	Anatomical Features	Human Subjects	Ionizing (I) or Non-ionizing radiation (N)	References
	UF Adult Male	CT images	Adult male		Tresser and Hintenlang 1999
	UF Newborn physical phantom	Based on UF Newborn voxel phantom including soft tissue, bone and lungs.	Newborn cadaver	I	Jones *et al* 2006, Staton *et al* 2006